MAYO CLINIC

Semi-Annual Status Report - NASA Research Grant NGR 24-003-00

October 1, 19

STUDIES OF THE EFFECTS OF GRAVITATIONAL AND INERTIAL FORCES ON CARDIOVASCULAR AND RESPIRATORY DYNAMICS

This report consists of comprehensive status reports of the investigative projects which have received support from this grant.

Summary

1) A number of papers describing the roentgen video system and physiologic studies carried out with the system have been published or prepared for publication during the last eight months. A list of these publications and copies of a number of recent, still unpublished manuscripts are appended to this report.

2) A prototype model of the new General Electric Epicon television camera has been tested in this laboratory in collaboration with General Electric engineers. Except for blemishes in its integrated diode target array, its dynamic response has been demonstrated to be considerably superior to the previously highest performance available television camera (the image orthicon) currently used in our biplane roentgen video system.

General Electric has recently succeeded in fabricating an Epicon tube free of blemishes in its target array. This tube is scheduled for tests in our laboratory in October 1971.

3) Analysis of the problem of determining the shape and dimensions of solid objects from silhouettes of the object has revealed that accurate measurements of these parameters for objects of unknown shape cannot be made from silhouette outlines alone, no matter how many angles of view are analyzed (for details, see Sections I and II).

4) It has been demonstrated that the shape and dimensions of solid objects can be measured by high-resolution orthogonal biplane roentgen videodensitometry if the objects are of uniform roentgen density and have a shape similar to that of the left ventricle (for details, see Section II).

5) High resolution orthogonal roentgen videodensitometry requires direct analog-to-digital conversion of video images and subtraction of these digitized video images in their exactly correct temporal array plus, for some applications, reconversion of the difference images or other types of computer generated images back to their analog video form (for details, see Section III).

a) The very high sampling speeds (20 megahertz) and 0.1 to 0.5 percent (8-9 bit) accuracy required for these conversion processes has recently been attained by TRW, Inc. under contract with the U.S. Air Force Avionics Laboratory and a 20-megahertz, 9-bit analog-to-digital converter has been given to this laboratory on an indefinite loan basis for use in digital processing of video images.

A complete prototype of this A-D and D-A system was tested in this laboratory in June 1971 in collaboration with TRW engineers and found to be capable of converting and reconverting the video image of an 0.5 mm wire superposed on a background of pressed wood with a roentgen opacity similar to the human thorax.

The frequency range of the laboratory's video system used to obtain this image of an 0.5 mm object extended from 4 to 15 megahertz. The required digital conversion sampling rate for reproduction of such an image is at least 20 meghertz. When the sampling rate was reduced to 10.7 megahertz, the silhouette of the 0.5 mm wire disappeared in the reconverted image.

b) A special sum of products arithmetic module has been incorporated into the laboratory's CDC 3500 digital computer system. This system will allow very high-speed processing of video images with minimal use of the central processing unit of the 3500. This will allow use of the 3500 system for video image processing without compromising its use on a time-shared basis with other investigators who are served by this system.

c) Successful digital subtraction of video images of the opacified left ventricle and reconversion of the subtracted image to analog form has been achieved in the laboratory.

6) A stereotronics system for providing true stereo television displays has been tested in the laboratory with excellent results.

The system is modest in cost and does not require modification of our existing split-screen television capabilities.

Computer programs have been developed for generation of stereo images of the left ventricular cavity on the basis of biplane videometry data obtained from left ventricular angiograms. Such images can be generated for each 60-per-second video field throughout successive cardiac cycles and then recorded and displayed by the video disc in static (stop action) or forward and reverse variable slow motion or real-time displays as desired for detailed study of the temporal inter-relationships of dynamic changes in ventricular geometry, hemodynamics, and length-tension relationships derived therefrom (for details, see Section IV).

The frequency modulated system, developed in this laboratory, for recording of seven (expandable to fifteen) variables such as mutliple pressures, electrical events, and flows, on the same videotape as the angiogram, has been perfected. The problem of synchronizing simultaneous hemodynamic variables with the dynamic video images of the heart chambers has been eliminated by this development. Also, the computer-generated display techniques, developed in this laboratory, for superimposing multiple parameters on the stereo images of the ventricle in correct anatomical and temporal relationship to all regions of the ventricular image and the heart cycle, respectively, are facilitated by recording the requisite original information in exact temporal synchrony on the same videotape (for details, see Section IV).

7) The current configuration of the biplane roentgen videometry system has been used during the last eight months to study:

a) The effects of rapid injections of contrast medium on left ventricular function.

b) The cardiac and circulatory effects of sustaining the circulation by an intraventricular balloon pump after severe myocardial damage in dogs.

c) Left-to-right shunts in experimental ventricular septal defects in dogs.

d) Blood flow in selected sites in the coronary circulation and aortic-to-coronary artery-saphenous vein grafts.

8) Preliminary experiments have been carried out comparing simultaneous measurements of the internal diameter of the ventricle by biplane videometry and sonar micrometry (for details, see Section V).

9) A biplane roentgenographic technique has been developed for study and display of the simultaneous movements of multiple sites in the lung parenchyma during the respiratory cycle, various respiratory maneuvers, changes in body position, and the force environment. From these data, changes in regional lung volumes and regional ventilation can be calculated, and the relationships of the spatial distribution of ventilation and blood flow to specific anatomical regions in the lung under various conditions studied more accurately (for details, see Section VI).

Use of biplane videograms to record dynamic movements of the lung markers used in this study has been facilitated by use of an operator interactive electronic video cursor peripheral computer station assembly, developed in this laboratory, by means of which orthogonal marker positions, lung, and vertebral outlines can be fed directly into the computer from the video disc.

Computer programs have been developed to:

a) Identify the sites of 40-60 individual lung parenchymal markers in the orthogonal video roengenograms of the intact thorax,

b) Correct the positions for geometric distortion due to the diverging character of the orthogonal roentgen beams,

c) Calculate the X, Y, and Z coordinates of each marker in reference to given anatomical site (the midpoint of the body of the sixth thoracic vertebra or peak of the carina have been used), and

d) To generate projections of the outlines of the lungs and the positions of the multiple parenchymal markers and their movement onto the coronal, sagittal, or cross-sectional planes of the thorax as desired (for details, see Sections VI and VII). The display of dynamic lung geometry is being expanded to computer generation of true stereo video images of instant-to-instant regional movements of lung parenchyma and changes in regional volumes and distribution of ventilation derived therefrom.

10) An isotonic saline immersion respirator has been developed to provide control of respiratory rate and volumes to facilitate studies of dynamic lung geometry and provide the respiratory assistance required for maintenance of normal blood oxygen and carbon dioxide tensions during breathing of organic liquids at 1G and during changes in the gravitational-inertial force environment generated on the laboratory's human centrifuge (for details, see prior progress reports).

11) This respirator assembly has been used in conjunction with a liquid oxygenator assembly to study the effects of liquid breathing on:

a) Pulmonary arterial-venous shunts,

b) Intrathoracic pressure relationships, including vertical gradients in pleural fluid pressures,

c) Respiratory variations in left ventricular stroke volume, and

d) The spatial distribution of pulmonary blood flow,

(for details, see Sections VIII and IX).

Detailed Report

Manuscripts, which are being prepared for publication containing more detailed descriptions of some of the recent developments outlined in the foregoing, are appended to this report under the following section numbers.

Section I Estimation of the contractile function of the intact heart by angiographic techniques,

Section II The problem of determination of the shape and dimension of homogeneous objects from roentgenographic data with particular reference to angiocardiography,

Section III Consideration of the relative merits of different analog-to-digital conversion systems for digitization of video images,

Section IV Computerized measurement and display of dynamic changes in shape and volume of solid objects derived from biplane roentgen videograms with particular reference to cardioangiography,

Section V Comparison of ultrasound cardiography with biplane angiography,

Section VI Effect of inflation levels and body position changes upon regional pulmonary parenchymal movement in dogs at 1G,

Section VII Effect of changes in the magnitude and direction of the force environment on regional distortion of lung parenchyma in dogs,

Section VIII Respiratory variations in left ventricular stroke volume during liquid breathing,

Section IX Effects of acceleration on pulmonary blood flow in dogs breathing organic liquids,

Section X Calibration of chronically implanted transducers for cardiorespiratory studies in intact chimpanzees.

Publications

1. Wood, E. H.:
STUDIES OF EFFECTS OF VARIATIONS IN THE DIRECTION AND MAGNITUDE OF THE GRAVITATIONAL-INERTIAL FORCE ENVIRONMENT ON THE CARDIOVASCULAR AND RESPIRATORY SYSTEMS.
Chapter in Recent Advances in Aerospace Medicine (D.E. Busby, editor), Reidel Publishing Company, Dordrecht-Holland, 1970, pp 309-314.

2. Smith, H. C., R. E. Sturm, and E. H. Wood:
SIMULTANEOUS INDICATOR-DILUTION CURVES AT SELECTED SITES IN THE CORONARY CIRCULATION.
Federation Proceedings 30:487 (March-April) 1971. Abstract

3. Sass, D. J., E. L. Ritman, P. E. Caskey, W. Van Norman, and E. H. Wood:
RESPIRATORY VARIATIONS IN LEFT VENTRICULAR STROKE VOLUME DURING LIQUID BREATHING.
Aerospace Medical Association preprint, 1971 Annual Scientific Meeting April 26-29, 1971, pp 80-81.

4. Tsakiris, A. G., G. von Bernuth, G. C. Rastelli, M. J. Bourgeois, J. L. Titus, and E. H. Wood:
SIZE AND MOTION OF THE MITRAL VALVE ANNULUS IN ANESTHETIZED INTACT DOGS.
Journal of Applied Physiology 30:611-618 (May) 1971.

5. Sturm, R. E. and E. H. Wood:
ROENTGEN IMAGE-INTENSIFIER, TELEVISION, RECORDING SYSTEM FOR DYNAMIC MEASUREMENTS OF ROENTGEN DENSITY FOR CIRCULATORY STUDIES.
Roentgen- Cine- and Videodensitometry. Fundamentals and Applications for Blood Flow and Heart Volume Determination. G. Thieme, Stuttgart, 1971 (Dr. P. H. Heintzen, editor) pp 23-44.

6. Williams, J. C. P. and E. H. Wood:
APPLICATION OF ROENTGEN VIDEODENSITOMETRY TO THE STUDY OF MITRAL VALVE FUNCTION.
Ibid. pp 89-98.

7. Amorim, D. deS., A. G. Tsakiris, and E. H. Wood:
USE OF ROENTGENVIDEODENSITOMETRY FOR DETECTION OF LEFT-TO-RIGHT SHUNTS IN DOGS WITH EXPERIMENTAL ATRIAL SEPTAL DEFECT.
Ibid. pp 99-107.

8. Smith, H. C., R. L. Frye, G. D. Davis, J. R. Pluth, R. E. Sturm, and E. H. Wood:
SIMULTANEOUS INDICATOR DILUTION CURVES AT SELECTED SITES IN THE CORONARY CIRCULATION AND DETERMINATION OF BLOOD FLOW IN CORONARY ARTERY-SAPHENOUS VEIN GRAFTS BY ROENTGEN VIDEODENSITOMETRY.
Ibid. pp 152-157.

9. Ritman, E. L., R. E. Sturm, and E. H. Wood:
A BIPLANE ROENTGEN VIDEOMETRY SYSTEM FOR DYNAMIC (60/second) STUDIES OF THE SHAPE AND SIZE OF CIRCULATORY STRUCTURES, PARTICULARLY THE LEFT VENTRICLE.
Ibid. pp 179-211.

10. Vandenberg, R. A., J. C. Williams, R. E. Sturm, and E. H. Wood:
EFFECT OF VARYING VENTRICULAR FUNCTION BY EXTRASYSTOLIC POTENTIATION ON CLOSURE OF THE MITRAL VALVE.
The American Journal of Cardiology 28:43-53 (July) 1971.

11. Bove, A. A., R. E. Sturm, H. C. Smith, and E. H. Wood:
CHANGES IN LEFT VENTRICULAR FUNCTION DURING INJECTION OF OPAQUE CONTRAST MEDIUM.
The Physiologist 14:114 (August) 1971. Abstract

12. Greenleaf, J. F., H. C. Smith, A. A. Bove, D. J. Sass, and E. H. Wood:
EFFECT OF CHANGES IN THE MAGNITUDE AND DIRECTION OF THE FORCE ENVIRONMENT ON REGIONAL DISTORTION OF LUNG PARENCHYMA IN DOGS.
The Physiologist 14:155 (August) 1971. Abstract

13. Miyazawa, K., H. C. Smith, A. A. Bove, and E. H. Wood:
ROENTGEN VIDEODENSITOMETRIC DETERMINATION OF LEFT TO RIGHT SHUNTS IN EXPERIMENTAL VENTRICULAR SEPTAL DEFECT (VSD).
The Physiologist 14:196 (August) 1971. Abstract

14. Sass, D. J., J. F. Greenleaf, H. C. Smith, A. A. Bove, and E. H. Wood:
EFFECTS OF ACCELERATION ON PULMONARY BLOOD FLOW IN DOGS BREATHING ORGANIC LIQUIDS.
The Physiologist 14:223 (August) 1971. Abstract

15. Smith, H. C., J. F. Greenleaf, D. J. Sass, A. A. Bove, and E. H. Wood:
EFFECT OF INFLATION LEVELS AND BODY POSITION CHANGES UPON REGIONAL PULMONARY PARENCHYMAL MOVEMENT IN DOGS AT 1G.
The Physiologist 14:232 (August) 1971. Abstract

16. von Bernuth, G., A. G. Tsakiris, and E. H. Wood:
EFFECTS OF VARIATIONS IN THE STRENGTH OF LEFT VENTRICULAR CONTRACTION ON AORTIC VALVE CLOSURE IN THE DOG.
Circulation Research 28:705-716 (June) 1971.

17. Wood, E. H.:
SOME EFFECTS OF CHANGES IN THE GRAVITATIONAL-INERTIAL FORCE ENVIRONMENT ON THE HEART AND LUNGS.
Proceedings Fourth International Man-in-Space Symposium on Basic Environmental Problems of Man in Space, Yerevan, U.S.S.R. October 1-5, 1971, in press.

18. Ritman, E. L., P. L. Spivak, R. E. Sturm, and E. H. Wood:
THE PROBLEM OF MEASUREMENT OF SHAPE AND DIMENSIONS OF THE LEFT VENTRICULAR CAVITY FROM ANGIOGRAMS.
Proceedings North American Radiology Society Annual Meeting, November 28-December 3, 1971, Chicago, in press.

20. Wood, Earl H., P. Spivak, E. L. Ritman, and B. K. Gilbert:
THE PROBLEM OF DETERMINATION OF THE SHAPE AND DIMENSIONS OF HOMOGENEOUS OBJECTS FROM BIPLANE ROENTGENOGRAPHIC DATA WITH PARTICULAR REFERENCE TO ANGIOCARDIOGRAPHY.
Proceedings of Fifth Hawaii Internation Conference on System Sciences and Computers in Biomedicine, Honolulu, January 11-13, 1972, in press.

Section I

ESTIMATION OF THE CONTRACTILE FUNCTION OF THE INTACT HEART BY ANGIOGRAPHIC TECHNIQUES

Erik Ritman

R. E. Sturm

and

E. H. Wood

Department of Physiology and Biophysics, Mayo Clinic and Foundation, Mayo Graduate School of Medicine, Rochester, Minnesota 55901

This investigation was supported in part by Research Grants HE-4664, FR-7, and HE-3532 from the National Institutes of Health, Public Health Service, NGR-24-003-001 from NASA and AHA-CI-10 and AHF-CIF-69073 from the American Heart Association.

The contractile elements in the myocardium generate the mechanical energy which produces the changes in length and tension of the myocardial walls required to maintain a stroke volume and heart rate necessary to meet the circulatory demands of the body. Consequently the time course of the changes in length and tension of the ventricular myocardium, are a relatively direct function of the state of the contractile elements. However estimation of tension in any selected segment of the myocardium requires accurate knowledge of the shape of this segment and its dimensions as well as the transmural pressure. Consequently a primary requirement for detailed analysis of left ventricular function is knowledge of its shape in three dimensions and of intraventricular pressure at successive instants in time at a rate of at least 30 per second (1).

Accurate left ventricular volume can be determined once the shape is known, but conversely, knowledge of the ventricular volume is insufficient data for the determination of ventricular shape. Even if only a "representative" length/tension relationship of the myocardium is desired, the shape of the ventricle must be known. The volume/pressure characteristics of the left ventricle are commonly held to be analogous to the length/tension properties of a "representative" muscle fiber, with ventricular volume used as a measure of fiber length. There are several objections to this direct analogy. In a perfectly homogeneous, thin walled spherical chamber, the length in any one direction along the surface of the wall changes as

$$L = \text{Constant} * \text{Volume}^{1/3}$$

so that there is not a linear relationship between length and volume even in this simplest model. Volume may remain constant despite considerable length (i.e. shape) changes. A prolate spheroid with a maximum radius of revolution of

0.7 R, and height 2R, would have a surface area of $4.7\ \pi R^2$ as against $4\pi R^2$ for a sphere of the same volume ($\frac{4}{3}\pi R^2$). This implies that the average length decrease of linear elements in the thin wall during an isovolumic shape change from a cylindrical to spherical shape is about 17%, which would be of the order of sarcomere shortening during normal ventricular ejection with ventricular volume decrease. This exagerated example shows that when volume measurement alone is used to give a measure of average fiber length this may not be relevant to the true lengths. The volume is not accurately known, thereby further limiting the use of the volume value.

Simplifications are used to calculate left ventricular volume. One to three "diameters" of the ventricle chamber are used to derive a volume for the ventricle on the assumption that the ventricle chamber is a prolate spheroid (2). It is clear that reasonable estimates of volume are made in this fashion as is demonstrated below in the section on left ventricular shape.

The range of uncertainty of the value of the calculated volume (up to 20%) may obscure significant changes in muscle length. Small changes in muscle length may be quite significant as was indicated by Pollack (3) who shows that a 4% length increase may be equivalent to a 150% increase in extra cellular calcium ion concentration in increasing the fiber active tension. There are further reasons which make the conversion of volume, or a length measurement, to a "representative" muscle fiber length of limited value. Heterogeneity of perfusion, the presence of non-contractile tissue, and the asynchronous activation of the ventricle wall, all contribute to interaction of the "populations" of muscle fibers. At the time of onset of ventricular activation the contractile elements have differing active states and initial lengths so that ventricular contraction occurs with the contractile elements

at different phases of their active states.

In addition to the irregular shape the myocardial wall has hellically oriented fiber directions. A theoretical consideration of the need for hellically oriented fibers is provided by Sallin (4). He points out that purely circular fibers (equatorial) cannot account for high ejection fractions. Helical fibers can cause large ejection fractions. Sarcomeres rarely contract more than 20% of their length, yet ejection fractions of more than 50% are commonly seen. A 20% contraction of a circumference along the equator of a sphere produces an ejection fraction of upto 0.48 and less if an ellipsoid. The angles of the fibers at the Endocardium and Epicardium (+60° and -60°) (5) are consistent with ejection fractions of 60%. With helical fiber shortening the long axis as well as the minor was of the ventricle cavity shorten during systole.

These considerations indicate the need for detailed knowledge of the shape of the left ventricle wall in three dimensional space and at frequent time intervals. This is necessary for reasonable accurate estimates to be made of changes in regional fiber lengths. Similar reasoning is applicable to defining the requirements for estimation of regional fiber tensions.

Ventricular pressure has been used as a measure of ventricular muscle fiber tension by virtue of Laplace's law,

$$\text{Tangential Tension} = \text{pressure} \times \text{Radius}$$

so that for a given volume, tension is directly related to pressure. A changing shape without change in ventricular volume must cause changes in the radius of curvature of some regions of the ventricle which alters the tension in these regions even if intraventricular pressure were unchanged. Furthermore, the known irregular shape of the ventricle implies variation in local tension

in the ventricle wall. Laplace's law applies only to thin walled chambers. The thick muscle wall has been shown experimentally and theoretically (6,7) to have a gradient of tension through its thickness as well. Mirsky (7) developed a set of stress differential equations of equilibrium for a hypothetical thick walled prolate spheroid. Analysis indicates that maximum stresses occur at the inner layers and decrease to a minimum at the epicardial surface. This theoretical result was confirmed by Ghista (8) and Wong (9) who also showed a linear stress distribution through the wall thickness. This result cannot be predicted from Laplace's law because it does not allow for transverse normal (radial) stress and transverse shear deformation which always accompanies bending stress. The maximum stresses occur at the equator of the ellipsoid and they appear prior to the attainment of peak left ventricular pressure.

Further experimental evidence of a stress gradient within the wall may be deduced from the distribution of sarcomere lengths in the myocardium (10). Spotnitz et al. fixed hearts at a certain phase of the cardiac cycle and measured the sarcomere lengths to find them longest endocardially (2.22 u at 5 mmHg, 2.9 u at 10 mmHg) and shorter epicardially (2.17 u at 5 mmHg, 2.22 u at 10 mmHg) indicating higher tension at the endocardial level. All sarcomeres measured were on the ascending limb of the active length/tension curve although the relation of the length after fixation to the length in the beating heart is not known.

Taking these varied but interdependent factors (e.g. sequence of activation, volume, shape) into account one may question the meanings of such generalizations as $(dP/dT)_{max}$ with respect to any one segment of muscle in the ventricle wall. Wiggers (11) and Randall (12) attributed a change in $(dP/dT)_{max}$ only to the summation effect over the reduced time intervals between onsets of fibers contractions. Neither considered the possibility that a change in

sequence of contraction of the muscle fibers (even though the time spread of contraction in the fibers remains constant) could cause an additional change in $(dP/dT)_{max}$ such as the effect of left ventricular geometry and fibers' different active status on the interaction of fibers.

The length/tension relationship of individual sarcomeres must be a complex compromise between local wall shape, fiber direction, fiber nutrition and delay of activation relative to surrounding sarcomeres as well as ventricular volume and intraventricular pressure, the latter two of which are often assumed to be an acceptable index of the length and the tension being generated in the contractile elements. Measurement of a few sarcomere lengths along the ventricular "equator" in the gluteraldehyde fixed heart indicates a fairly consistent relationship between the sarcomere length and diastolic pressure (10). However the location of the samples (at the ventricular equator) would be expected to behave in this fashion whereas the more curved apical fibers would not be expected to necessarily show this relationship. In the actively contracting ventricle the stretching of the as yet not activated muscle by the already activated muscle could significantly alter the initial preactivation contractile element length. That the "prestretch" is significant in cardiac muscle was shown in papillary muscle experiments (13). Change in length before contraction can greatly alter the "inotropism" of that sarcomere relative to the state determined by the end-diastolic pressure and volume just before activation. These interactions occur within a few milliseconds once every heart cycle, so that the chance of "capturing" this distribution of the sarcomere lengths in the fixed heart wall is small. Moreover, the fixative requires a long time (relative to the activation time of the ventricle) to affect the entire ventricle wall. If 0.3 seconds is taken as an average capillary transit time, then the "wave" of fixation traverses the myocardium sufficiently

slowly to permit nonfixed myocardium to mechanically interact with the fixed myocardium. Use of the volume/pressure - length/tension analogy for the estimation of a "representative" muscle fiber function is further hampered, because unlike the isolated muscle strip preparation the ventricle does not have a phase equivalent to the isometric and isotonic states. During the isovolumic phase shape changes occur (14) so that length changes must also occur during this phase of the cardiac cycle. During ejection, even if intraventricular pressure is held constant artificially, the variation in curvature in the ventricle wall causes various muscle fibers to "see" different tensions.

It is clear that detailed knowledge of the shape of the ventricle is required if consistent estimates of ventricular volume and muscle fiber operating conditions are to be calculated. Anisotropy and heterogeneity of functional status in the myocardial wall would be expected to manifest as localized shape changes in relation to adjacent myocardial wall regions over short time intervals. Detection and quantization of these manifestations requires high spatial and temporal resolution of the ventricular shape in three dimensions.

It can be seen that until a theory is developed which includes both the effects of anisotropy and nonhomogeneity, Laplace's law will remain the basis of stress calculations even though it is known to be inappropriate. This is unfortunate because localized regions of muscle fibers with loss of contractile effectiveness (such as ventricular aneurysms or abnormal spread of electrical excitation) remain inaccessible to quantitative analysis. Such detailed data is required for meaningful diagnosis of ventricular functional status and evaluation of therapeutic interventions.

In order to reconstruct the three dimensional shape of the left ventricle the shape of both the endocardial and epicardial surfaces must be known. Clearly the epicardial surface is most readily accessible in only a few favorable situations where there is sufficient contrast of tissue radio-opacity. The use of border enhancement and recognition techniques can facilitate and extend the analysis. Nonetheless, regardless of the accessory techniques used, the quantitative data derived from ventricular roentgenograms is usually limited to silhouette outlines and degree of roentgen opacity. For both the analysis of endocardial and epicardial roentgen images the primary concern therefore is the understanding of the properties of roentgen silhouettes and roentgen opacity profiles in relation to the three dimensional bodies which generate them.

The following sections discuss work that has been done to clarify the properties of silhouettes generated by roentgen opacities in a biplane x-ray system, and a series of proposed experiments designed to apply this work to the beating ventricle observed by biplane angiography.

DYNAMIC SHAPE OF THE LEFT VENTRICLE.

High resolution orthogonal silhouettes of the left ventricle obtained at 60 exposures per second (aperture time 2 msec) using biplane roentgen videometry can be used to estimate the shape of the left ventricle in three dimensions (18). Numerical modelling and analysis of silhouettes of models of known shapes have been used to ellucidate the theoretical and practical limits of the information about the three dimensional shape of the body obtained by measurement of its silhouettes.

Analytic Considerations.

A radio opaque object of known cross section in the plane of the x-ray beams is considered to be held at the intersection of the two orthogonal x-ray beams as is shown in Figure 1. By keeping the x-ray source to object distance large relative to the object diameter the x-ray divergence can be ignored. The degree of indeterminancy of the information contained in a pair of orthogonal silhouettes can be illustrated by the fact that a cube cannot be distinguished from two orthogonally oriented square plates intersecting at their mid=points and with their respective areas equal to the cross sectional area of the cube as illustrated in Figure (I). The implication is that large volume changes, and radii of curvature changes, can occur without a concommitant change of the silhouettes. Practical experience tells us however that the left ventricular cross section is some what elliptical in shape. For this reason an elliptical cross section was subjected to analytical manipulation in order to more closely mimic the effect of positional change on the silhouette produced.

Volume Calculation and Shape Reconstruction From Silhouettes.

An ellipse with its major axis at an angle other than 90° or 0° to the x-ray beams presents a silhouette the length of whose diameters are intermediate between the lengths of the major and minor axes (Figure II).
If the diameters of these silhouettes are assumed to be the true major and minor diameters of the ellipse (as is invariably the case when Chapmans method (16) is used) then the reconstructed cross section shape will be distorted so that the calculated curvatures and the "disc" volume will be incorrect (Figure III). The variation of the calculated volume with angle of the major axis to the x-ray beam shows this to be a considerable fraction of the total volume (25% for an ellipse with the major axis two times the minor axis). This effect is also seen

SILHOUETTES. OF. CROSS. AND. SQUARE. ARE. IDENTICAL.

ROTATION. OF. SQUARE. AND. CROSS. ABOUT. OO. DOES. NOT. ELLIMINATE. AMBIGUITY. OF. THE. SHAPE. PRODUCING. THE. SILHOUETTES..

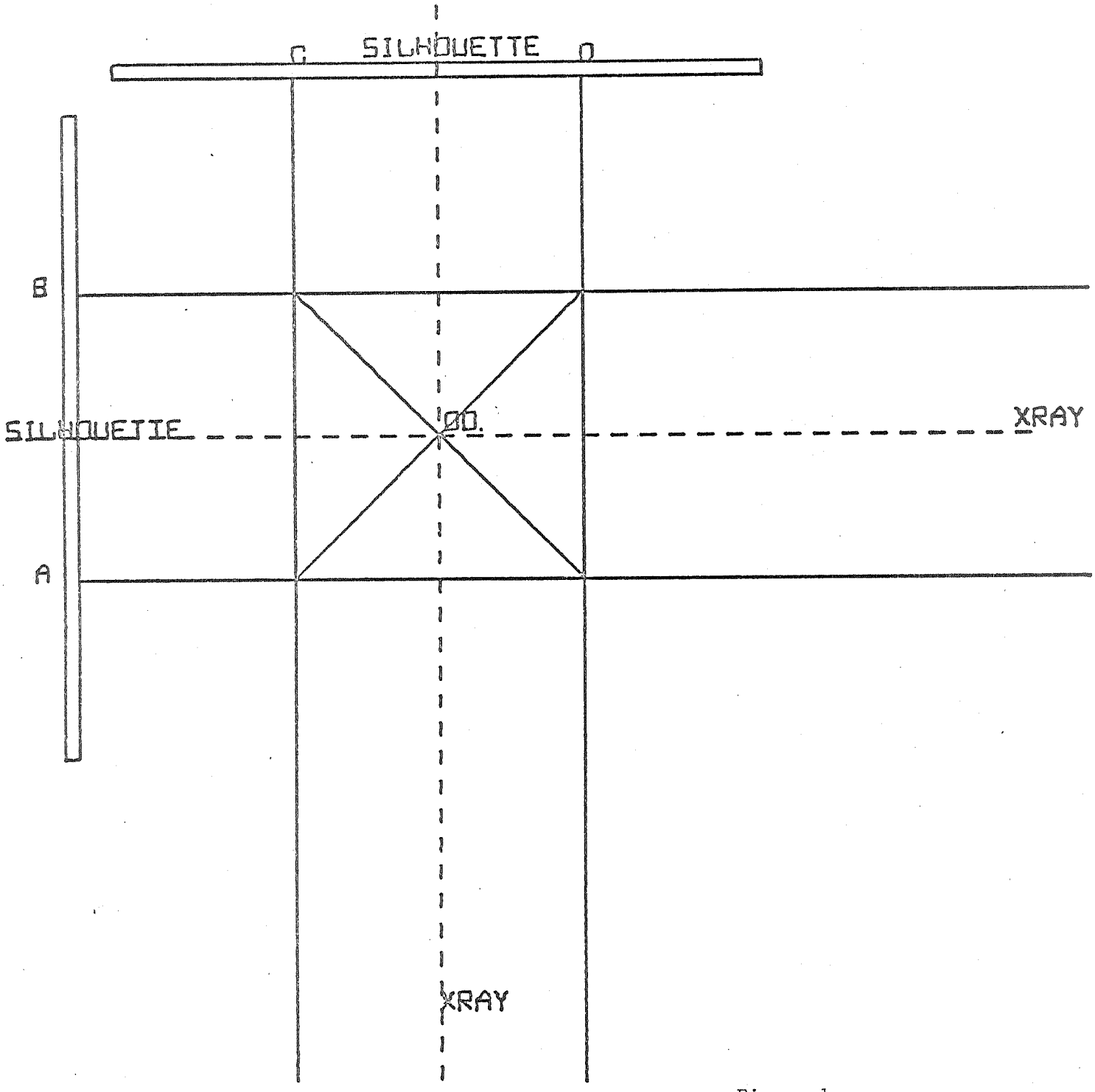

Figure 1

SILHOUETTES. PRODUCED. BY. AN. ELLIPSE.

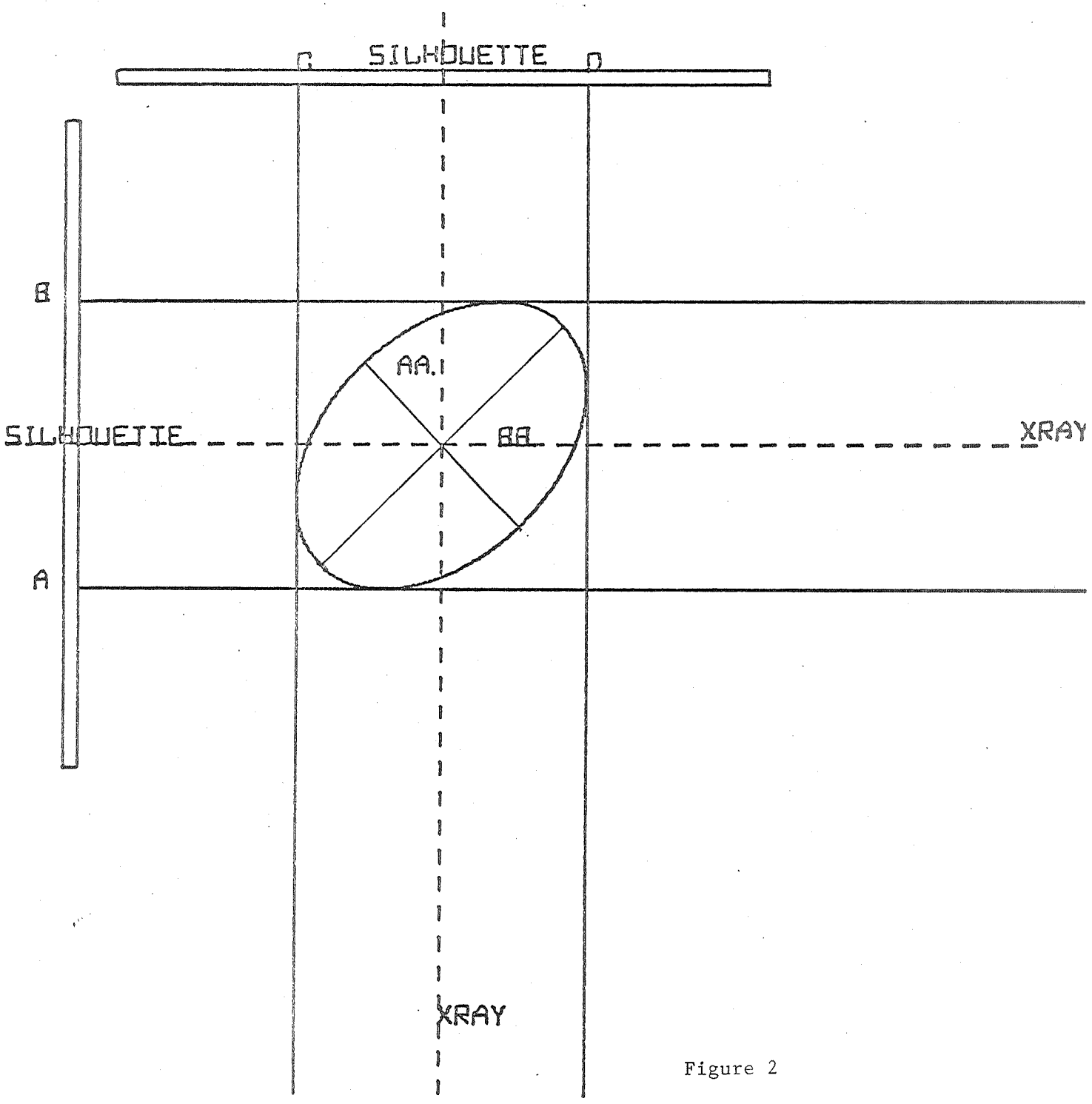

Figure 2

SILHOUETTES. AB. AND. CD. MAY. BE. PRODUCED. BY. DIFFERENT. ELLIPSES..

CONVENTIONALLY. ALWAYS. ASSUME. THE. ELLIPTICAL. DISC. TO. HAVE. ITS. MAJO
AND. MINOR. AXES. ALLIGNED. WITH. XRAY. BEAMS..

(VOLUME. OF. ORIGINAL. ELLIPSE. 6.3. CC).

(VOLUME. OF. ASSUMED. ELLIPSE. 7.3. CC).

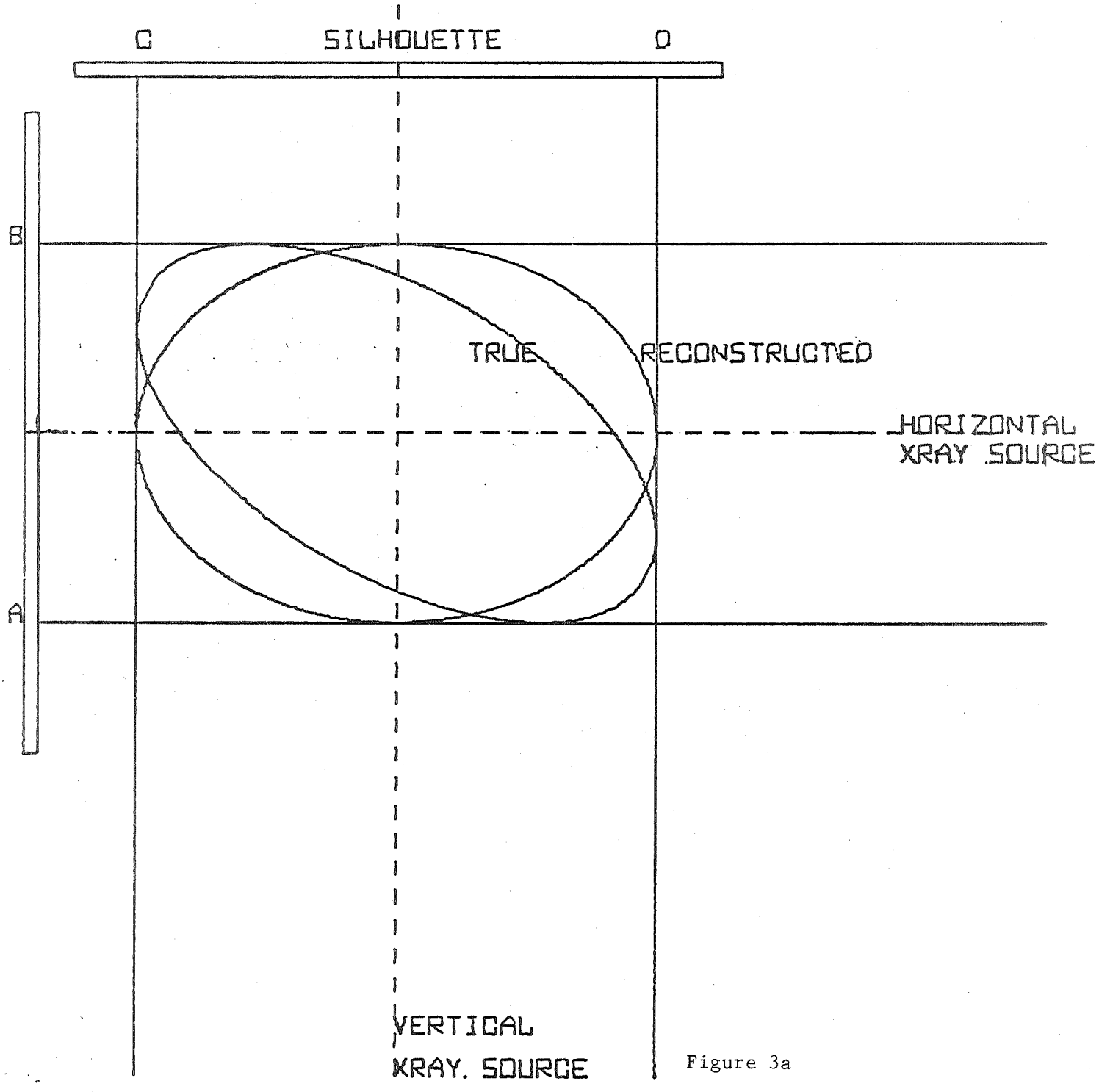

Figure 3a

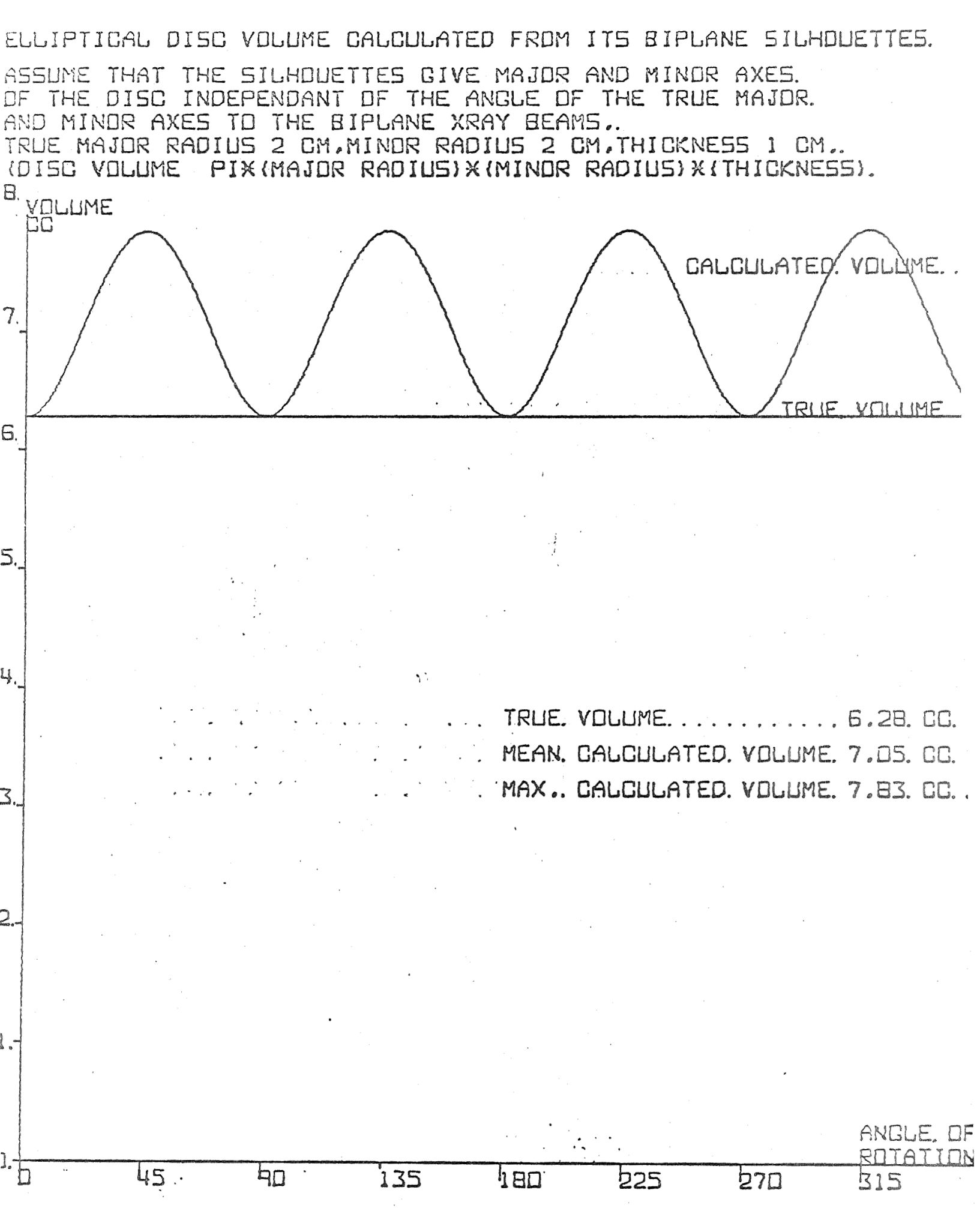
ELLIPTICAL DISC VOLUME CALCULATED FROM ITS BIPLANE SILHOUETTES.
ASSUME THAT THE SILHOUETTES GIVE MAJOR AND MINOR AXES.
OF THE DISC INDEPENDANT OF THE ANGLE OF THE TRUE MAJOR.
AND MINOR AXES TO THE BIPLANE XRAY BEAMS..
TRUE MAJOR RADIUS 2 CM.MINOR RADIUS 2 CM.THICKNESS 1 CM..
(DISC VOLUME PI*(MAJOR RADIUS)*(MINOR RADIUS)*(THICKNESS).
VOLUME
CC
8.
7.
6.
5.
4.
3.
2.
1.
CALCULATED. VOLUME. .
TRUE. VOLUME
TRUE. VOLUME. . . . . 6.28. CC.
MEAN. CALCULATED. VOLUME. 7.05. CC.
MAX.. CALCULATED. VOLUME. 7.83. CC. .
ANGLE. OF
ROTATION
0
45
90
135
180
225
270
315

Figure 3b

in the ventricle (15). A 51.5 cc silastic cast of a canine left ventricle was rotated about its aorta to apex axis and the volume calculated from the silhouettes obtained at every 3° interval as illustrated in Figure IV. For each angle the volume was calculated at each of 78 cross sections which were assumed to be elliptical in shape and whose major and minor cross axes were given by the silhouette cross sections. It is clear that a few degrees rotation of a ventricle of constant volume would result in a different volume being calculated.

In an attempt to further study the properties of silhouettes the outline of each of the 60 to 80 "disc" cross sections of the ventricle casts was reconstructed from the multiple sets of orthogonal silhouettes obtained during the rotation of the cast about its aorta to apex axis. This method is of limited value for reconstructing the cross sectional shape as is readily shown by analytical considerations which show that a cross sectional shape other than a circle cannot be reconstructed irrespective of the number of sets of orthogonal silhouettes (angles of view) obtained by 180° rotation about an axis normal to the plane of the cross section. The projections of the major and minor extremes of the "disc" "over-shadow" other adjacent regions thereby causing the outline reconstructed from multiple orthogonal silhouettes to be rounded out, somewhat like a cloverleaf (Figures V and VI).

The basis for this distortion in shape is illustrated in Figure VII. The calculated radius AA used for reconstruction of the ellipse is equal to $A\cos\theta$ which is an overestimate of the actual radius R_A. Similarly the calculated orthogonal radius BB is equal to $B\cos\theta$ which is also an overestimate of the true radius R_B for this particular set of orthogonal silhouettes. Consequently all calculated radii from respective orthogoneal silhouettes will overestimate

COMPUTER PLOT OF VOLUMES CALCULATED 60/SECOND FROM BIPLANE VIDEOROENTGENOGRAM DURING ROTATION OF 51.5ml CAST OF CANINE LEFT VENTRICULAR CAVITY AROUND ITS LONG AXIS
(Simpson's Rule Using 78 Biplane Diameters)

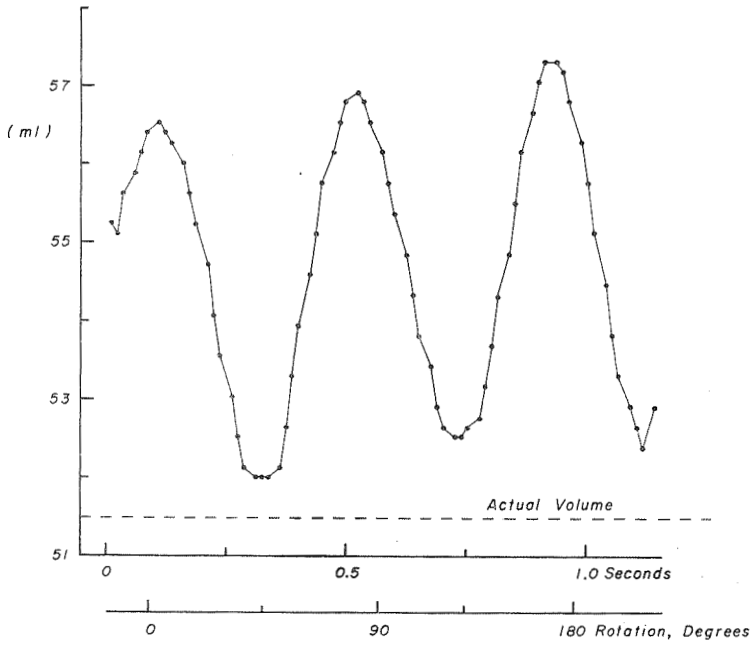

Figure 4

RECONSTRUCTION OF DISC OUTLINE FROM BIPLANE SILHOUETTES AND ANGLES.
ANGLE THETA BETWEEN INSTANTS WHEN SILHOUETTES MEASURED DURING.
ROTATION OF THE DISC ABOUT AXIS THROUGH OO..

$$\text{VOLUME} \propto \sum_{I=2}^{N} (1/2) * (R(I) * \cos(\theta)) * (R(I-1) * \cos(\theta)) * (\theta) * \text{THICKNESS}.$$

WHERE N*O 360 DEG.

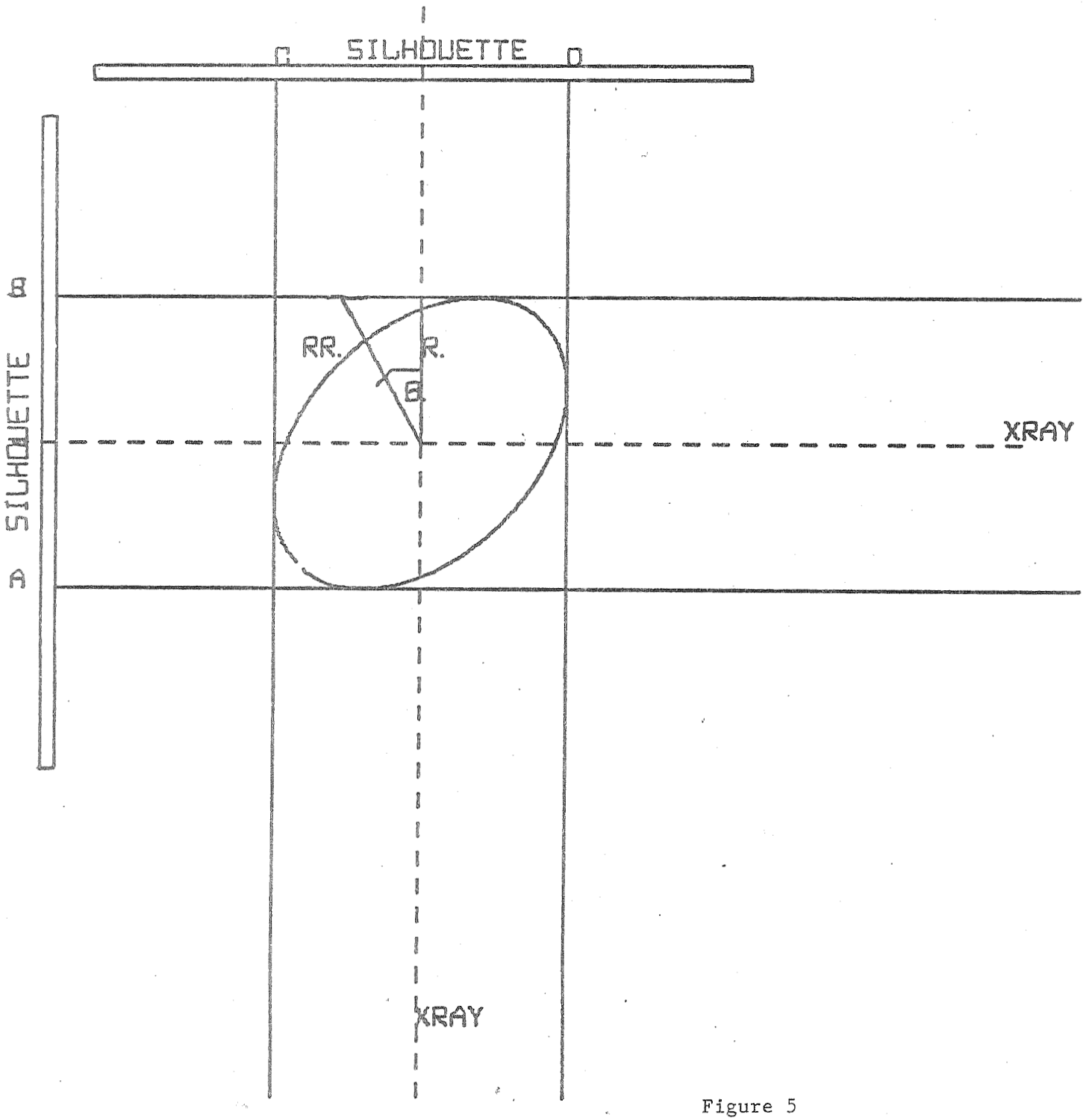

Figure 5

CLOVER-LEAF. EFFECT. IN. RECONSTRUCTION. OF. ELLIPTICAL. DISC. OUTLINE. FROM. SILHOUETTES. ONLY..

SILHOUETTES. OBTAINED. WHILE. THE. DISC. IS. ROTATED. ABOUT. AN. AXIS. THROUGH. OO,. THE. PROJECTION. OF. RADIUS. RB. (OO-BB). ONTO. THE. EXTRAPOLATED. LINE. THROUGH. RA. (OO-AA). CAUSING. THE. TRUE. RADIUS. ORTHOGONAL. TO. THE. TANGENT. TO. BE. OVERESTIMATED..

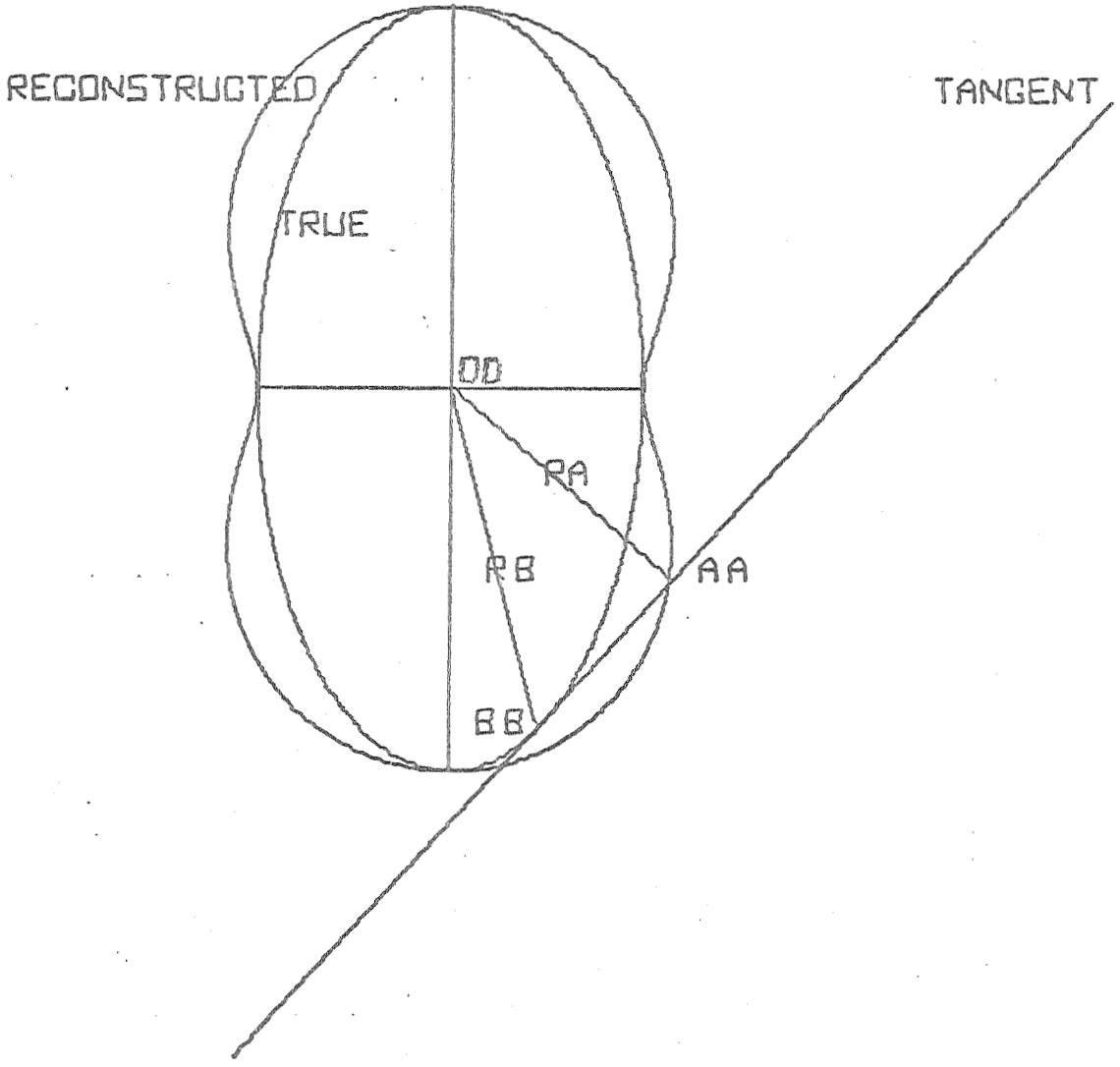

Figure 6

the actual radii except for the orthogonal pair obtained when the orientation of major and minor axes of the transradiated ellipse coincide with the central axes of the orthogonal x-ray beams. The magnitude of the errors in the reconstructed shape of the elliptical cross section is proportional to the eccentricity of the ellipse. When an ellipse is reconstructed from its silhouettes obtained during rotation about its axis the bulging effect in the regions between its maximal dimension is obvious.

Clearly there will be an overestimate of volume and incorrect curvature calculated. The left ventricle cross section is irregular so that this effect cannot be detected apriori from the reconstructed silhouette as shown in Figure VII. The dye filled ventricle chamber is distinguishable from the background only if a certain depth of dye (at a given concentration) is present. Consequently recognition of the ventricle border is dependent on the shape of the ventricle at the edge producing the silhouette. This effect is readily mimicked analytically (Figure VIII). The calculated volume is less than if the true edge is observed, but the variation with angular position is not significantly less (Figure IX).

The shape of the left ventricle is complex and probably differs from heart to heart and even from beat to beat. The above considerations clearly indicate that the biplane silhouettes, even when a large number are obtained by using multiple angles of view, do not contain enough information to fully describe true three dimensional shape of the ventricle. The ventricle is somewhat egg shaped and reasonable approximations to ventricular volume and shape have been devised (Figure X). A simple approximation requires only the silhouette area and the long axis length (2). This method is applicable to

CROSS. SECTION. OF. A. SILASTIC. CAST. OF. A. CANINE. LEFT. VENTRICLE. RECONSTRUCTED. FROM. 20. SETS. OF. BIPLANE. SILHOUETTES. OBTAINED. DURING. ROTATION. OF. THE. INTACT. CAST. ABOUT. ITS. LONG. AXIS.

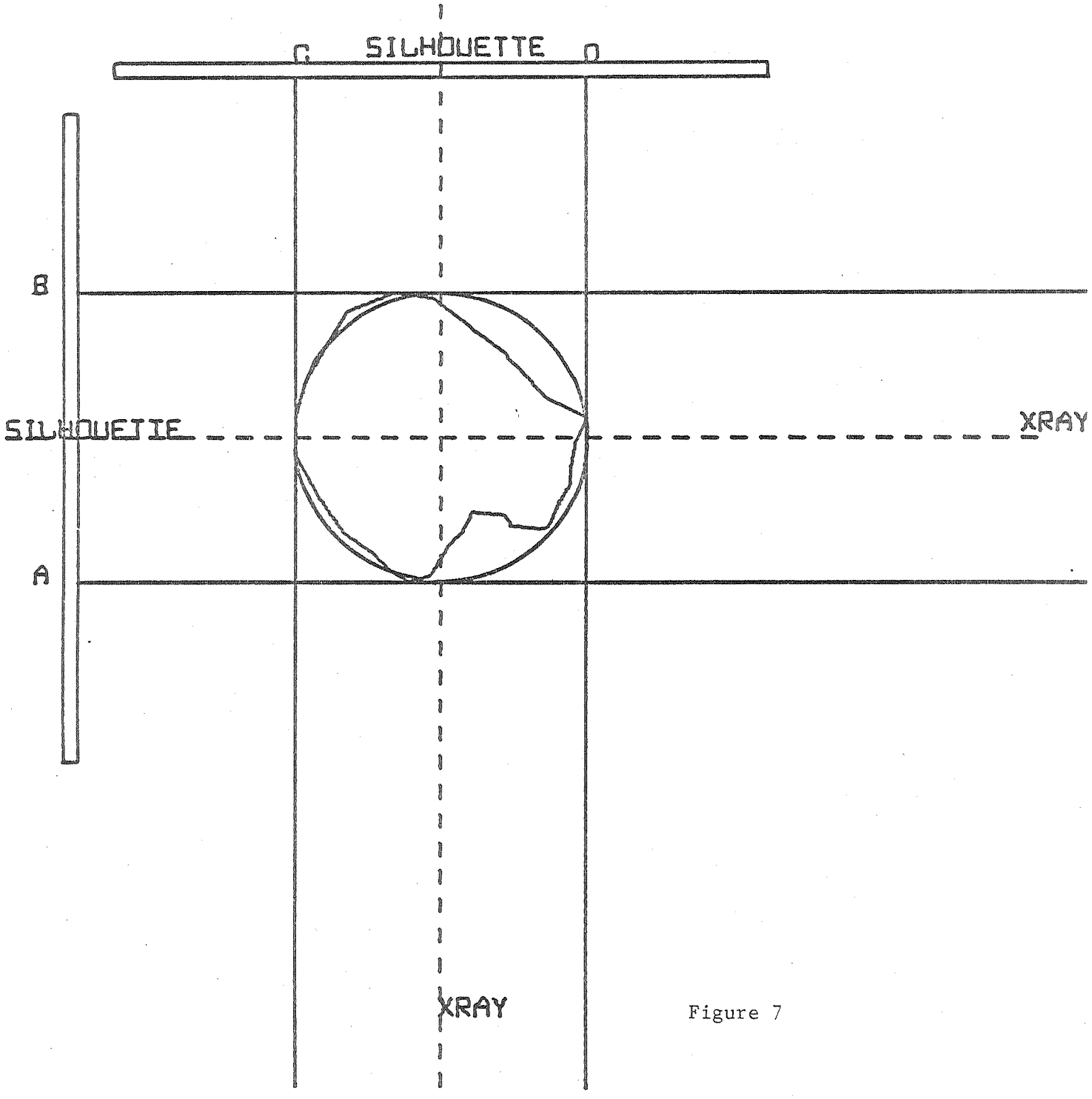

Figure 7

SILHOUETTES. AB. AND. CD. PRODUCED. BY. A. RADIOLUCENT. ELLIPTICAL. DISC. IN. BIPLANE. XRAY. BEAMS..

(MINIMUM. DEPTH. OF. DYE. THAT. MUST. BE. PENETRATED. IS. 1/4. OF. MINOR. DIAMETER).

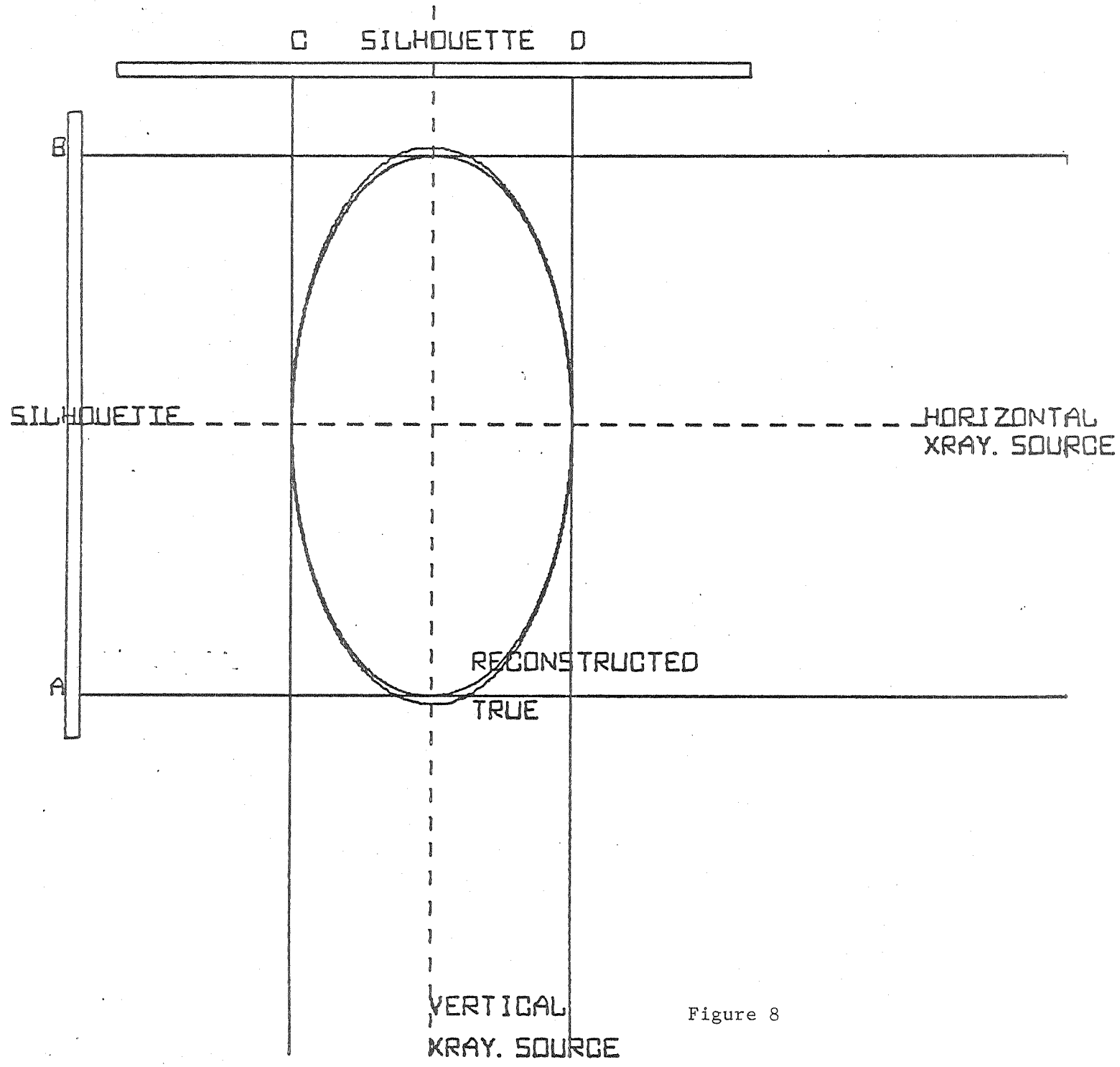

Figure 8

ELLIPTICAL DISC VOLUME CALCULATED FROM ITS BIPLANE SILHOUETTES.

ASSUME THAT THE SILHOUETTES GIVE MAJOR AND MINOR AXES.
OF THE DISC INDEPENDANT OF THE ANGLE OF THE TRUE MAJOR.
AND MINOR AXES TO THE BIPLANE XRAY BEAMS..
TRUE MAJOR RADIUS 2 CM, MINOR RADIUS 2 CM, THICKNESS 1 CM..
(DISC VOLUME = PI*(MAJOR RADIUS)*(MINOR RADIUS)*(THICKNESS).

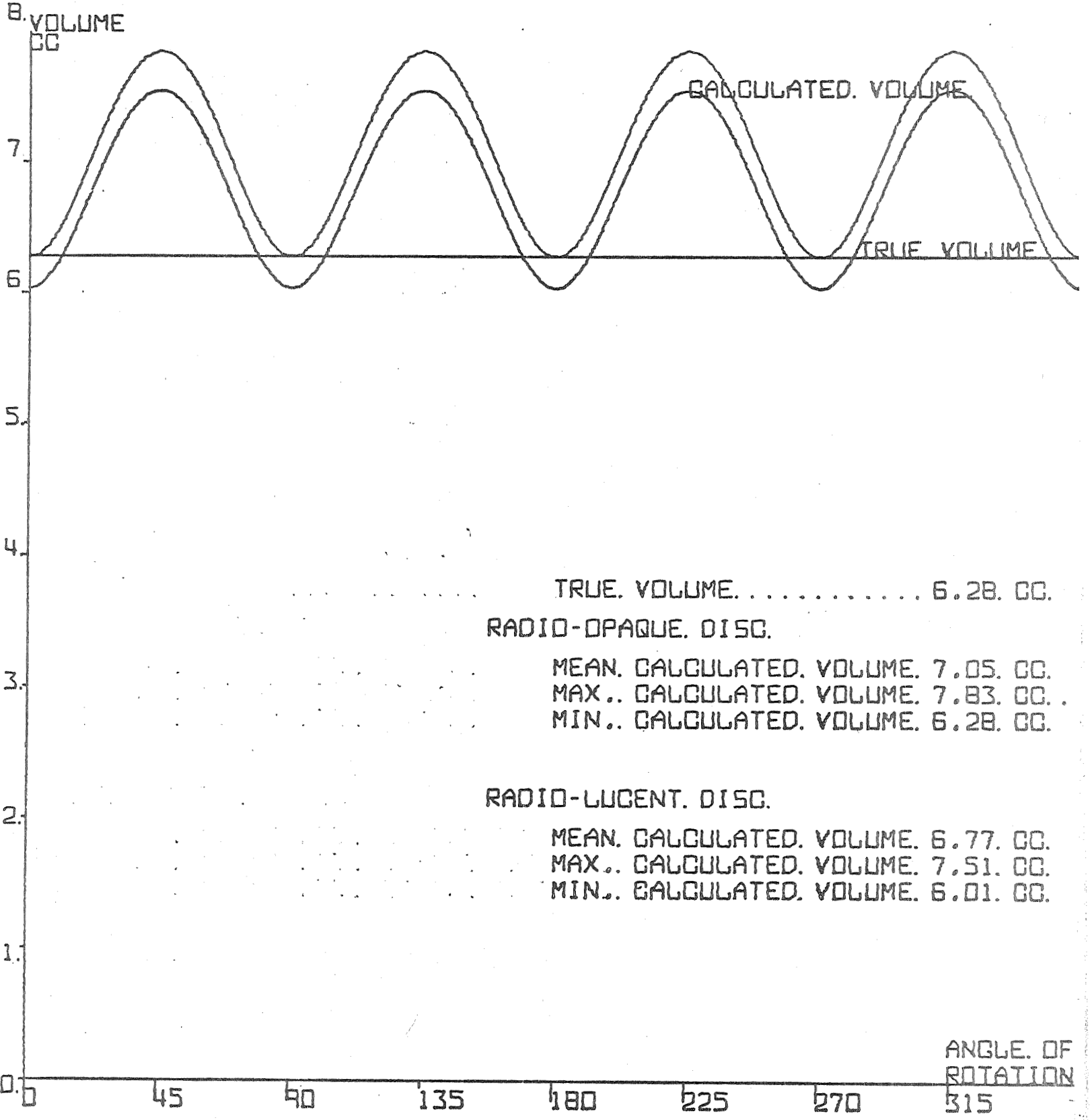

TRUE. VOLUME. . . . . 6.28. CC.

RADIO-OPAQUE. DISC.

MEAN. CALCULATED. VOLUME. 7.05. CC.
MAX.. CALCULATED. VOLUME. 7.83. CC..
MIN.. CALCULATED. VOLUME. 6.28. CC.

RADIO-LUCENT. DISC.

MEAN. CALCULATED. VOLUME. 6.77. CC.
MAX.. CALCULATED. VOLUME. 7.51. CC.
MIN.. CALCULATED. VOLUME. 6.01. CC.

Figure 9

THREE METHODS OF CALCULATING LEFT-VENTRICULAR VOLUME. ASSUME ELLIPTICAL SHAPE OF THE VENTRICULAR CAVITY.

$VOL = \pi \times L \times D1. \times D_{1.} / 6.$

$VOL = \pi \times L \times D_{1.} \times D_{2.} / 6.$

$D_{1.} = 4 \times A_{1.} / (\pi L).$

$D_{2.} = 4 \times A_{2.} / (\pi L).$

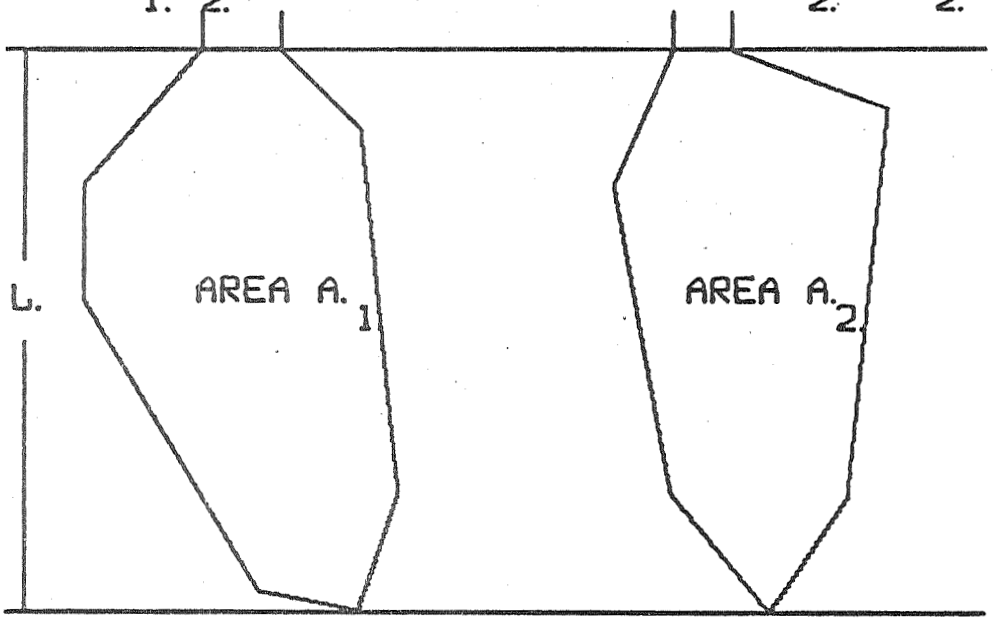

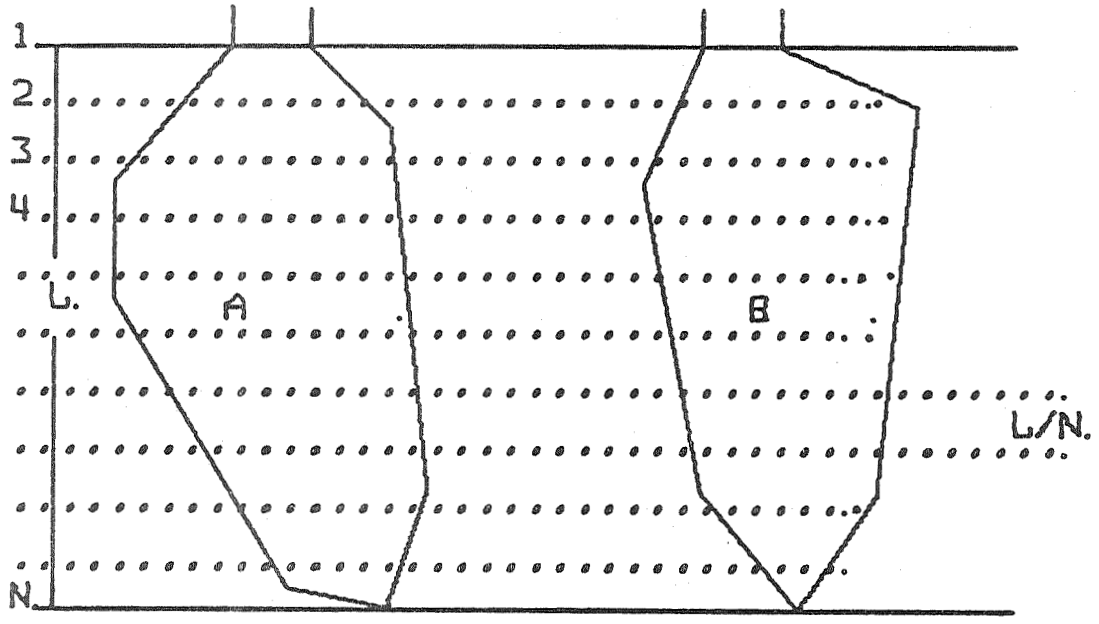

$$VOL = \sum_{J=1.}^{N.} \pi \times (A/2) \times (B/2) \times (L/N).$$

Figure 10

CORRELATION CALCULATED VENTRICULAR VOLUMES
ASSUMING DIFFERENT SHAPES OF CAVITY

(Simultaneous 60/second Values from Biplane Videoroentgenogram During Rotation of 51.5 ml Cast of Canine Left Ventricular Cavity Around Long Axis)

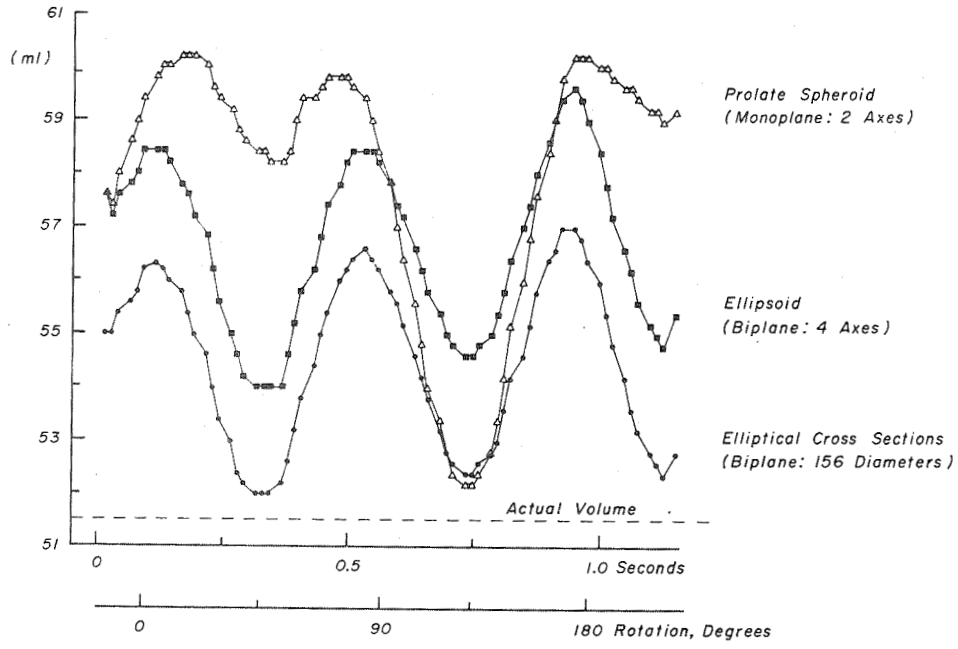

Figure 11

biplane and monoplane silhouettes. The approximation based on the assumption that the left ventricle cavity can be divided into a large number of elliptical discs although inherently in error is less so than monoplane area-length method (16). Figure XI shows the calculated values of volumes from the same silhouettes according to three different methods (15). Similar data was obtained for five different casts of canine left ventricles. All show that the monoplane method results in the greatest range of error (about 17% of true volume) whereas the two biplane methods show about equal variation at about 8 to 9% of true volume. It is concluded that accurate determinations of the shape of the ventricle cannot be obtained from measurements of the dimensions of multiple orthogonal pairs of its silhouettes. Despite these limitations for determinations of shape, measurements from multiple silhouettes provide reasonable accurate measurements of the volume of casts of the left ventricular cavity as shown in Table 1.

TABLE 1

CAST	TRUE VOLUME*	PAPILLARY MSL VOLUME	CALCULATED VOLUME
End diastole	51.7	1.4	56.2 ml
Mid systole	35.5	1.7	37.1
End systole	19.9	1.4	21.3

* (True volume determined by displacement of mercury).

The calculated volumes are independent of angle of observation provided at least 10 pairs of orthogonal silhouettes are used. However two pairs of orthogonal silhouettes obtained with the respective position of the orthogonal roentgen video system differing by 45° provide a calculated volume which is virtually independent of the angle of observation in respect to the axis of rotation of the cast under study as illustrated in Figure XII.

INCREASED NUMBER OF ORTHOGONAL VIDEO ROENTGEN SILHOUETTES.
OF LEFT VENTRICLE CAST REDUCES VARIABILITY OF CALCULATED VOLUMES.
(EQUI-ANGULAR SEPERATION OF MULTIPLE VIEWS FOR EACH VO

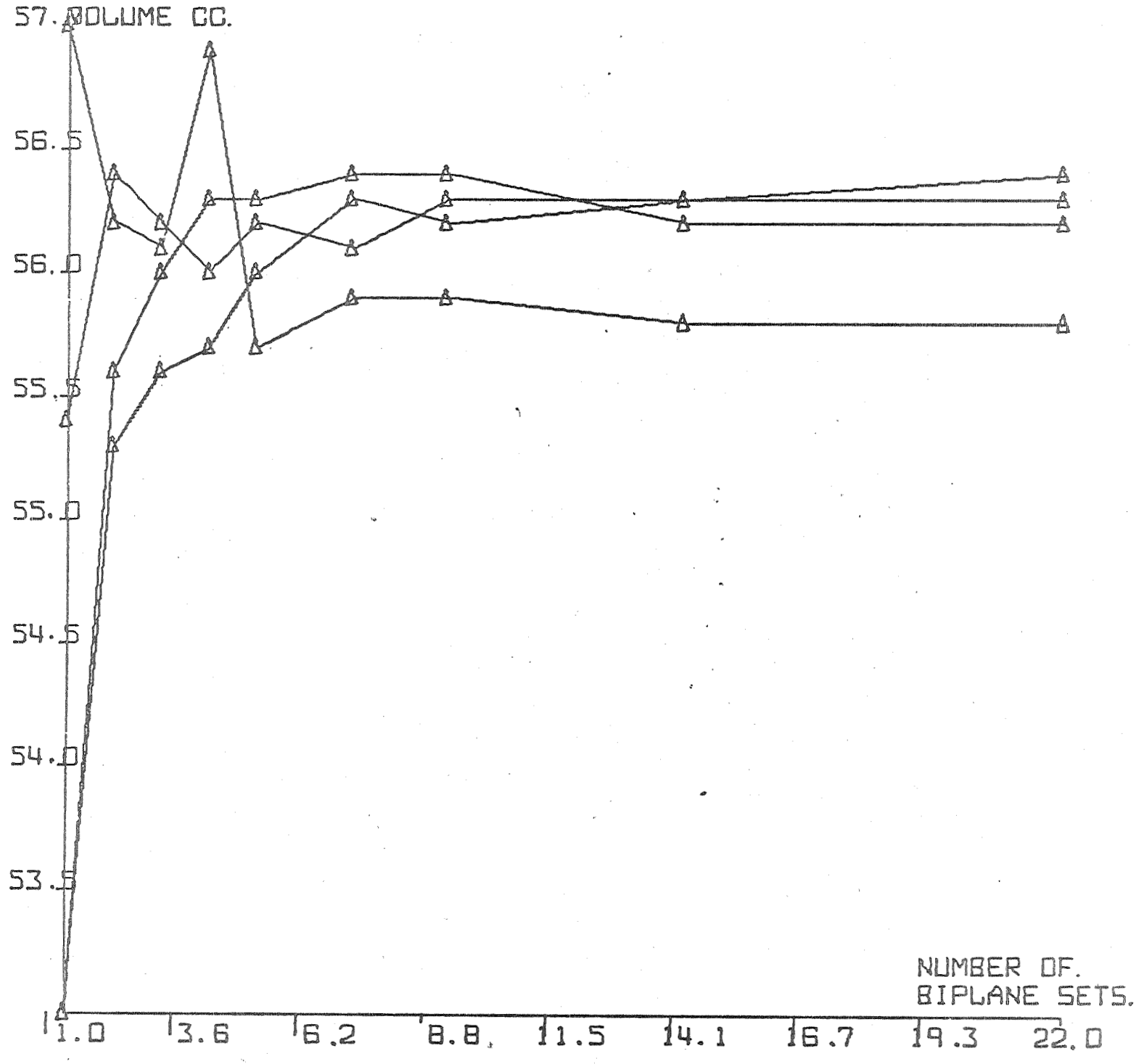

Figure 12

The variation in the calculated value for the volume of a 51.5 ml ventricular cast was about 1 cc when two pair of orthogonal views was used, as against 4 cc when only one orthogonal pair was used. The same pattern was observed in video roentgenographic measurements of other casts made at different phases of the cardiac cycle. Considerable angle dependent variation in calculated volume values of one very small irregularly shaped cast (made at end systole) was obtained when less than 8 pairs of orthogonal silhouettes were used.

angle between was decreased
If the/two pairs of orthogonal silhouettes/when the positions of the respective biplane roentgen systems differed by less than 45° then an increase of angle dependent variation in calculated volume resulted as shown in Figure XIII.

Several important conclusions can be drawn from these data. The calculated values for the volumes of cross section of the left ventricle behave in a predictable fashion provided its dimensions at 8 points around its circumference are known.

(2). The true shape of cross sections of the ventricle cannot be obtained from measurements of the dimension of ventricular silhouettes. It is possible however that the assumption of an elliptical shape of ventricle cross sections may be acceptable if in addition it is assumed that the angular orientation of the major and minor axes of successive cross sections varies along the long axes of the chamber as illustrated in Figure XIV. This differs from the traditional assumption (16) that the major and minor axes alligned with the biplane x-ray beams. For this assumption to be of value in relation to estimations of volumes and approximate shape from orthogonal shapes it is necessary that technics be developed for measurement of the true major and minor axes and the angular orientation of the major axis of each elliptical cross

EFFECT OF ANGLE BETWEEN TWO ORTHOGONAL ROENTGEN BIPLANE. PROJECTIONS ON THE VOLUME CALCULATED FOR LEFT VENTRICLE CAST.. CASTS HELD AT INTERSECTION OF THE BIPLANE BEAMS.

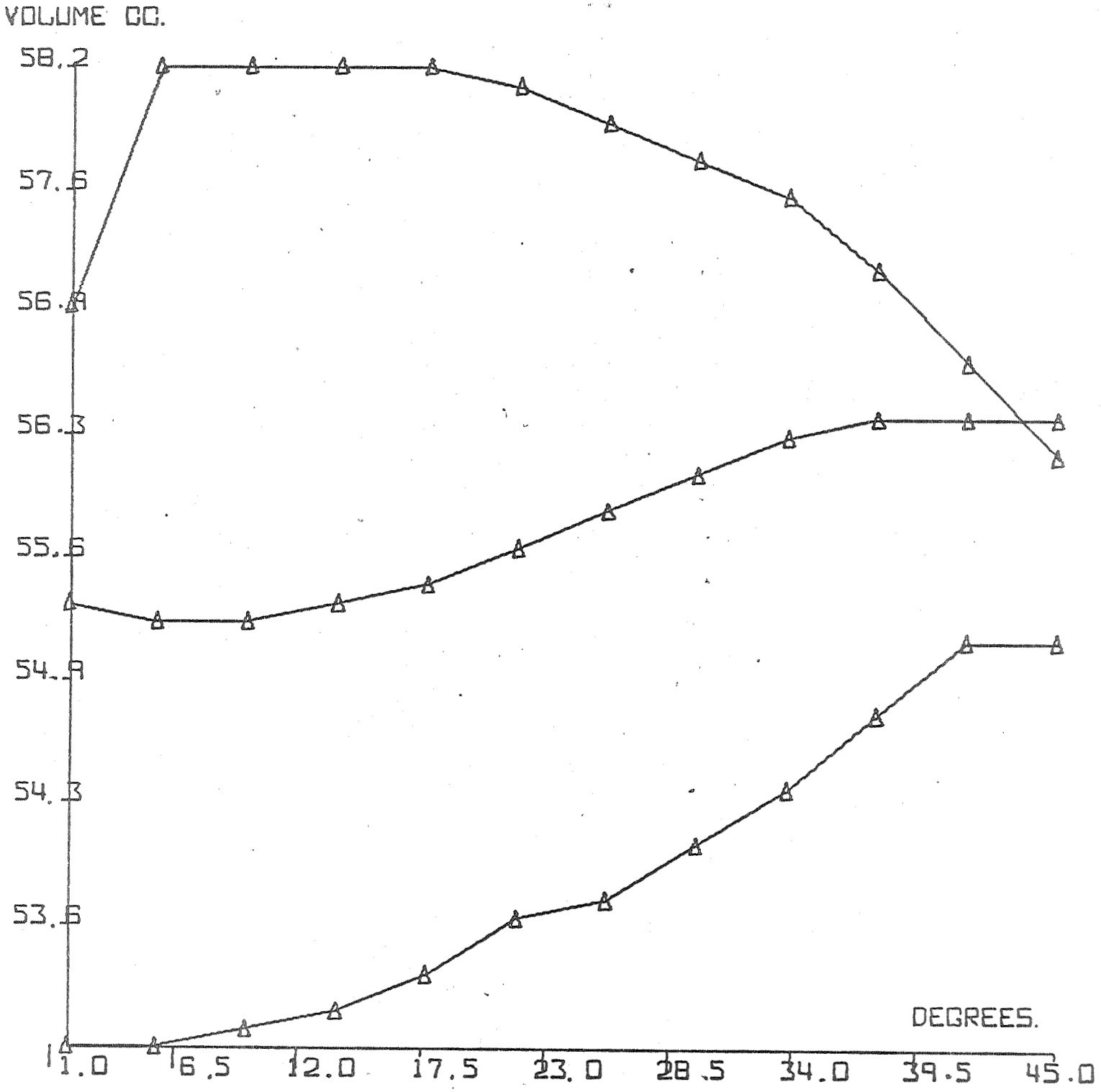

Figure 13

RECONSTRUCTION. OF. LEFT. VENTRICLE. FROM. BIPLANE. SILHOUETTES.
APPLICATION. OF. TRADITIONAL. AND. IMPROVED. ASSUMPTIONS.

TRADITIONAL. RECONSTRUCTION.

(MAJOR. AND. MINOR. AXES. ALIGNED. WITH. XRAY. BEAMS)

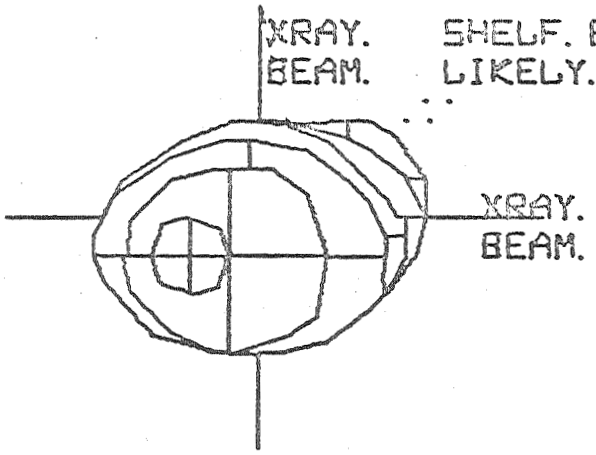

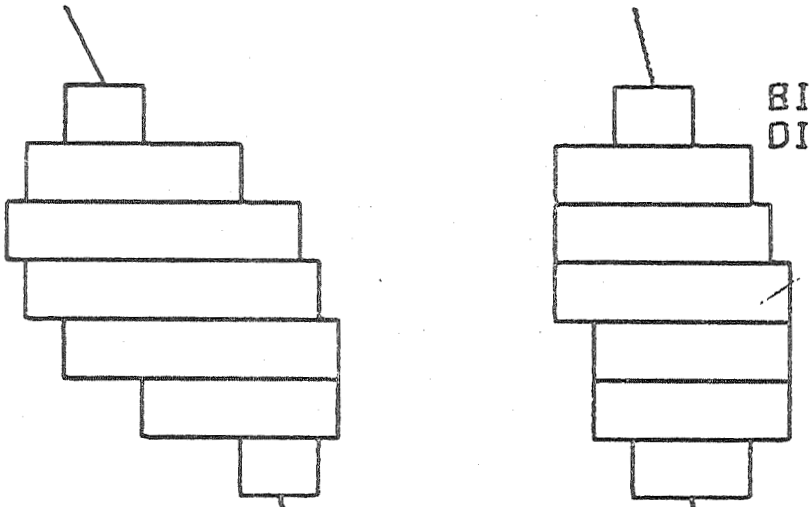

IMPROVED. RECONSTRUCTIONAXES. AT. ANGLES. TO. XRAY. BEAMS).

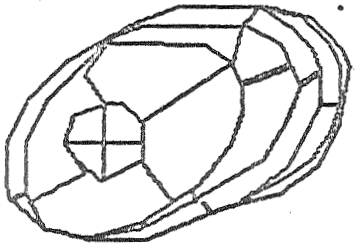

Figure 14

section about the long axis of the ventricle. It is impossible to calculate this angle from the silhouette data alone, but if the orthogonal roentgen opacity profiles of each cross section of the ventricle is measured this can be accomplished. This is illustrated for a truly elliptically shaped cross section in figure XV. It is assumed that the roentgen opacity of the cross section is uniform over its full width and depth and that the opacity can be expressed in roentgen density units. The dimension of a transirradiated cross section in a direction perpendicular to its surface is directly proportional to its roentgen density at this point in its roentgen silhouette. Therefore the orthogonal roentgen density profiles of a cross section are a direct function of the depths (dimensions) of the cross section at points perpendicular to each point on the respective orthogonal profiles. If the cross section is truly elliptical in shape and is of uniform roentgen opacity its orthogonal density profiles will be parabolic as illustrated in Figure XV.

The problem of determining the true shape and dimensions of such a cross section falls into the general problem of determination of binary patterns from their orthogonal projections which has been considered in relation to computer technology (17). The solution proposed are applicable to radio density profiles are applicable to cross sections of the ventricle if the concentration of the contrast medium is uniform across the cross section. Ambiguous shapes which cannot be determined from density profiles are possible but the added restriction that the cross section must be ellipse like in outline greatly reduces the ambiguity. The further restriction that contiguous cross sections must match reasonably closely further reduces ambiguity.

BIPLANE\ DEPTH. PROFILE\ OF. AN. ELLIPTICAL. DISC.

ORTHOGONAL. DEPTH. PROFILES. PERMIT. CALCULATION. OF. THETA,. THE. ANGLE. BETWEEN. THE. XRAY. BEAM. AND. THE. MAJOR. AXIS. OF. ELLIPSE..

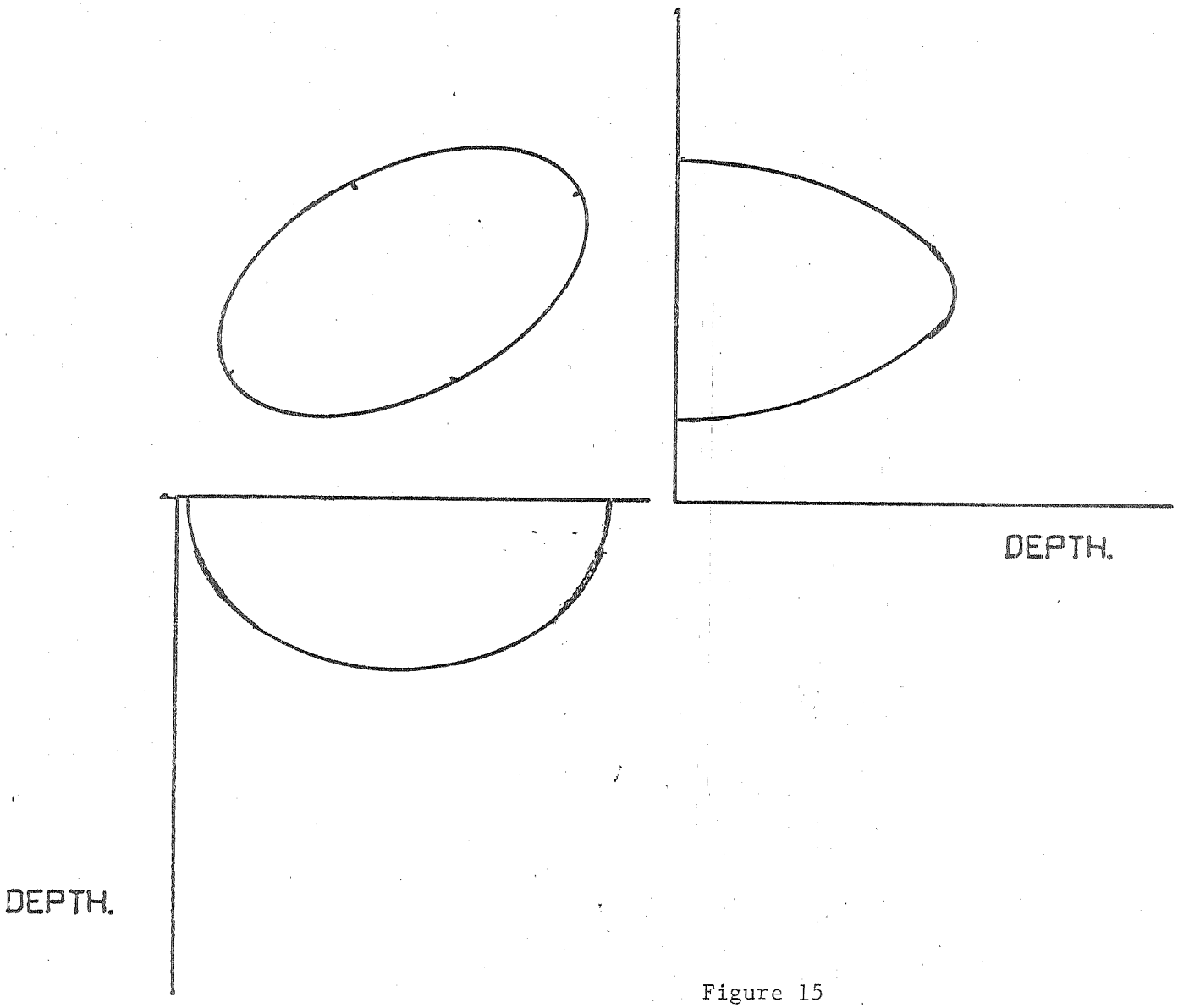

Figure 15

An important consequence of the knowledge of the radio density profiles is that these represent encoded versions of the original cross section. This represents a considerable data compression. An "n" by "n" binary pattern needs up to n^2 bits of storage while its horizontal and vertical projections together need only up to $2n\log_2 n$ bits of storage.

Analysis of ventricular three dimensional shapes may well utilize these profiles at great saving of computing time and computer memory, limiting use of the true three dimensional shape to those of display purposes only.

If the true cross sectional shape of the ventricle can be calculated using the roentgen density profile method outlined above the true curvature at any one point on the circumferences and the volumes of successive cross sections can be calculated. That cross sections of ventricular casts do present paraboloid depth profile has been demonstrated by testing the goodness of fit of a least squares fit parabola to each of some 70 cross sections in three silastic casts of ventricular chambers studied in this laboratory. The depth profile in each case was calculated from the reconstructed shape of the approximately 0.7 mm thick cross section as shown in Figure XVI. In the region of the papillary muscles there were obvious deviations from the parabolic profile but on the whole the fit was good. This hypothesis was further tested by plotting the ventricle chamber depth obtained from a left ventricular angiogram. This was performed by digitizing the gray level value of the angiogram to 64 levels (performed by Salt Lake City and JPL groups) at about 260 points across the angiogram for each of about 270 scan lines. The results demonstrate clearly that the Log transform values fall close to a parabolic distribution.

ORTHOGONAL DEPTH PROFILE OF A LEFT VENTRICULAR CAST CROSS-SECTION.

THESE DATA GREATLY REDUCE THE AMBIGUITY OF THE SHAPE PRODUCING THE SILHOUETTES.

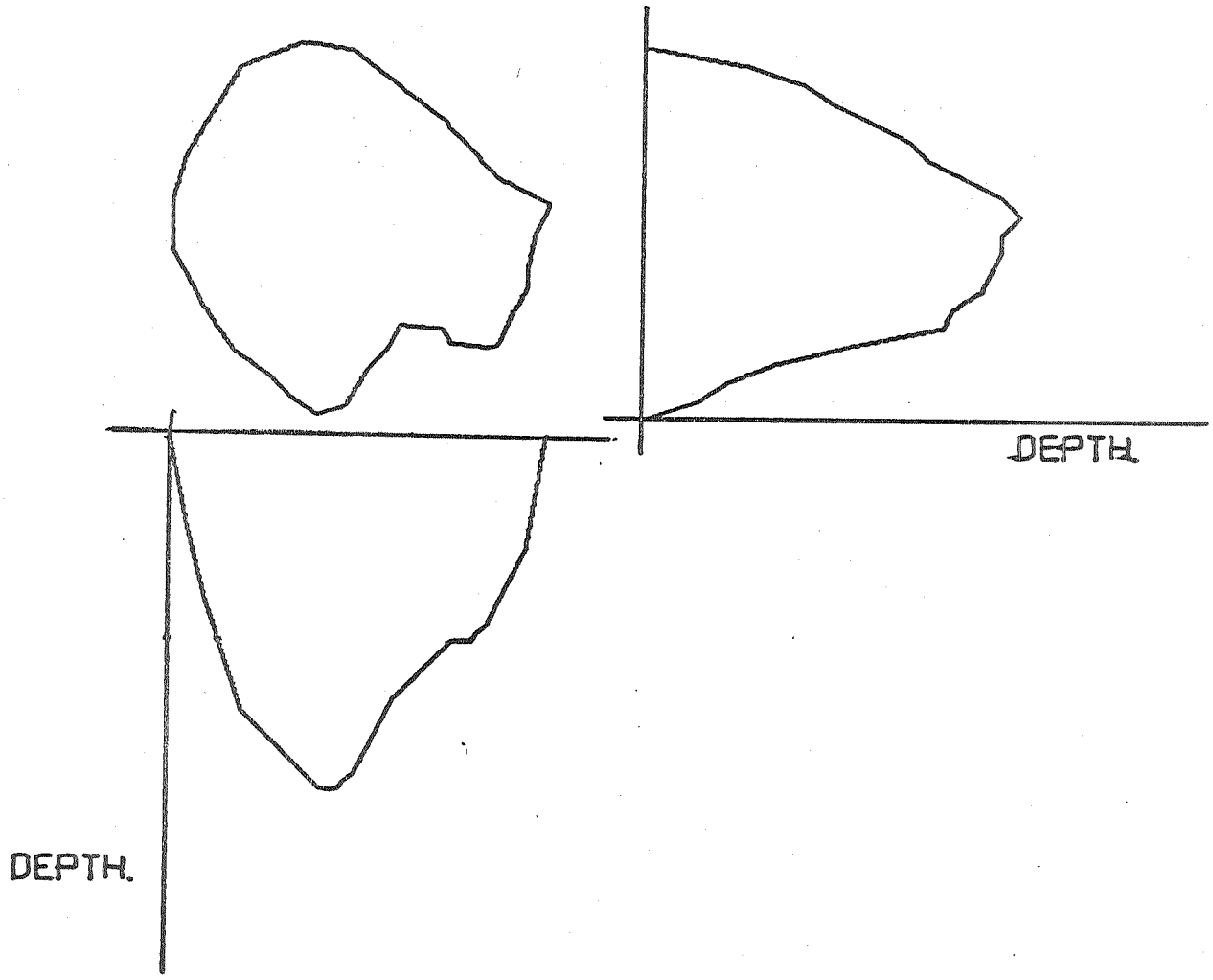

Figure 16

The biplane roentgen videometry systems developed in this laboratory provide sixty per second simultaneous measurements of the positions of the borders of orthogonal silhouettes of the ventricular chamber as well as the variations in roentgen density over the entire surface of both silhouettes. With the incorporation into the system of a TRW 20 megahertz analog-to-digital converter being supplied to the laboratory by the Avionics Lab of the Air Force high resolution orthogonal roentgen density grams can be fed into the CDC 3500 system. This system will give about six to twelve hundred roentgen density values for each horizontal line before and after injection of contrast medium. Very accurate spatial point to point subtraction of these digital values from video images recorded in identical phases of cardiac cycles before and after injection of contrast medium will provide point to point roentgen density values of the left ventricular cavity proper which cover the entire orthogonal surfaces of each orthogonal silhouette of the ventricle. For use with inaminate ventricular casts and isolated ventricle experiments there will be no problems due to nonuniform mixing in the ventricular chamber. In the intact animal the roentgen opacity profiles will be meaningful, however only if uniform cross sectional mixing the contrast media in the ventricle is achieved however uniform mixing along the longitudinal axis of the chamber is not required.

The capability provided by this system for simultaneous automated border and roentgen density measurements of orthogonal silhouettes of the ventricle will provide measurements of regional shape and volume of the ventricular cavity with far more certainty than heretofore. With this capacity for a greatly improved data base a series of experiments is proposed to further test and develop these techniques. Inanimate solid objects of known shape will be used to test this system and also to calibrate it for use on intact beating ventricles.

REFERENCES

1. Bove, A. A., Ziskin, M. C., Freeman, E., Giminez, J. L. and Lynch, P. R.: Selection of optimum Cineradiographic frame rate. Relation to accuracy of cardiac measurements. Investigative Radiology. Vol. 5 No. 5 (Sept.-Oct.) 1970.

2. Davila, J. C. and Sanmarco, M. E.: An analysis of the fit of mathematical models applicable to the measurement of left ventricular volume. Amer. J. Cardiol. 18:31, 1966.

3. Pollack, G. M.: Maximum velocity as an index of contractility in cardiac. Circ. Res. 26 (Jan.) 1970.

4. Sallin, E.: Fiber orientation and ejection fraction in the human left ventricle. Biophysics Journal. 9:954-64 (July) 1969.

5. Streeter, D. D. and Bassett, D. L.: An engineering analysis of myocardial fiber orientation in pigs left ventricle in systole. Anat. Rec. 155:503-512, 1966.

6. Baird, R. J., Markelow, R. T., Shake, P. A. and Amble, F. M.: Intra-myocardial pressure - a study of its regional variation and its relationship to intraventricular pressure. J. Thorac. Cardiovasc. Surg. 59:810-23 (June) 1970.

7. Mirsky, T.: Left ventricular stresses in the intact human heart. Biophysical Journal. 9:189, 1969.

8. Ghista, D. N. and Sandler, H.: An analytical model for the shape and the forces in the left ventricle. NASA Amer. Research. 1967.

9. Wong, A. Y. K. and Rasbahaym, P. M.: Stress distribution within the left ventricle wall approximated by a thick ellipsoidal shell. American Heart J. 15:649, 1968.

10. Spotnitz, H. M., Sonnenblick, E. H. and Spiro, D.: Relation of ultrastructure to function in the intact heart. Sarcomere structure relative to pressure-volume curves of intact left ventricles of dog and cat. Circ. Research. 18:49, 1966.

11. Wiggers, C. J.: The interpretation of the intraventricular pressure curve on the basis of rapidly surmated fractional contractions. Amer. J. Physiol. 80:1, 1927.

12. Randall, W. C., Wecksler, J. S., Pace, J. B. and Szentovarzi, M.: Alterations in myocardial contractility during stimulation of the cardiac nerves. Amer. J. Physiol. 214(5):1205-1212, 1968.

13. Tyberg, J. V., Parmley, W. W. and Sonnenblick, E. M.: In vitro studies of myocardial asynchrony and regional hypoxia. Circ. Res. Vol. XXV (Nov.) 1969.

14. Hawthorne, E. W.: Dynamic geometry of the left ventricle. Am. J. of Cardiol. 18:506-573, 1966.

15. Ritman, E. L., Sturm, R. E. and Wood, E. H.: Comparison of volume of canine left ventricular casts and angiograms using biplane and monoplane roentgen vidometry. The Physiologists. 13:294 (August) 1970 (Abstract).

16. Chapman, C. B., Baker, O., Reynolds, J. and Bonte, F. J.: Use of biplane cinefluorography for measurement of ventricular volume. Circulation. 18:1105, 1958.

17. The Reconstruction of Binary Patterns from their Projections. Shi-Kno Chang. Vol. 14, Number 1 Jan. 1971. Communications of the ACM.

18. Spivak, P. L., E. Ritman, B. Gilbert, and E. H. Wood: The problem of determination of the shape and dimension of homogeneous orbjects from roentgenographic data with particular reference to angiocardiography. Section II, Addendum Progress Report, NIH Grant HE04664, 1971, pp 1-7.

Section II

The Problem of Determination of the Shape and Dimension of Homogeneous Objects from Roentgenographic Data with Particular Reference to Angiocardiography

Patricia L. Spivak, Erik Ritman, Barry Gilbert, and Earl H. Wood
Department of Physiology, Mayo Graduate School of Medicine,
Rochester, Minnesota

Present methods of calculating the volume and dimensions of the left ventricular cavity by means of left ventricular angiography all presuppose some form of elliptical shape for this chamber. The data used for these calculations are obtained from one or at most two angiographic silhouettes of this chamber. However, it can be readily demonstrated that the relatively simple problem of reconstructing the shape of an elliptical disc (similar to a cross section of the left ventricle) cannot be solved from projections (silhouettes) of this disc recorded in planes perpendicular to the surface, no matter how many angles of view are used.

It follows that the actual shape and dimensions of the left ventricle cannot be determined by conventional multiple plane angiography no matter how many silhouettes obtained from an infinite number of views around the long axis of the ventricle are used, and the number of cross sectional dimensions of the resulting infinite number of multiple silhouettes of this chamber which are measured.

If uniform cross sectional mixing of roentgen contrast medium in the left ventricle can be achieved, the inability to measure the shape of the left ventricular cavity or its cross sections from angiographic silhouettes of this chamber can be overcome; if point to point variations in roentgen opacity across single orthogonal projections of successive cross sections, extending from the base to the apex of the chamber can be measured. Measurements of this type are possible by means of roentgen videometric and computer analysis techniques being developed in this laboratory (1,2). Digitization of the image from our biplane roentgen video system yields the orthogonal roentgen densities at, for example, 100 discrete intervals covering a particular cross section of the ventricle traversed by the corresponding horizontal television line; the thickness of each cross section is determined by the length of the two ventricular silhouettes covered by

this particular television line. For example, if 80 television scan lines cross the silhouette of the ventricle from apex to base, the thickness of each cross section to be considered is 1/80 of the ventricular length. The question posed in these studies is, how can the shape of each cross section be determined from the biplane density data?

If the roentgen density of the cross section is uniform over its full area, and the density of extraneous structures superposed in its orthogonal projections is corrected for by subtraction in the exact spatial array of the matrix of density values obtained prior to opacification of the cross section with contrast medium, then the roentgen density matrix of the cross section proper can be considered as a binary array: i.e. contrast medium present = 1, contrast medium absent = 0. The digitized value from any point on the television scan line crossing the ventricle represents the thickness of the ventricle at that point, in the direction perpendicular to the plane of view of the image. Stated another way, the digitized value represents the number of squares of unit size needed to span the thickness of the ventricle at any point (Figure 1). A given ventricular cross section can be represented by two orthogonal vectors whose elements are the projections of ventricular thickness at the respective points.

Recreating the exact shape of the ventricular cross section given only the sum (projection) vectors becomes a special case of the general problem of reconstructing binary patterns from their projections. Algorithms for solution of this class of problem are under study in our laboratory and are the subject of the following discussion.

Theoretical Considerations

The use of digitized values derived from a single television line crossing a biplane view of the left ventricle has been suggested as a means of reconstructing the border of the ventricle in the plane defined by the television lines. The first attempt was to multiply the two vectors together: this method is not helpful, since it does not provide a clear delineation of the ventricle border. By applying the knowledge of the magnitude of the decrement in the roentgen video signal equivalent to transradiation of one unit volume of radiopaque substance in each biplane image, we can convert the elements of the horizontal and vertical density vectors A and B to unit density sums. This implys that the pattern matrix which we are trying to establish is a binary one with the elements of the vectors A

and B being the sum of the rows and columns respectively (Figure 1). In this scheme the vectors are not required to be the same length. In a recent publication, Chang (3) defines two types of binary arrays, ambiguous and unambiguous; further, he states that an unambiguous matrix can be defined solely by and reconstructed unequivocally from its projection vectors. An ambiguous pattern, on the other hand, has a number of elements whose values cannot be determined solely from their projections. An unambiguous pattern, which might represent a ventricular cross section, is shown below. Chang's Algorithm 1 sets forth a technique for reconstruction of the matrix by writing a set of ~~m+n~~ simultaneous equations in m times n unknowns, where m is the number of rows and n is the number of columns. Denoting the elements in the array by f(i,j), where i is the row index and j is the column index, and with f(i,j) taking on only the values 0 or 1,

y	
3	1 1 1
3	1 1 1
1	0 1 0
	2 3 2 X

the equations for the array are:

$$f(1,1) + f(1,2) + f(1,3) = 3 \quad (a)$$
$$f(2,1) + f(2,2) + f(2,3) = 3 \quad (b)$$
$$f(3,1) + f(3,2) + f(3,3) = 1 \quad (c)$$
$$f(1,1) + f(2,1) + f(3,1) = 2 \quad (d)$$
$$f(1,2) + f(2,2) + f(3,2) = 3 \quad (e)$$
$$f(1,3) + f(2,3) + f(3,3) = 2 \quad (f)$$

These equations can be solved with standard techniques of back substitution, especially when it is noted that the terms on the left hand sides of equations a, b, and e must be identically equal to unity.

We have developed an algorithm for the solution of unambiguous arrays, based upon the last comment in the preceding paragraph. While it is more difficult conceptually, it is easier to program for a digital computer and should require less computation time. Referring to figure 1, note that in this example one column and one row are composed entirely of ones, detectable by the fact that their respective column and row sums are equal to the number of rows and columns in the array. A zero row or column can be detected by the same reasoning. The simplification of Algorithm 1 is straightforward. If a row or column is all ones or all zeros, cross it out, thereby decreasing the size of the matrix under consideration by one

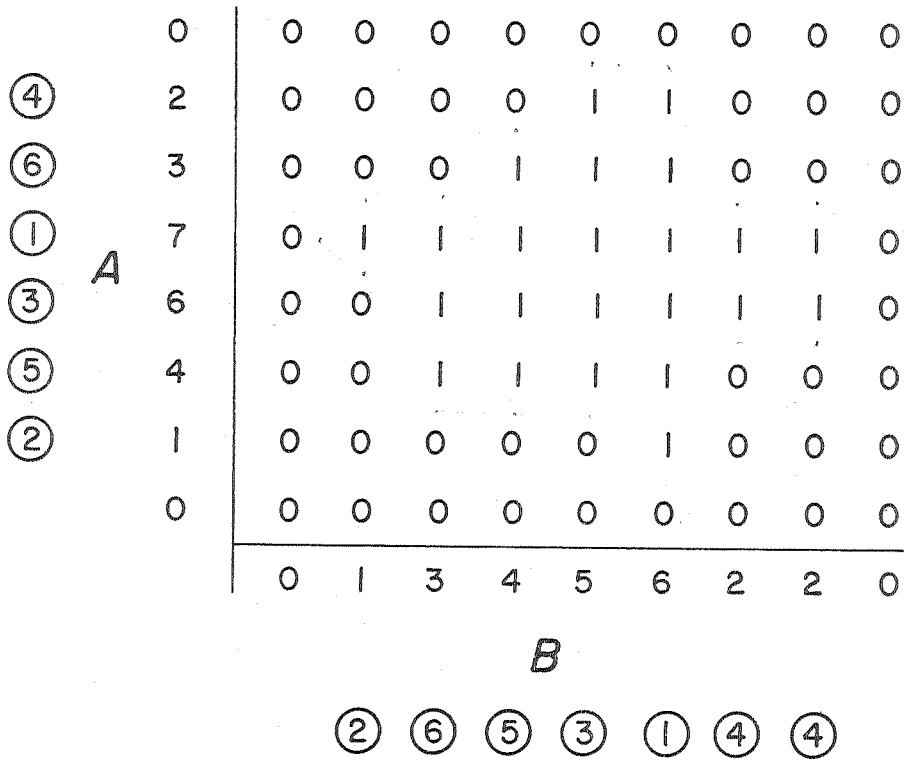

Figure 1

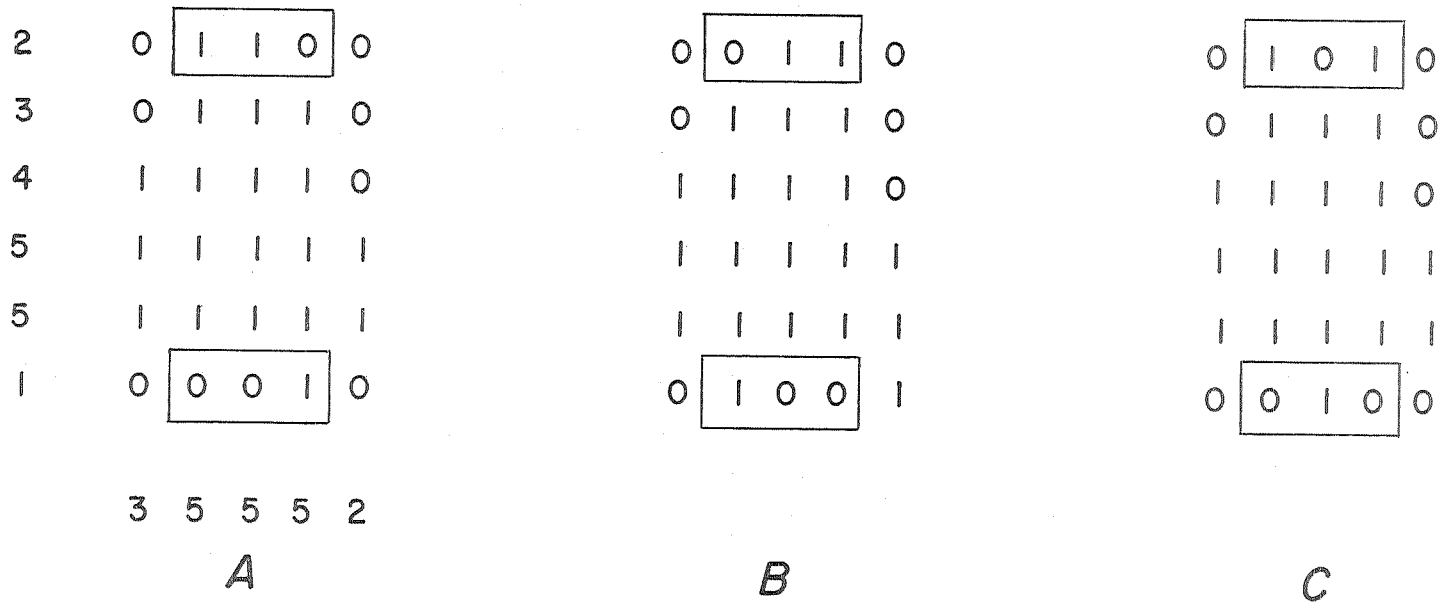

Figure 2

row or column. If a row of ones is crossed out, subtract one from each column sum. If a row of zeros is crossed out, decrease the row count as stated above but do not change the column sums. The process is carried out on the rows, then the columns, and then the rows again. As the contents of each row and column are accounted for in this manner, the two-dimensional pattern is reconstructed from the identified elements in the array. Finally, both rows and columns in the last two by two submatrix will have been accounted for, and the iteration is terminated. The circled numbers in figure 1 indicate the order, in this example, in which the rows and columns are crossed out or accounted for.

Chang proves that Algorithm 1 (and the adaptation of it discussed above) is also a test for the presence of indeterminate elements and thereby an ambiguous array.

The ambiguous case is much more prevalent, especially in the outline of the left ventricle. Figure 2 shows an example of the ambiguous case. First note that by employing our implementation of Algorithm 1, three reconstructions are possible because the elements enclosed in the rectangles cannot be assigned unequivocal values. Secondly, note that the difference between a and b or c is just the placement of a set of $\begin{matrix}1&0\\0&1\end{matrix}$ for $\begin{matrix}0&1\\1&0\end{matrix}$. These, in Chang's terminology, are denoted as switching components. One changes from a to b or c by a switching operation. Ambiguous patterns can be formed by carrying out many switching operations on patterns with the same row and column sums. Patterns so related are defined as similar patterns. Chang's third algorithm establishes a method for the recreation of a "similar" pattern from a set of projection vectors. Algorithm 3 as stated by Chang leaves too much uncertainty in constructing the endocardial border of the ventricle (defined as the line separating the zeros and the ones in Fig. 1), and therefore can be used in this application only with great care. However, Algorithm three does imply that the pattern so constructed, if incorrect, should be alterable into the "correct" configuration by a finite number of switching operations. Our present reasoning is that one additional piece of information may be sufficient to reduce the ambiguities to the level of the measurement errors; accordingly, we have assumed that the ventricular cross section is approximately elliptical in shape.

With these constraints it should be possible to prove that, given the projections, the ellipse-like form can be restored with the use of Algorithm III and a finite number of switching operations. A corollary to this supposition is that if it is not possible to reconstruct the proper pattern using switching operations and a knowledge of the general shape of the figure, then no method whatsoever can be developed to reconstruct the pattern. Since at this time we are developing two promising algorithms which do not use switching operations but which do reconstruct ambiguous figures very well, reference to the corollary seems to imply that a positive proof of the supposition is possible. Further, the assumption of an ellipsoidal cross section implies that a continuous set of ones must appear in each column and row, i.e., all unity values are continuous in the binary matrix. The first of the two algorithms under development in this laboratory employs this property in an iterative solution of the pattern, which requires no guesswork on the part of the operator or the computer program. In addition, the algorithm appears to form the basis for a proof that a general figure of unknown, but approximately ellipsoidal shape, can be reconstructed from its projections to within a few switching operations at most. Most of the major steps of the proof are in hand at present.

The second algorithm under consideration entails the placement of the proper number of adjacent unity values in the rows or columns of the matrix, as specified by the respective density sums. Each string of ones is then shifted en bloc within its own row or column until the proper number of ones appears continuously in the columns or rows. This algorithm appears to be easier to implement than the one discussed above, both for hand and for computer solution, although a large number of iterations may be required.

As a further aid to reduction of residual ambiguities, we believe that it may be useful to examine the binary patterns of the planes which are formed "above" and "below" the one under discussion. It is of course unlikely, that the same switching operations would have to be performed on adjacent planes (taken three at a time), thus giving some indication as to which of several possible ambiguities would be the correct one.

In summary, our studies of binary pattern arrays indicate that a proof is in hand of the possibility of reconstructing the shape of a general ellipsoidal pattern from its projection vectors. Two computational algorithms for this reconstruction are presently under development, one of which forms the basis for the proof that reconstruction is possible.

References

1. Sturm, R. E. and E. H. Wood:

Roentgen image-intensifier, television, recording system for dynamic measurements of roentgen density for circulatory studies.

Roentgen- Cine- and Videodensitometry. Fundamentals and Applications for Blood Flow and Heart Volume Determination. G. Thieme, Stuttgart, 1971 (Dr. P. H. Heintzen, editor) pp 23-44.

2. Ritman, E. L., R. E. Sturm, and E. H. Wood:

A biplane roentgen videometry system for dynamic (60 per second) studies of the shape and size of circulatory structures, particularly the left ventricle.
Ibid. pp 179-211.

3. Chang, Shi-Kuo:

The reconstruction of binary patterns from their projections.
Communications of the ACM 14:21-25 (Jan) 1971.

Section III

CONSIDERATION OF THE RELATIVE MERITS OF DIFFERENT ANALOG-TO-DIGITAL CONVERSION SYSTEMS FOR DIGITIZATION OF VIDEO IMAGES

Barry K. Gilbert and Earl H. Wood

In the initial studies of the feasibility of processing roentgen-video information by digital computer, several alternatives in terms of hardware design and implementation appeared; the decisions which resolved these possibilities, while not discussed in the original grant request, have substantially shaped the philosophy of our overall development plans. The two most critical choices concerning hardware implementation, and the reasons for our final decisions, are discussed below.

The present standard technique for converting pictorial information into digital form for computer processing employs an electromechanical scanning device which passes a light beam through successive small areas, called pixels, of a photographic negative, recording in digital form the amount of light remaining in the beam after passage through the emulsion. The technology requisite for these so-called film scanners is well known; the devices are available commercially. Several major difficulties are inherent in their design, however. If the information to be processed is originally in electronic (video) form, as in our facility, an increasing number of clinical cardiac catheterization laboratories, and all electron microscope facilities, for example, the data must be placed on photographic film before digitization. This reformating is undesirable, as Information Theory states that loss of information is unavoidable with each additional step in the processing of data, regardless of the degree of care with which this is done. Direct electronic digitization of the original signal would save one or two intermediate processing steps compared with conversion to photographic film format (i.e., electron beam to film, or

electron beam to phosphor target to film), and thereby decrease information loss, assuming the same accuracy of conversion of a given pixel to digital form (e.g., six or eight bits). In addition, the accuracy of a film scanner is dependent upon the precision of its mechanical components, requiring careful fabrication and care in its use; degradation of mechanical performance is immediately apparent in a reduction in the quality of the digitized data.

The duration needed to process a single frame of film is excessive, as the film must be carefully developed following exposure, and then mechanically scanned (present devices scan a single frame of film of dimensions 24 mm by 36 mm in one to ten minutes). One of the major motivations for digitization is the opportunity to employ the speed and computational power inherent in modern digital computers, a benefit which is largely dissipated if the digitization requires minutes or hours compared with a processing time measured in seconds. The disparity becomes devestatingly clear if it is desired to process multiframe, real-time data, as is the case in a clinical catheterization laboratory. Clearly, the conversion times should be of the same order of magnitude as the requisite processing times. Short overall conversion and processing durations, inherent in an all-electronic system but hard to envision in an electromechanical system, would make possible in the future the development of true operator-interactive image enhancement, feature-selection and extraction techniques, and even automated or computer-aided diagnosis of visual information (1-3). Rapid, inexpensive processing of great numbers of individual roentgenograms of many varieties is also more likely with entirely electronic systems.

Film scanning techniques suffer from similar electronic signal-to-noise ratio problems as do electronic systems, but have the additional liabilities of the nonuniformity from one batch to another in film emulsions of any given type, and the variability introduced during chemical processing. Effective safeguards

against equivalent electronic variations can be designed into entirely electronic hardware with much greater ease.

Projected refinement of the two techniques was also considered. Improvements in analog video systems over present systems are foreseen, in the areas of increased system signal-to-noise ratio and image resolution (which are two sides of the same coin); several such improvements are already at the testing and installation stages (see Section II A2 of grant request) and others will follow. Analog-to-digital converters with twice the resolution and half the noise of present units are already in the discussion stage. The nature of the electronic system is such that an improvement in any single component such as pickup tubes etc. usually improves the performance of the entire system. Contrarily, film scanning techniques are limited by improvements in mechanical precision and progress in emulsion technology, which, while still continuing, no longer appears to have the momentum of advancement so obvious in the world of microelectronics; it is our opinion that present emulsion technology is maturing, whereas the equivalent area of video electronics is still in its infancy.

Finally, our current estimates of the cost of implementing either a prototype system of the all-electronic variety, or of an off-the-shelf precision film scanning system, is $50,000 to $100,000. While advanced technology or mass production may reduce the cost of scanning systems somewhat, the Air Force Avionics Laboratory and TRW, Inc. have projected a multiple unit cost for an all-electronic system of ten to twenty-five percent of the amount required for the prototype system under consideration, using presently available technology, and even greater reduction employing implementations which are still in the research and development stages. Operating expenses for the film scanning system include computer time, maintenance, film, and processing, whereas the electronic

system dispenses with the latter two items.

The above comparisons have convinced us that it is worth the extra effort to develop an image conversion system which is entirely electronic. However, one of the critical difficulties in such a system is the rate at which samples must be taken, or inversely, the intersample spacing. This spacing is dictated by the Shannon Sampling Theorem and was discussed in the January 1971 grant request (pages II-12 through 18). To recover all the information present in a commercial video system (with 4 MHz bandwidth) requires 600 equally spaced samples from every line, and approximately 1200 to 2400 such samples from every line of the specialized wideband system employed in this laboratory (bandwidth greater than 12 MHz). If the sampling is done in real time, the equivalent sampling frequency is ten to forty million samples per second (Megasamples/second, or simply Ms/s), a difficult task even with state-of-the-art electronics.

Accordingly, we discussed with Ampex, Inc., the possibility of recording the video information on magnetic tape or disc at standard speeds and playing the information back at a much slower speed, which would have the effect of lengthening the duration of each video line, thereby increasing the intersample time interval and decreasing the speed requirements of the A-D converter employed. For their own reasons, Ampex had already explored this possibility and readily provided the following comments. As recorder bandwidth increases, the design interrelationships between electronics, magnetic recording surface characteristics, and recording and playback head characteristics become more critical, making retrieval of information at varying head-to-surface speeds (i.e., different playback speeds) progressively more difficult. In an actual test, the best which could be achieved for practical reasons was a two-to-one reduction in playback versus recording speed, but with a concommitant loss in signal strength and a decrease in system bandwidth. Any additional reduction in

speed would require different electronic components and recording beads for record mode and for playback mode, a prohibitively difficult and expensive task. Ampex has apparently abandoned this concept, as has our laboratory.

Another technique, which in effect decreases the sampling rate by increasing the duration of sampling, calls for replaying a given field to be digitized many times, each time taking one sample from all video lines, thereby increasing the intersample interval to 63.5 microseconds. On the first replay, the first sample is digitized from all lines; on the second replay, the second sample is digitized from all lines, and so on. Sampling 1200 values from each line would require 1200 replays of the field, or about twenty seconds.

While at first examination this technique appears suitable (twenty seconds is a reasonable digitizing duration), the method has a serious theoretical weakness. The Sampling Theorem implies that if the intersample spacing varies randomly by, for example, one percent, then the noise added to the digitized data from this source alone is one percent. Consider the implications of this statement in the present case. If all required samples from a given line are digitized in a single pass, as in the application of a very high speed A-D converter, and if, for example, the intersample spacing were 100 nanoseconds (i.e., 10 Ms/s), a one percent variation (i.e., a one nanosecond variation) in sample spacing implies one percent added digitizing noise. A variation of one part in one hundred is easy to achieve with present electronic technology, even at 10 Ms/s. However, using the repetitive playback system, two consecutive samples ostensibly separated by 100 nanoseconds are actually separated by one field replay time (16.6 milliseconds); a one percent noise addition will now require a stability of one nanosecond in 16.6 milliseconds, or one part in 16.6 million, an impossible degree of precision in an electromechanical device such as a video disc or tape recorder. (This is the best case; many machines replay

only entire frames, thereby requiring a stability of one part in 33.2 million). In point of fact, the laboratory's Ampex DR-10 video disc has an interfield stability of thirty nanoseconds, which, using the repetitive sampling scheme, implies the addition of thirty percent noise to the digitized data, assuming an equivalent 10 Ms/s sampling rate. Since we intend from the outset to sample at 20 Ms/s, this technique would add sixty percent noise from intersample error alone, clearly an unacceptable amount. Therefore, our conclusion is that it is absolutely necessary to sample the video image in real time, at the desired rates, because although difficult, it is by far the simplest and most reliable method.

In summary of this discussion, we believe that an all-electronic data handling system is worth the additional effort when long-term advantages are considered, and that high-speed direct A-D conversion is the only practicable means for achieving an adequate quality of digitized data.

Bibliography

1) Preston, K.: Feature Extraction by Golay Hexagonal Pattern Transforms. IEEE Transactions on Computers C-20(9): 1007-1013 (September) 1971.

2) Klinger, A., Kochman, A. and Alexandris, N.: Computer Analysis of Chromosome Patterns: Feature Encoding for Flexible Decision Making. IEEE Transactions on Computers C-20(9): 1014-1022 (September) 1971.

3) Hall, E. L., Kruger, R. P., Dwyer, S. J., Hall, D. L., McLaren, R. W. and Lodwick, G. S.: A Survey of Preprocessing and Feature Extraction Techniques for Radiographic Images. IEEE Transactions on Computers C-20(9): 1032-1044 (September) 1971.

Section IV

COMPUTERIZED MEASUREMENT AND DISPLAY OF DYNAMIC CHANGES IN SHAPE AND VOLUME OF SOLID OBJECTS DERIVED FROM BIPLANE ROENTGEN VIDEOGRAMS WITH PARTICULAR REFERENCE TO CARDIOANGIOGRAPHY

J. F. Greenleaf

E. L. Ritman

C. M. Coulam

R. E. Sturm

and

E. H. Wood

Department of Physiology and Biophysics, Mayo Clinic and Foundation, Mayo Graduate School of Medicine, Rochester, Minnesota 55901

This investigation was supported in part by Research Grants HE-4664, FR-7, and HE-3532 from the National Institutes of Health, Public Health Service, NGR-24-003-001 from NASA and AHA-CI-10 and AHF-CIF-69073 from the American Heart Association.

Videometry and Display: A computer automated biplane roentgen videometer has been developed for dynamic measurement of the shape of the left ventricle (1,2). This system generates data sets at the rate of about 60,000 points per second representing the shape of the ventricle 60 times per second. Comprehension of information resulting from such a mass of data can be facilitated by recently developed techniques of display utilizing computer generated oscilloscopic plots of contour maps and simulated three dimensional surfaces (3-5). The purpose of this paper is to describe the combination of computerized videometry with computerized display, and to illustrate examples of the resulting display formats. Videometric data acquisition has been described in detail elsewhere (2,6)but will be briefly outlined here.

Biplane Videometry

A biplane roentgen videoangiographic system is shown in Figure 1 as set up for alignment and volumetric calibration through the use of a rubber sphere of known dimensions. The sphere is positioned at the intersection of the axes of the biplane systems. The x-ray sources (HS and VS) and image intensifier systems (HI and VI) are shown for each of the biplane assemblies. Dynamic video roentgenographic biplane images of left ventricular angiograms are recorded on a single vidotape simultaneously with left ventricular pressure, ECG, and the rate and volume of injection of radio-opaque indicator (69% Renovist, 0.5 cc/kg body weight) into the left ventricle (2). A hardware system has been designed to recognize the spatial position of the biplane borders of a properly placed radio-opaque geometric form for subsequent calculation of its volumes (7,8). This is done in the following way.

The signals representing the video images of each of the biplane projections of the solid, for example the calibration sphere, are electronically switched and delayed such that one of the biplane images appears on the left and

one on the right half of a TV monitor screen. The position in space of the four border points encountered by each video line traversing the angiographic image of the object under study are then determined from the video signal of each respective line by an operator interactive quantizing sensor circuit (7). Figure 2 shows an oscilloscopic example of this signal after traversing the image of the calibration ball along with the biplane video roentgen images of the ball. Points A, B, C and D on the signal represent the four borders as recognized by the quantizer system. These quantized borders are displayed as bright spots on the video images (Figure 2, lower panel). If the sync pulse (S) is taken as the origin, then the time axis of the video line can also be considered to be the distance axis since the line is swept at a constant rate across the image. The times (distances) required to sweep the video beam from the sync pulse (S) to the various recognition points are fed into a CDC 3500 digital computer at the end of each line (i.e., four 10 bit time measures every 63.5 usec). This requires a data transfer rate of about 63,000 data words (10 bits/word) per second.

Any noncardiographic shadows which may interfere with the ventricular border recognition, such as the diaphragmatic border of the liver, can be preferentially shaded out by the operator with the use of a flying spot scanner system. The flying spot scanner system allows the operator to increase or decrease the opacity of a sheet of translucent plastic film* with a pencil or an eraser respectively and generate a video signal as

*Color-key negative acting magenta color films manufactured by 3M Company, St. Paul, Minn.

though the video image was being viewed through this film. By subtracting this signal from the original video image one can adjust the brightness (voltage level) of any desired portion of the images. The operator, on an interactive basis, used the flying spot scanner system and voltage level controls of the video signal to process each of the biplane views. The views are adjusted independently so that, in the judgement of the operator, the video display of the brightened border recognition points generated automatically by the quantizer system circumscribes and coincides with the borders of the calibration ball (Figure 2), or of the opacified left ventricular cavity (Figure 17).

Undyed blood entering the left ventricle via the mitral valve during diastole produces a less radio-opaque area or "hole" in the roentgen silhouette of the ventricular cavity just downstream to the mitral valve. This problem is overcome by the operator being able to preferentially darken the affected area within the confines of the ventricular silhouette using the flying spot scanner system. Small regions of erroneous border recognition which still remain can be removed at a later time during computer analysis by digitally interpolating across the defect in the cardiac border.

After a complete video field has been scanned in 1/60th of a second, data representing the digitized outline of the object for that field are transferred to digital magnetic tape. Real-time scanning (digitization and storage) of data representing one to three heart cycles lasting several seconds can be achieved by using a standard 2200 word computer program written in basic assembly language using the Medlab time sharing monitor ( ).

After the data are transferred from the video disc (Ampex VR10) to the digital tape the data is analyzed and displayed on a storage oscilloscope at a peripheral computer station juxtaposed to the video-tape-videodisc data processing assembly.

Acceptance of certain assumptions allows the data obtained from this system to be used to calculate the volume of the object being viewed. The following method is one used by this laboratory and has been extensively reviewed (2).

It is assumed that the shape of each of the 60 to 80 cross sections of the ventricular chamber delineated by the horizontal video lines traversing the biplane images of the chamber is elliptical. It is further assumed that the two orthogonal diameters (B - A, and D - C in Figure 2) measured from each of these horizontal lines is the major and minor axes of the elliptical disc representing the cross section of the object at the level of that line. Based on these assumptions:

$$\text{del } v_n = \pi * K * \left(\left[(B_n + B_{n-1}) - (A_n + A_{n-1}) \right] * \left[(D_n + D_{n-1}) - (C_n + C_{n-1}) \right] /16 \right), \qquad \text{Equation 1}$$

where del v is the volume of the disc; K is the scaling factor and A, B, C, D are the coordinates of the four borders at video line level n. Ventricular volume is obtained from the equation

$V = \sum_{n=1}^{N} \text{del } Vn$, where N is the total number of horizontal video lines traversing the ventricular image.

The accuracy and reproducibility of the data has been assessed. Calculated volumes of radio-opaque dye filled balloons were correct to within 0.2 ml for balloons in the 30 to 40 ml range (2). Variations of about 1.5 percent in the computed volume of an average size left ventricular chamber correspond to an error of less than 0.4 mm in the measurement of the diameters of the real object at the magnifications used.

Photographs of oscilloscopic displays generated by the program used to calculate volume are shown in Figure 3. The reconstructed biplane silhouettes based on the digitized border recognition points fed into the computer from one video filed in real time are shown in the left panel. A plot of 60 per second calculated volumes of a balloon filled with 32 ml of a 10% renovist solution and suspended in water during a one second injection of an additional 8 ml of this solution into the balloon is shown in the right panel.

The spatial coordinates of each of the border recognition points making up the digitized outline of the biplane silhouettes can be derived from the number in the particular horizontal line and the position along this line (point in time) at which the recognition point occurs relative to the left side of the picture marked by the horizontal sync pulse (Figure 2), i.e., $X = A_n$ or B_n, $Z = n$ and $y = C_n$ or D_n. Where Z is the vertical axis, X is the left to right axis, and Y is the front to back axis of the video image and n is the number of the horizontal video line. Therefore, each point can be located in space by the coordinates (X, Y, Z).

Simulated Three-Dimensional Display: A mathematical model for simulated three dimensional oscilloscopic display was constructed from the elliptical discs used for volume determinations by interpolating equispaced data points around their circumference and stacking them in order from top to bottom. The centers of the ellipses, points $(\left[A_n + B_n\right]/2, \left[C_n + D_n\right]/2)$, were aligned in space exactly as they occurred in the video images. Figure 4 illustrates a simulated three dimensional image representing the surface of such a model derived from videographic data obtained from the radio-opaque dye filled balloon whose computer reconstructed biplane silhouettes are shown in figure 3.

Techniques for computer generation of simulated three dimensional displays of surfaces have been described elsewhere (3-5) but will be described briefly here. Figure 4 is a polaroid time exposure photograph of the face of a computer driven oscilloscope. The picture is made up of a mosaic of light spots arranged in a 256 x 256 square array. Modulation of the brightness of each spot is achieved by varying its time of illumination. The film then integrates the light of each spot up to the desired level of brightness.

The illusion of three dimensions is achieved by the combination of three characteristics:

1) The surface is continuous; although the data are known at approximately 1600 points in space only, linear spatial interpolation is used to fill in the triangles resulting from the projection of each triplet of neighboring data points onto the viewing plane (scope face). Thus, the surface consists of flat triangular sections connected along their edges. The spots of the mosaic are close enough together to give an appearance of continuity when each spot of the mosaic falling within the triangle is illuminated.

2) The surface is shaded as if illuminated by a beam of parallel light rays. The brightness of each triangle depends upon its orientation relative to a theoretical arbitrary illumination vector. The triangles are plotted brightly if they face the light vector and darkly if they are oriented at 90 degrees to the light vector.

The light vector of Figure 4 is directed from the right at 45 degrees and results in the body appearing as if it were lit by parallel light from that direction.

The light function used is:

$$\text{Brightness} = \text{EXP}\ (C\,[V_1 \times V_2] \cdot L), \qquad \text{Equation 2}$$

where V_1 is a vector representing one side of the triangle being plotted and V_2 represents another side. L represents the light vector, X represents cross or vector product and . represents dot or scaler product. C is a constant controlling the range of illumination and is a function of taste and of the characteristics of the film.

Since we take the absolute value of $(V_1 \times V_2 \cdot L)$, triangles facing 180 degrees from the light source are also plotted brightly. This results in the figure appearing to be lit from behind as well as from the front.

3) Hidden sections are not plotted. Although the data for the entire surface are known, various hidden portions of the surface should not be plotted. This is accomplished in two steps. First by plotting the triplets of data points in sequence from nearest to fartherest from the selected viewing plane (the theoretical position of the scope face) and second by allowing each light spot in the mosaic to be illuminated as a member of only one triangle, thus sections or portions of sections which are to be hidden are not added to the image.

Examples of two formats to display multidimension data will be described: First a simulated 3 dimensional plot of changes in the contours of a surface in space is used to display simultaneous variations of two parameters with time. The plot of calculated volumes of successive multiple cross sections of a chamber in relation to their position along the long axis of this chamber against time is an example of this type of display. The second format is in the form of a three dimensional display of the shape of the chamber derived from digitized loaders of its orthogonal silhouettes and the assumed shape of its cross sections.

Displays From Biplane Videometry of a Balloon: In order to demonstrate the previously described technics several displays will be illustrated using a few selected functions. These functions were derived from data measured by the videometry system from orthogonal roentgen silhouettes of a balloon suspended in water as it was inflated with a known volume of roentgen contrast media over a period of 1 to 2 seconds.

Although inflation and deflation of a balloon is a complex process, at an analytical level, it is much simpler than that of a beating ventricle (which has an asymetric shape as well as a heterogeneous wall structure). Consequently we chose to use data from balloon inflation to illustrate the use of simulated 3 dimensional figures for data dense displays of vary large volumes of data in readily comprehensible forms.

Figure 5 represents a computer generated three dimensional surface display and corresponding contour map for a volume function V(L,t) derived from videometry data. The height above the X Y plane of each point on the surface represents the calculated volume (delV) of an elliptical disc whose major and minor axes were measured from biplane silhouettes by the automated videometry system and whose position along the longitudinal axis of the balloon from inlet to tip are indicated by the X coordinate (rightward and toward the viewer). The time at which the volume measurements were made is indicated by distance along the Y axis (rightward and away from the viewer).

The panel on the right is a contour map whose contours are virtually the same as those inscribed on the surface, but are plotted as viewed from directly above. Exact coordinate values of features of interest on the surface can be determined from the contour map.

This surface indicates that the entire length of the balloon gains volume as the injection progresses. The relative distribution of volume to the elliptical discs does not seem to change greatly during inflation.

Figure 6 illustrates a function representing the slope (in the direction of time, i.e. $\frac{\delta V(L,t)}{\delta t}$) of the surface in Figure 5. One can see that this plot affords a different look at the balloon inflation and reveals that the rate of changes in volume in the inlet and in the tip regions of the balloon are less than in the center region.

Although functions such as this are not independent of the original data, they can greatly increase the comprehension of such data by generating a description in an entirely new domain of reference.

Circumference C(L,t) of the elliptical discs comprising the mathematical model of the balloon are plotted in Figure 7, as a function of disc position along the long axes of the balloon and of time during inflation in the same format as Figure 5. Circumference of an ellipse is equal to $\pi * (A + B)$ where A and B are the major and minor axes of the ellipse and correspond to the distances (times) (A - B) and (C - D) on the video signal for each line, an example of which was shown in Figure 2.

If the circumference surface of Figure 7 is expressed as percent change relative to the circumferences at minimal volume, one obtains a surface representing a measure of strain, i.e. the fractional change in circumference of each elliptical disc, plotted as a function of the time of inflation. Such a surface derived from the data of Figure 7 is plotted in Figure 8 in the same format as Figure 7.

The tip of the balloon showed much greater strain than the center and inlet regions. This was apparently due to movement of the balloon toward the tip during inflation and to stiffening of the large diameter regions (center

and inlet regions) of the balloon. In addition, one can see from Figure 4 that the tip region has a very large axial radius of curvature giving rise to large axial tensions in the wall in this region (Tension $\propto$ Pressure x radius of curvature).

Figure 9 represents the slope of Figure 8 in the direction of time (i.e. $\frac{\delta C(L,t)}{\delta t}$). This surface is the normalized velocity of lengthening of the balloon during inflation. The highest strain velocity occurs in the tip even though the greatest change in absolute volume occurred in the mid region (Figure 6).

Under the rather strict assumptions of thin shell theory one can calculate wall tension (T) in the balloon given the shape of the balloon (curvature) and the pressure within and without (transmural pressure). The thin shell equation for wall tension is T = P * R, where radius, R, is radius of curvature in a direction of the tension and P is the transmural pressure. We can easily calculate the radius of curvature along the circumference of the ellipses comprising the balloon model with the following equation:

$$R(X,Y) = \frac{\left(1+\left(\frac{dy}{dx}\right)^2\right)^{3/2}}{\left(\frac{d^2y}{dx^2}\right)} \quad \text{where } \left(\frac{X}{a}\right)^2 + \left(\frac{Y}{G}\right)^2 = 1 \text{ represents the ellipse.}$$

Equation 3

Therefore, the equation T(X,Y,P) = P * R (X,Y),(equation 4) gives the tangential tension (i.e., tension in the plane of the assumed eliptical disc) for any point on the surface of the mathematical balloon model given the transmural pressure, P and the coordinates X and Y of the point in the plane of the elliptical disc.

Figure 10 is a surface plot and contour map of the tangential tension in the wall of the balloon during an inflation of 8 ml of roentgen contrast medium (12% Renovist). Note the ordered appearance of the tension. Since tension in the wall of a balloon is a vector (assuming no radial tension), this surface could be plotted for each possible orientation of the surface tension vector although the tangential tensions plotted in figure 10 was the simplest to calculate.

Displays From Biplane Videometry of the Left Ventricle: Figure 11 shows comparisons of photographs of orthogonal views of a silastic cast of the left ventricular chamber of a dog, biplane roentgen video silhouettes of this cast from the same angles of view, and computer generated reconstructions of the shape of this cast from the same angles of view derived from the biplane silhouettes and the assumption that the cross sections of the cast are elliptical in shape.

The data for the computer generated images were obtained by recording biplane roentgenogram /silhouettes of the cast on video tape as it was rotated through 90° using the assembly shown in Figure 1. The spatial coordinates of 320 points circumscribing the borders of the silhouettes for each video field were then obtained by the videometry system. The image was reconstructed from the particular sets of border points whose orientation in space corresponded to the orthogonal photographs of the cast. This set of border points was then used by the computer program to generate the simulated three-dimensional representaton and to shade the surfaces (as described previously) to correspond to the illumination of the cast which was used when the actual orthogonal photographs were obtained. There is a recognizable similarity between the photograph and the computer

constructed images although the trabeculations on the endocardial surface of the case are not reproduced.

Figure 12 illustrates computer generated displays from a biplane left ventricular videoangiogram of a dog. The shape and size of the left ventricular cavity have been reconstructed by the computer at 5 instants in time separated by 66 msec intervals and encompassing one cardiac cycle.

Although these reconstructed pictures of the ventricular cavity are shown for only five instants, data for 60 such images per second were recorded on the videoangiogram. The entire set of images of the ventricular chamber can be calculated by the computer in a period of ninety minutes.

A summary of the dynamics of the individual elliptical volumes for a period of several heartbeats can be obtained by displaying a heart volume surface such as that of Figure 13, which is analogus to and in the same format as the balloon volume surface of Figure 5. Synchronization of instant to instant changes in regional volume of the ventricular chamber throughout individual heart beats with the simultaneous changes in intraventricular pressure associated with these changes in volume plus the electrocardiogram and volume of contrast medium injected as illustrated in this figure is facilitated by recording these parameters on the same video tape (8). The sequential filling and emptying of the ventricle in diastole and systole can clearly be seen. The mean height of the surface decreases with time as the 8 ml of contrast material are washed out and the ventricle returns to its original mean volume.

The contour map indicates that virtually the entire ventricle participates in relaxation (increase in volume) and contraction (decrease in volume). Note the slight lag in time of contraction of the apex relative to the base.

Figure 14 illustrates the changes in volume of a heart during a period in which ectopic extrasystoles occurred and is shown in the same format as Figure 13. The surface representing volume and the contour map are very different from the normal heartbeats shown in Figure 13. The change in volume due to the ectopic beats appears to be located in the base region of the heart although its exact localization is not possible.

Figure 15 illustrates a technic of superimposing iso-lines of a function on the surface of a three dimensional image. This image of the left ventricular chamber is inscribed with iso-tension lines indicating the level of tangential wall tension (derived from equation 4) for each point on the surface of the chamber. The middle panel shows the distribution of these values for tangential tension over the surface of the ventricular chamber on the Z axis as a function of axial length of the chamber from base to apex on the X axis and circumferential length on the Y axis at the instant in time represented by the left panel. The left panel is the contour map of the regional distribution of iso-tension lines in relation to these two anatomical dimensions of the chamber.

This display format gives the investigator the ability to correlate points of interest on parametric functions (stress, velocity, strain, etc.) with their exact anatomical locations on the ventricular chamber.

Discussion

Study of the dynamic changes in shape and dimensions of the left ventricle covering the full anatomical and temporal extents of the chamber and individual cardiac cycles respectively requires that sufficient dimensional information be obtained to accurately outline the shape of the entire chamber at 30 to 60 successive instances in time during each second of the period under study (A. A. Bove and co-workers, Physiologist. 13:153, 1970). The development of a computerized biplane roentgen videometry system in this laboratory is an attempt to meet these requirements. This system, by an automated technique, divides the chamber into multiple successive cross sections about 0.7 mm thick covering its entire length and measures the orthogonal diameters of each of these 50 to 200 cross sections 60 times each second. This is a data accumulation rate of about 60,000 samples per second.

Clearly collection of volumes of data of the magnitude required to obtain reasonably accurate information concerning the dynamic changes in shape and dimension of the ventricle, is not feasible for routine use by manual technics.

Furthermore, transformation of these data to instant to instant determinations of shape, dimensions, position and volume of the chambers requires a similarly large number of arithmetic calculations. In addition to attaining real values for meaningful studies of cardiac functions, this instant to instant anatomic information must be accurately synchronized with simultaneous measurements of intraventricular pressure so that calculations of the changes of the tension-length relationships of the myocardial wall generated by its contractile elements during successive instants in the cardiac cycle can be made.

The biplane roentgen videometry system has the capability to collect and process these very large volumes of data. However, comprehension by the investigator of interrelationships between multiple time varying parameters and their spatial relationships to sites on the surface of a three-dimensional chamber in space is a problem which must be solved to attain the maximum value from such a system.

Solution of this problem requires development of operator interactive computer display technics for rapid generation of data dense readily comprehendible displays of multidimensional data. The display techniques illustrated herein are a first step toward information dense formats of reduced forms of such data. Although these types of displays are qualitative, their combination with contour maps tends to add quantitative information. The use of color displays would add greatly to the information content in that additional dimensions may be depicted by various hues.

The data density of these displays depends a great deal on the illusion of three dimensions achieved by the display format. The illusion of three dimensionality can be greatly enhanced with stereo pairs generated by mathematically rotating the original surface by a small angle and repeating the display. An illusion of true three dimensions can be achieved by viewing one of the pictures with one eye and the other with the other eye. Figure 16 shows a stereo pair which should be viewed by focusing the right eye on the left image and the left eye on the right image.* The increase in comprehension of this surface with this method of display is striking. A more adaptable and potentially valuable means of viewing such stereo pairs is to display the images side by side on a television scan converter which converts the images to a composite video signal which can be viewed on conventional telev sion screens or recorded on video tape or disc.

Use of the relatively inexpensive stereotronics system (12) makes it possible to view these images in true stereo form. The time delay recording capability of a video disc such as the ampex DR10 makes it possible to record stereo images field by field as they are generated in a time lapse mode by the computer for successive instants of time (e.g., 60 images per second) during individual cardiac cycles.

These images can then be played back from the video disc in stop action, reverse or forward variable time base modes as desired by the operator for detailed analysis of the temporal relationships of the multiple parameters. By use of multiple angles of view the operator can accurately delineate their spatial positions on the surfaces of the object under study.

These displays allow the opportunity to apply mental as well as mathematical identification processes to correlate various surface forms with

*It helps a great deal to use ones hands to make blinds such that the right eye cannot see the right image and the left eye cannot see the left image.

various heart functions. Much more information than that described here is available from these displays and many other functions can be derived from these data and displayed in this fashion.

Although the biplane roentgen videometry method has no advantage over biplane cine-angiographic method (10,11) in terms of accuracy, videometry seems to be advanced in terms of speed and ease of acquisition, making it a valuable tool for possible on-line experimental or diagnostic laboratory use. This is especially true when the method is combined with high information density, methods of data analysis and display.

The effectively greater spatial and temporal resolution of angiographic analysis using the electronically assisted videometry system, as compared to hand analysis of the same angiograms is possible because of the ability for real-time computer analysis to reduce analysis times to practical dimensions while still maintaining a high resolution in time and space of the videoangiographic images.

Instead of relying entirely on electronic methods and mathematical algorithms in recognition of cardiac records, this system utilizes the experience and pattern recognition ability of the operator to judge the accuracy of the electronically detected borders of the ventricular silhouettes. This capability prevents the possibility of bizarre borders being analyzed by a completely automated system, thereby removing the possibility of grossly incorrect data being collected.

A disadvantage of the system is that videometric measurements of both the left ventricular cavity and balloon as outlined by the radio-opaque dye, contain very limited information about the positions of particular elements of the left ventricular or balloon wall. The subsequent analysis of change in shape of the cavities is, therefore, limited in that the mechanical properties

of a particular element of the left ventricular or balloon wall cannot be deduced from the angiographic data without delineation of the wall elements themselves.

One of the most valuable contributions of these display formats is to give the investigator the ability to obtain quick qualitative evaluations of heart function which, by directing his attention to specific areas of interest, allow him to proceed immediately to detailed quantitative analysis and study of the region of interest.

References

1. Wood, E. H., R. E. Sturm and J. J. Sanders: Data processing in cardiovascular physiology with particular reference to roentgen videodensitometry. Mayo Clinic Proceedings 39:849-865 (Nov) 1964.

2. Ritman, E. L., R. E. Sturm, and E. H. Wood: A biplane roentgen videometry system for dynamic (60/second) studies of the shape and size of circulatory structures, particularly the left ventricle. Roentgen- Cine- and Videodensitometry. Fundamentals and Applications for Blood Flow and Heart Volume Determination. G. Thieme, Stuttgart, 1971 (Dr. P. H. Heintzen, editor) pp 179-211.

3. Coulam, C. M., W. H. Dunnette, and E. H. Wood: A computer-controlled scintiscanning system and associated computer graphic techni ues for study of regional distribution of blood flow. Computers and Biomedical Research 3:249-273 (June) 1970.

4. Greenleaf, J. F., J. S. Tu, and E. H. Wood: Computer-generated three-dimensional oscilloscopic images and associated techniques for display and study of the spatial distribution of pulmonary blood flow. IEEE Transactions on Nuclear Science 17:353-359 (June) 1970.

5. Coulam, C. M., J. F. Greenleaf, A. G. Tsakiris, and E. H. Wood: Three-dimensional computerized display of physiological models and data. Computers in Biology and Medicine (in press).

6. Sturm, R. E. and E. H. Wood: Roentgen image-intensifier, television, recording system for dynamic measurements of roentgen density for circulatory studies. Roentgen- Cine- and Videodensitometry. Fundamentals and Applications for Blood Flow and Heart Volume Determination. G. Thieme, Stuttgart, 1971 (Dr. P. H. Heintzen, editor) pp 23-44.

7. Sturm, R. E. and E. H. Wood: The video quantizer: an electronic photometer to measure contrast in roentgen fluoroscopic images. Mayo Clinic Proceedings 43:803-806 (Nov) 1968.

8. Wood, E. H. and R. E. Sturm: Use of videometry and electronic data processing for hemodynamic investigation by angiographic techniques. Chapter, Proc on Conf on Pathophysiology of Congenital Heart Disease, spon by American Heart Assn., Berkeley, University of California Press, April, 1970, pp 419-434.

9. Gardner, R. M. and J. J. Osttend: Communications system for remote access to a biomedical computer. Am Conf Eng in Medicine and Biology 8:141, 1966.

10. Williams, J. C. P., R. E. Sturm, A. G. Tsakiris, and E. H. Wood: Biplane videoangiography. Journal of Applied Physiology 24:724-727 (May) 1968.

11. Tsakiris, A. G., D. E. Donald, R. E. Sturm, and E. H. Wood: Volume, ejection, fraction, and internal dimensions of left ventrcile determined by biplane videometry. Federation Proceedings 28:1358-1367 (July-August) 1969.

12. Butterfield, J. F.: Three-dimensional televison. Proceedings SPIE, 15th Technical Symposium, Anaheim, California (September) 1970.

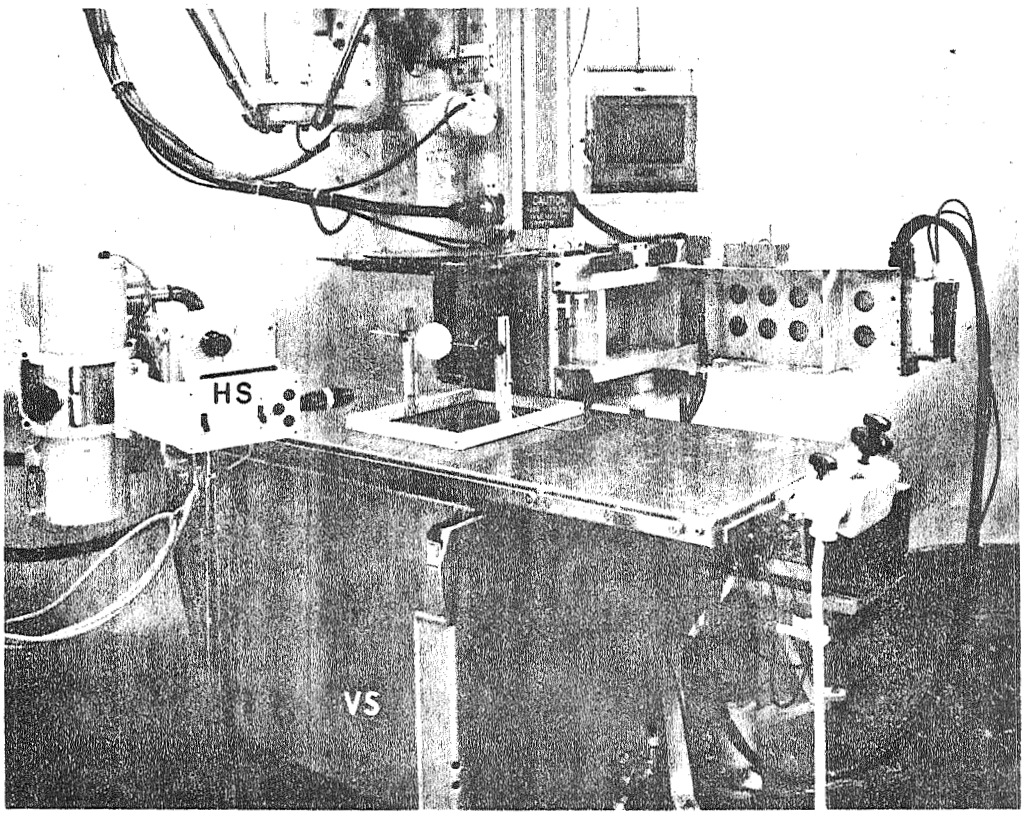

Figure 1: The biplane x-ray image intensifier system as set up for calibration with a radio-opaque ball of known dimensions. The ball is centered at the intersection of the axes of the biplane videoroentgenograph assemblies for the horizontal (source at HS, intensifier at HI) and vertical (source at VS in support of table, intensifier at VI) systems. Since the dimensions of the sphere are accurately known, the image amplifications (and distortions) of the system can be calculated.

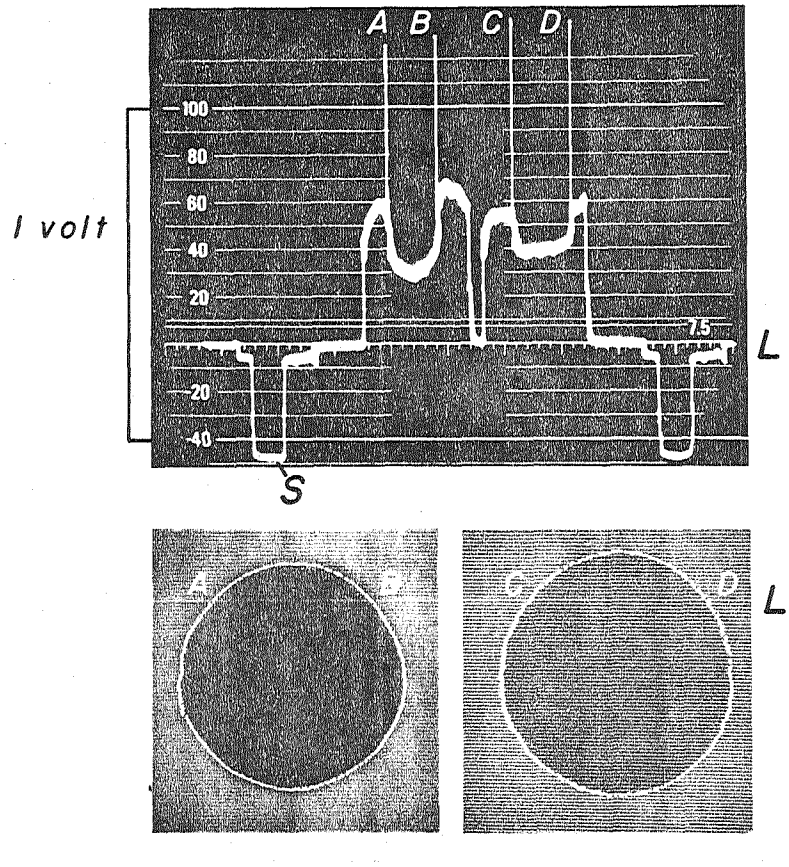

Figure 2: The lower panel shows one frame of biplane videoimages of the radio-opaque calibration sphere as it was played back in stop action from a video disc recorder. The brightened line indicates the video line for which the voltage is displayed on the oscilloscope in the upper panel. A, B, C and D on the video signal and on the biplane image indicate the points at which the line crosses the calibration sphere. These points were recognized by a voltage level sensing circuit and were brightened on the monitor to indicate to the observer where the borders were detected. The borders may be adjusted by adding various voltages to the original signal, independently correcting for any unequal biases in the two systems as frequently results from unequal background x-ray illumination due to varying chest thickness in the case of ventriculograms.

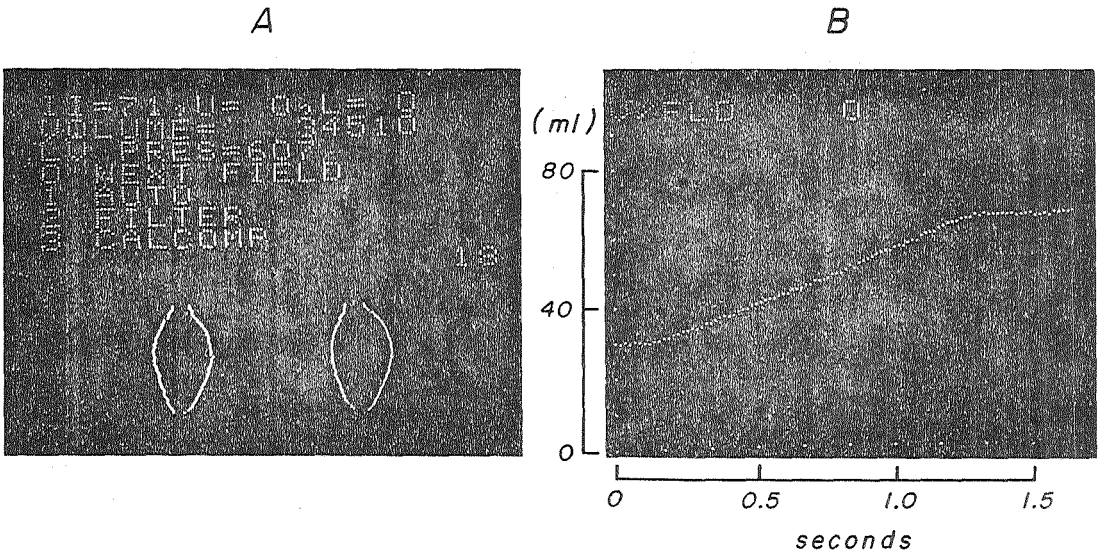

Figure 3: Panel A: Computer generated oscilloscopic output of videometry analysis program. Photograph of face of oscilloscope screen at a peripheral computer station showing below the orthogonal silhouettes of the balloon, the borders of which were recognized from the video images by the videometry system and transferred to the computer. The number, 18, is the particular video field from which there data were obtained and corresponds to the field number on the video disc recorder. The upper portion of the display gives the number of video lines in the image, 71; the volume of the balloon in cubic millimeters and the pressure in the balloon in mm of water options (0-3) in the computer programs which can be called by depressing the designated button in the peripheral station keyboard action as listed. A 60 per second sequence of these balloon outlines was used to calculate the volume versus time plot of Panel B by the method described in the text.

Panel B: Oscilloscopic output representing volume versus time (video field) calculated from 100 successive fields of a video tape recording of a biplane roentgenogram of a water suspended balloon during its inflation from 32.1 to 41.9 ml in a period of .4 seconds. Volume was calculated from equation 1 in the text.

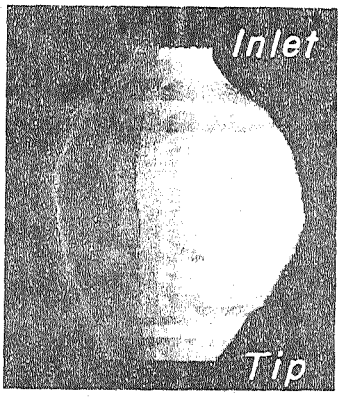

Figure 4: A computer generated simulated three dimensional plot depicting the surface of a renovist filled balloon suspended in water whose spatial dimensions were measured by the biplane roentgenographic videometry system. The picture is a time exposure photograph of the face of an oscilloscope and the image is a mosaic of 256 x 256 light spots. The figure is made up of a stack of approximately 30 elliptical discs (originally 60 discs, but reduced to every second disc) whose orthogonal diameters and their positions in space were derived videometrically from the orthogonal roentgen silhouettes of the balloon during playback from a video disc recorder. Three properties are illustrated which enhance the illusion of three dimensions: 1) The surface is solid; 2) shading is relative to a light source; and 3) surfaces which are hidden are not plotted.

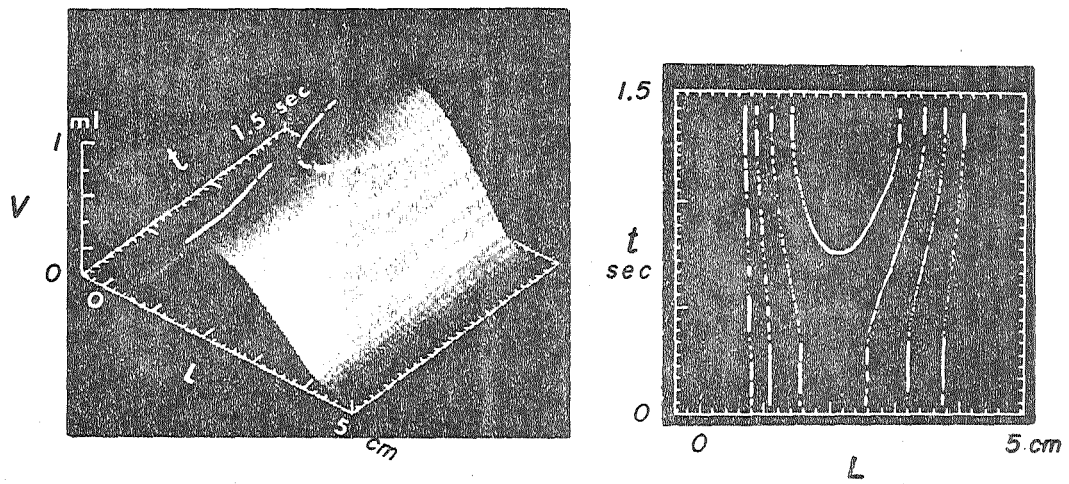

Figure 5: Computer generated spatial versus time displays of the regional volume V(L,t) of a balloon. The data were determined from a biplane roentgenogram recorded on videotape during injection of 20 ml of roentgen contrast medium into balloon suspended in water. The left panel is an oscilloscopic display of the volume of 0.5 mm thick cross sections of the balloon (in ml on the Z axis) plotted against the position of these sections from inlet to tip (in cm on the X axis) and against time from the onset of the injection (in seconds on the Y axis).

The right panel is a contour plot of the distribution of the 0.5 mm thick cross section volumes from inlet to tip on the axis against time in the axis. The contour lines in each panel delineate volume increments of 0.1 ml and are identical to those inscribed on the surface.

The large volume of data that are included in this type of easily understood surface display is indicated by the fact that this display is based on 28,000 videometric data points (10 bits each) collected over a period of 1.5 seconds.

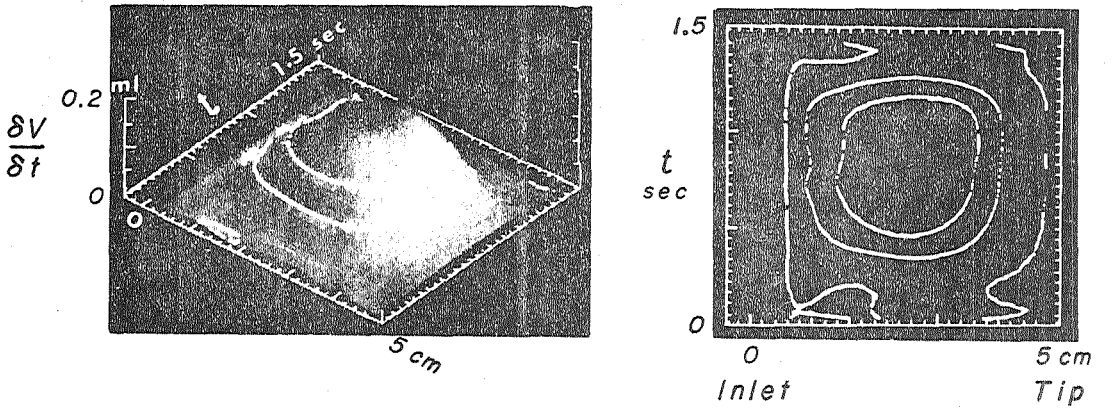

Figure 6: Surface representing the slope of the surface of Figure 5 in the direction of time, i.e., $\frac{\delta V(L,t)}{\delta t}$, plotted in the same format as Figure 5. Note the constant rate of increase in volume in the mid-region of the balloon indicated by the centrally located plateau. The inlet and tip regions exhibit the least volume rate of change. This surface indicates the possibility of additional information being obtained from an original set of data with the use of a simple mathematical operation, in this case first order differences, in combination with a suitable display format.

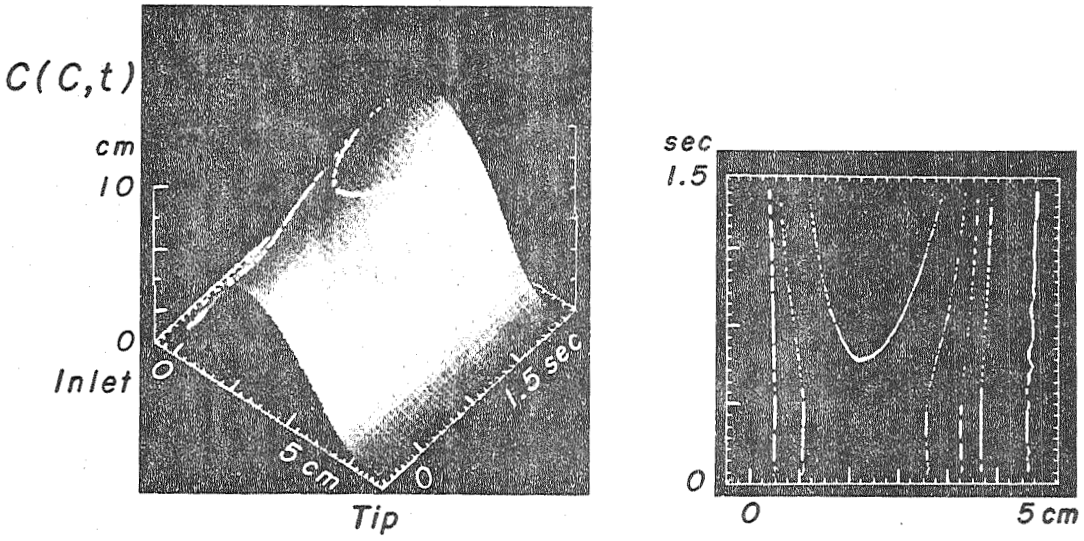

Figure 7: Surface representing the length of the circumference of each of the elliptical cross sections assumed to make up the surface of the balloon during the injection illustrated in Figure 5. Note that the largest change in circumference occurred in the central portion of the balloon, however, this was not the region of greatest stress (see Figure 10).

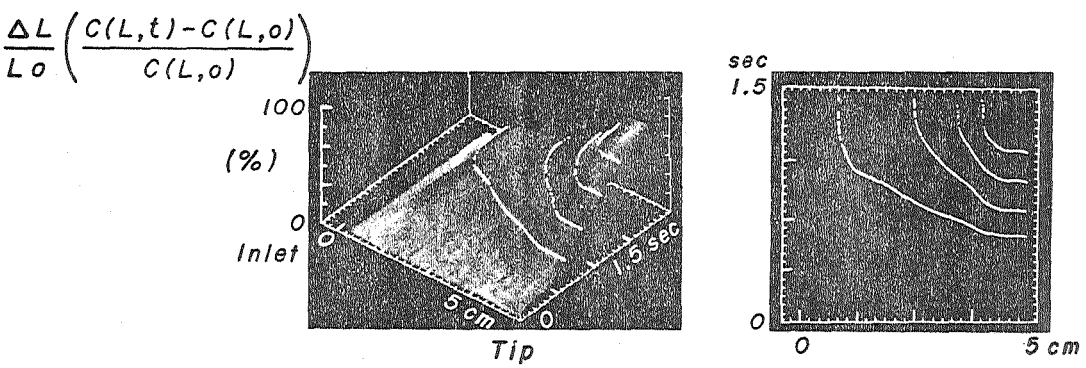

Figure 8: Fractional change in circumferential length. Each value of elliptical circumference in the surface of Figure 7 has been divided by the value at that point along the X axis at the onset of the inflation of the balloon. This gives a surface representing tangential strain, $\frac{\Delta L}{Lo}$, the strain in the plane of the ellipses. Tangential strain appears to be greatest in the tip regions of the balloon even though tangential radius of curvature is minimal in that region. This is apparently due to the large radius of curvature in the axial direction (normal to the plane of the ellipses, see Figure 4) which causes large stresses, thus strains, in that region.

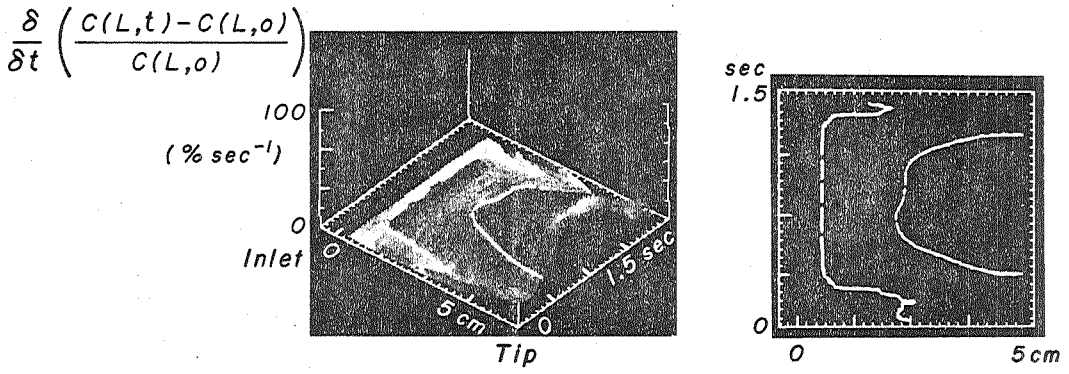

Figure 9: Surface representing the time rate of change of each point on the surface of Figure 8. This surface is $\frac{\frac{\Delta L}{\delta Lo}}{\delta t}$ and is proportional to strain velocity, commonly called velocity of shortening in cardiac muscle, but in this case it would be velocity of lengthening. Note the highest strain rate is in the tip region where the largest radius of curvature in the balloon occurred (in the axial direction, see Figure 4).

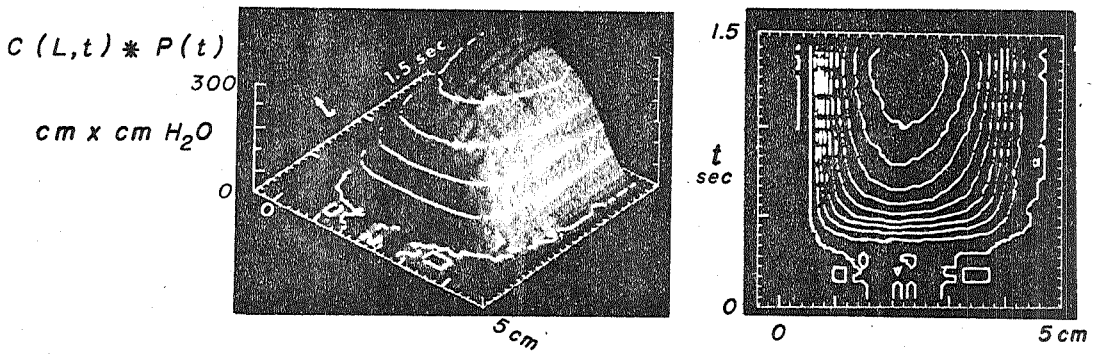

Figure 10: Surface representing tangential stress in a balloon as it is inflated under the conditions of Figure 5. The height of each point on the surface represents the stress in the tangential direction (in the plane of the elliptical cross sections defined by the successive video lines which make up the orthogonal roentgen silhouettes of the balloon). The independent variables are L and t as in Figure 5. Tangential stress was assumed to be proportional to pressure times the mean radius of curvature of the ellipses. Stress in a thin walled balloon is a vector, however, and the magnitude of tangentially oriented stress shown here is easy to calculate and was chosen for the purpose of illustration.

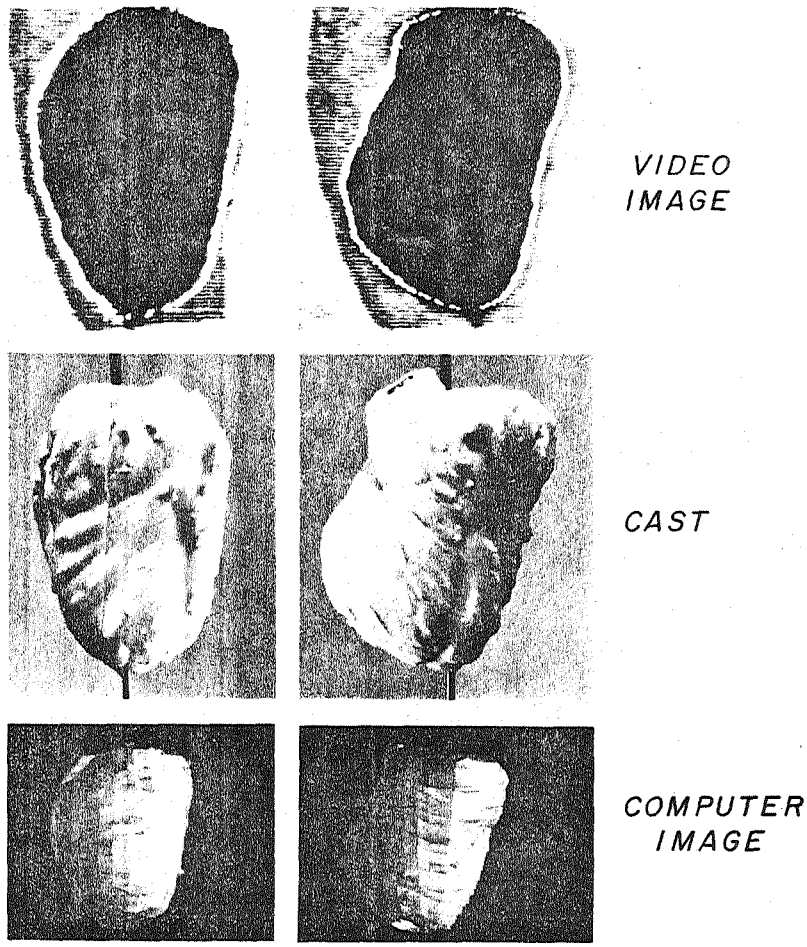

Figure 11: Comparison of the computer generated outlines of the orthogonal roentgen images of a silastic cast of the left ventricle of a dog with orthogonal photographs of the cast taken from the same angle of view as used for recording the video roentgen images, and a simulated three dimensional computer reconstruction of the cast based on the assumption that each of the 80 cross sections measured by the videometry system were elliptical in shape. Although detailed invaginations of the cast were missed by the measurement and display technique, the computer reconstructed shape of the cast is similar to the photographs.

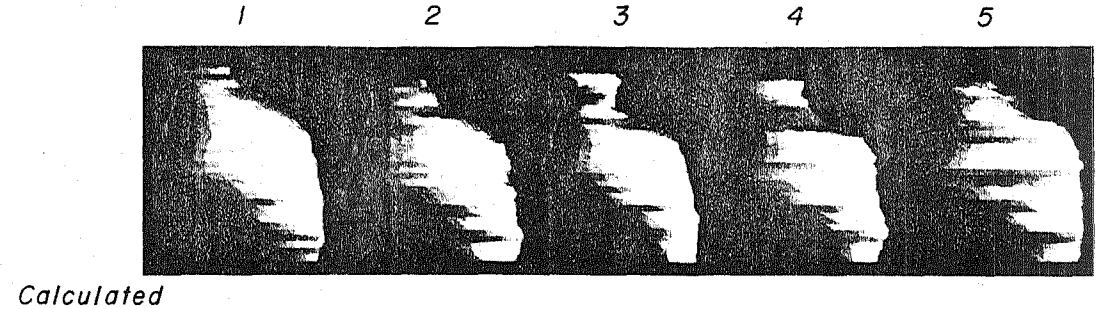

	1	2	3	4	5
Calculated Volume (ml)	47.9	34.9	21.0	24.8	41.6

Figure 12: Computer generated simulated three dimensional displays of the left ventricular cavity of an anesthetized intact dog derived from data obtained by the biplane videometry system described in the text. The left ventricular cavity is depicted at intervals of 66 msec. during the cardiac cycle. Note the large relative decrease in size of the apex during systole. Such displays can be sequentially stored on a video disc recorder and played back in real time, slow motion or stop action for detailed dynamic study of the ventricular dynamics.

COMPUTER GENERATED DISPLAYS OF SPATIAL AND TEMPORAL DISTRIBUTION OF CHANGES IN VOLUME IN DIFFERENT REGIONS OF LEFT VENTRICLE DURING SUCCESSIVE CARDIAC CYCLES

(60/sec Biplane Roentgen Videometric Values during Injection 8 ml 69% Renovist into Left Ventricle of 14 kg Dog with Heart Block - Morphine Pentobarbital Anesthesia)

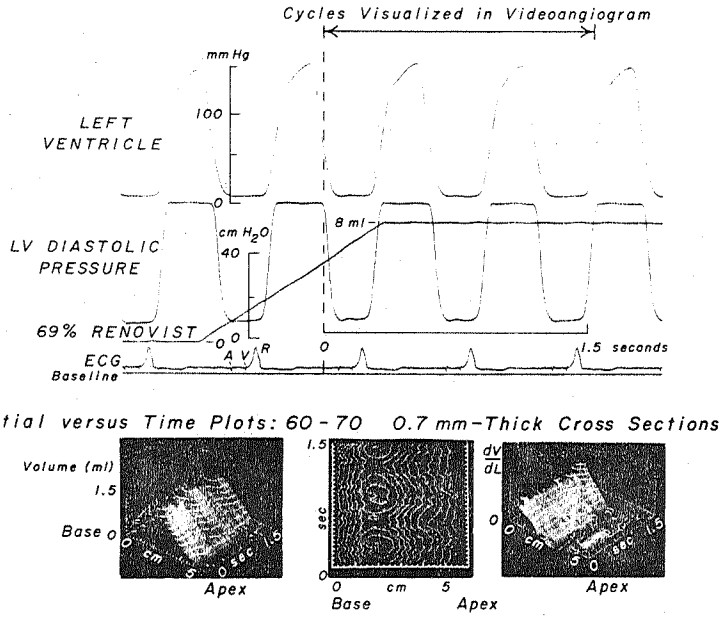

Figure 13: Volume surface V(L,t) and contour map of the left ventricle of an intact dog derived from a biplane angiogram, along with simultaneous recordings left ventricular pressure, ECG and the amount and duration of the injection of contrast medium from which the angiogram was obtained. The cycles analyzed by the videometry system are indicated by the double ended arrow. The bottom panels are volume surface and contour map displays in the same format as Figure 5. The assumed elliptically shaped cross sections of the heart represented by each point on the surface plot are 0.7 mm thick. The contour lines designate increments of 0.2 ml. The atrial contribution to diastolic filling can be seen, and the anomalus bulging near the apex in early systole is also visible.

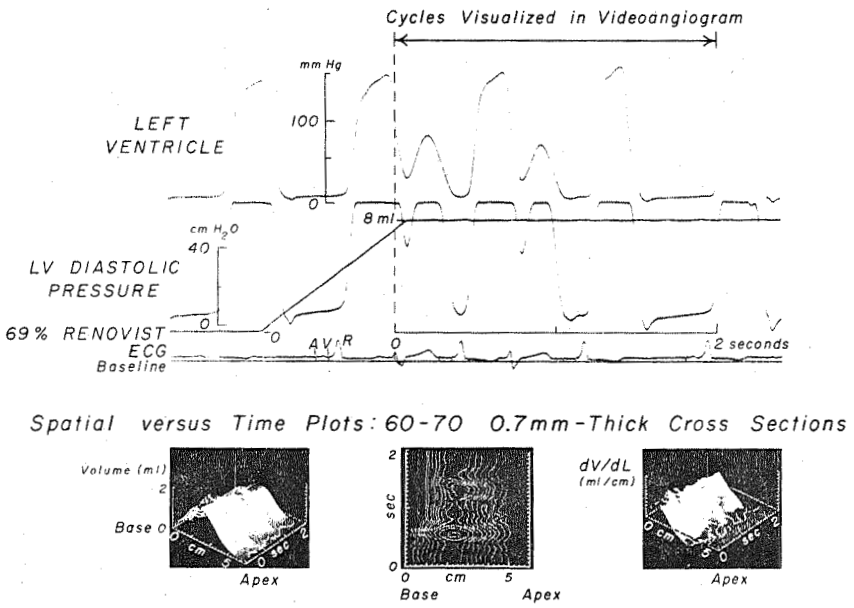

Figure 14: Volume surface and contour map of the left ventricle of the same dog as shown in figure 13 derived from another left ventricular angiogram during which true ventricular extra systoles occurred. The extra systole clearly affected the volume and contour maps. The mean volume of the ventricle was decreased by the extra systoles as can be seen by the decrease in length of the contour map during these extrasystolic cycles.

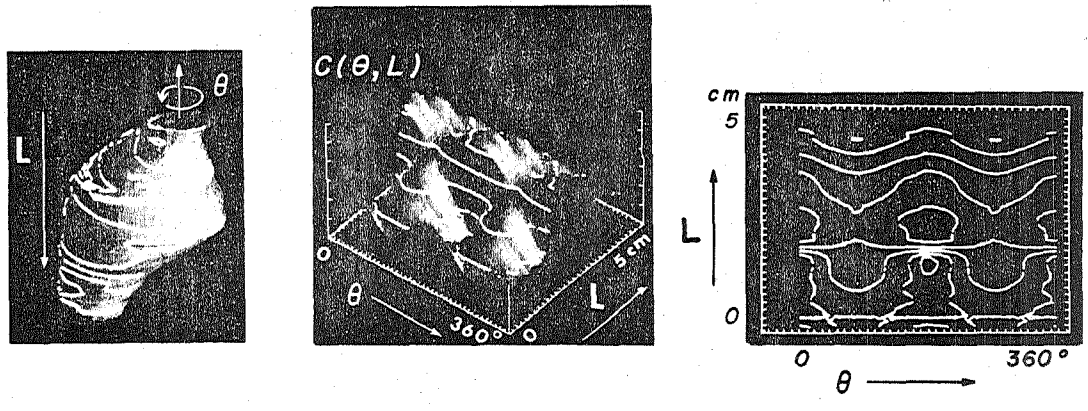

Figure 15: A computer generated display of the left ventricular chamber of an intact anesthetized dog derived from biplane videometry data. The left panel is the left ventricular cavity circumscribed with contour lines representing tangential stress calculated in the manner described in Figure 10. The center and right panels represent the stress surface and stress contour map for the surface of the left ventricular chamber. The X axis (left and toward the viewer) represents the spatial coordinate along the base to apex while the Y axis (right and away from the viewer) represents the circumferential coordinate.

STEREO VIEW of COMPUTER GENERATED
LEFT VENTRICULAR CAVITY

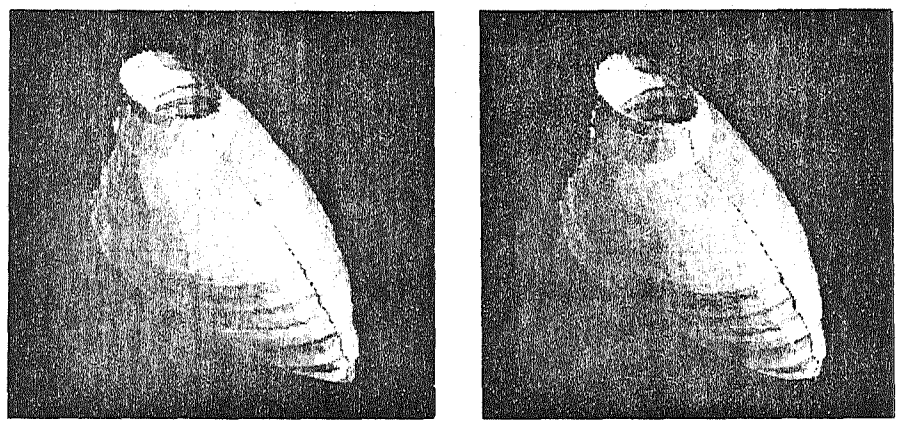

Figure 16: Stereo views of a computer generated left ventricular cavity. The right panel should be viewed by the left eye while the left panel should be viewed by the right eye. The illusion of three dimensions is nearly complete in this display format, greatly increasing the information content and comprehension of the display. This type of display can be generated by the computer field by field and recorded on a video disc in the time lapse mode. Detailed analysis of temporal relationships of the anatomical changes can than be carried by study of the instant to instant changes in shape and volume of the stereo images of the chamber throughout individual cardiac cycles by use of the field by field stop action, forward or reverse, or real-time replay capability of the video disc recorder.

Section V

COMPARISON OF ULTRASOUND CARDIOGRAPHY WITH BIPLANE ANGIOGRAPHY

J. F. Greenleaf, S. J. Johnson and E. H. Wood

Left ventricular diameters have been recently measured with the use of ultrasonic sound for the determination of cardiac output, end systolic volume, end diastolic volume and ejection fraction (1).

The noninvasive character of the ultrasonic method makes it particularly desirable as a method of measurement in the clinical setting. It is important then to determine the accuracy of the method and the sensitivity of its accuracy to various methodological and procedural variations.

The purpose of this project is to study the efficacy of ultrasonic sound in measuring the shape and volume of the left ventricular cardiac chamber and to substantiate these measurements with simultaneous measurements by the biplane videometry system. There are four parts to this description of the study: data acquisition, data analysis, data display and the experimental procedures.

The problems of data analysis and display of ultrasonic signals will be shown to be directly solveable by the use of the advanced techniques of signal conditioning, analysis and display which have been developed in this laboratory for biplane video angiographic data.

Data Acquisition: Ultrasonic data is obtained with the use of an ultrasonic transducer crystal which can transmit and receive ultrasound. The echoes produced by a pulse of sound energy reflecting from various interfaces

of material with different refractive indices are the signals which we wish to analyze and display. These echoes represent the various surfaces of the heart tissue and blood if the transducer produces a sufficiently narrow beam of sound energy.

Transducer: Several transducers are available. We are using crystals supplied by Dr. Harold Sandler, Ames NASA. Their / fundamental frequency of 500 kHz gives a wavelength in tissue of about 0.33 cm. We plan in the future to use about 2.25 mHz for a wavelength of less than 1 mm. The transducer will be mechanically scanned at first although the authors are aware of phase scanning of arrays of transducers (2). The mechanical scanning will be carried out by moving the transducer by hand, or automatically, while measuring its spatial coordinates and orientation with the use of a gimbal arrangement of potentiometers. The voltages generated across the potentiometers, representing the orientation of the transducer, will be recorded on video tape along with the echo signal in a manner to be described.

Recording: The echocardiograph signal contains frequencies up to the fundamental frequency of the crystal, i.e. about 2.25 mHz. Most physiology laboratories do not have recorders of this bandwidth. However, we are very fortunate in that we have several television video signal recorders (video having frequencies up to 4.5 mHz). Therefore, the echocardiograph signals can be recorded with the video tape facilities already available in this lab.

The voltages representing the spatial coordinates will be recorded on the analog data channels of the video recording system which are described elsewhere in this report. In order to store the echocardiographic signal on a video recording device the crystal must be pulsed at a rate $R = \frac{HS}{N}$ where HS

is the horizontal sync rate (17,250 Hz), and N is an integer such that echoes are recorded from a given pulse for a period equal to 62.5 N microseconds.

Therefore at the beginning of every N horizontal video lines we pulse the crystal and record the echo for N lines. However, every 63.5 μsec (each line) horizontal blank will blank out the signal for about 5 μsec. This loss of data can be overcome by pulsing the crystal every N/2 lines and alternately shifting the pulse by 5 μsec, so that at least every N lines we have measured the missing data. The signals for the two alternately pulsed echoes can later be averaged, except for the regions in each where horizontal blank occurred. The use of the existing high performance recorders of this laboratory will greatly facilitate the acquisition of this data.

Apparently the fastest pulse rate required would occur every 6 or 7 lines (about 2500 pulses/second) for the following reason. Ultrasonic sound travels in tissue a little faster than 1 mm/ μsecond, therefore, we can theoretically measure 10^6 mm of sound travel per second. If we are interested in measuring to a tissue depth of 20 cm we must allow the sound to travel at least 40 cm (in 20 cm then out 20 cm) between transmitter pulses. Thus we can pulse at a maximum rate of $10^6/400$ or 2500 pulses per second.

If a "picture" consists of a 10 x 10 array of measurements we can produce 25 pictures per second. This high scanning rate would probably require phased array scanning as opposed to mechanical scanning, however.

Data Analysis: These data will lend themselves to software methods of analysis which are much the same as those required for video image analysis. Digital filtering and deconvolution techniques consisting of many matrix-like manipulations will be greatly facilitated by the SPAM unit (described elsewhere) which carries out these manipulations as a peripheral device.

One of the operations required will be deconvolution of the signal with the impulse response of the transducer. This is because the transducer does not give a single pulse of voltage but rather a "ring" when it is hit with a wavefront or impulse of sound. Therefore, the signal we will measure from the transducer will consist of a sum of many "rings." A deconvolution process (3) will be used to determine the individual amplitudes and positions in time of these rings.

Data Display: Since the point of our study of echocardiography is to measure the volume and shape of the left ventricle, the data will be displayed with the use of previously developed methods of computerized oscilloscopic display of one, two and three dimensional functions (4). The x,y spatial coordinates of each echo, determined from the position of the transducer, and the z coordinate or depth, determined from the echo delay, will make up the three spatial coordinates which can be rotated and projected onto a scope face. Stereo views can also be obtained from these echoes in the manner described in the manuscript by Greenleaf and coworkers included in the appended progress report.

Procedure: The study will consist of two parts, first a highly controlled *in vitro* study and second an *in vivo* study. The echocardiographic measurements of ventricular shape obtained in each part of the study will be compared with those obtained simultaneously from biplane videometry. Since we have two video recorders, both forms of data can be recorded simultaneously.

In vitro Study: The *in vitro* study will consist of measuring the shape of an excised heart suspended in a fluid plethysmograph in a manner described previously in this report. An ultrasonic crystal will be mounted within the plethysmograph chamber and both ultrasonic and biplane roentgen videometric measurements will be made.

The two measurements will be compared at various heart rates, ventricular volumes and orientations of the ventricle to the measurement system. An absolute measure of ventricular volume can be obtained with the fluid plethysmograph.

This study will give us an upper limit to the accuracy of the ultrasonic measurement system. In addition to measurements of single diameters we will obtain multi-dimensional measurements by mounting the transducer on a gimbal device (yet to be designed) and mechanically scanning the heart while recording the echo and the position signals on video tape in the manner previously described. After digitization and software analyses the result will be a three dimensional array of points representing the positions of reflective surfaces of the scanned domain. Such data can be analyzed in the same manner as videometry data and displayed in a three dimensional format.

In vivo Study: The study of in vivo measurements of cardiac dimensions in dogs by ultrasound will be carried out through two main methods of approach: 1) the transducer will be placed on the surface of the chest at an intercostal margin, a method used by many investigators (1,5); and 2) the transducer will be placed in the esophagus at the level of the heart in a manner recently described by (6). Single diameter measurements and multiple dimension scanning will be carried out and compared with simultaneous measurements obtained from the videometry system.

BIBLIOGRAPHY

1. Pombo, Joaquin, F., Troy, B. L. and Russell, R. O.: Left ventricular volumes and ejection fraction by echocardiography. Circulation. 18:480-490 (April) 1971.

2. Somer, J. C.: Electronic sector scanning for ultrasonic diagnosis. Ultrasonics. :153-159 (July) 1968.

3. Greenleaf, J. F., Dobbs, W. A. and Bassingthwaighte, J. B.: Determination of a systems impulse response by parallel pathway analysis. Biophysical Society Abstracts, February 25-27, 1970.

4. Greenleaf, J. F., Tue, J. A. and Wood, E. H.: Computer generated three-dimensional acilloscopic images and associated techniques for display and study of the spatial distribution of pulmonary blood flow. JEEE Trans. Nuclear Science. 17:353-359 (June) 1970.

5. Dillon, J. C., Haine, C. L., Craig, S. and Feibnbaum, H.: Use of echocardiography in patients with prolapsed mitral valve. Circulation. 18:503-507 (April) 1971.

6. Olson, R. M., Sheldon, D. K. and Stone, H. L.: A nondestructive technique to measure wall displacement in the thoracic aorta. The Physiologist. 14(3):204 (August) 1971 Abstract.

Section VI

EFFECT OF INFLATION LEVELS AND BODY POSITION CHANGES UPON REGIONAL PULMONARY PARENCHYMAL MOVEMENT IN DOGS AT 1G*

H. C. Smith, J. F. Greenleaf, D. J. Sass, A. A. Bove, and E. H. Wood

The spatial distribution of inspired air and pulmonary blood flow of man and animals during various respiratory manuevers, and in various body positions, has been extensively investigated, but there is little or no experimental data on the spatial distribution of the third component of the lung, namely the parenchyma - under these conditions.

The purpose of this paper is to describe a method of measurement of regional pulmonary parenchymal shifts in dogs during various respiratory manuevers and body position changes.

In three dogs, 37 to 50 I mm metal tags were implanted percutaneously in the pulmonary parenchyma in a grid pattern 10 days to 2 weeks prior to study. This was achieved without significant pneumothorax or hemorrhage in the following manner; the dogs were anesthetized and intubated; and saline-filled catheters were inserted percutaneously into their right and left pleural spaces and pleural fluid pressures were monitored continuously.

A number 16 gauge needle - 28 cms long (Figure 1B) was fitted with a rubber gasket (A) so that with the trocar (C) in place, the assembly was essentially airtight. The small metal tags were placed in the needle; the dog was given several large positive pressure breaths, and the needle was inserted under fluoroscopic control through the appropriate intercostal space into the pulmonary parenchyma up to the mediastinum during the postventilation apneic period. The beads were then extruded at appropriate intervals as the needle was withdrawn. After each insertion the pleural catheters were aspirated to determine the presence of any blood or air in the pleural space, and upon completion of the procedure, roentgenograms were taken to confirm the presence or absence of pneumo or hemothorax. This procedure was repeated at each interspace overlying the lung on both sides of the dog until a grid pattern was obtained as shown on the bilateral roentgenograms of the chest illustrated in Figure 2.

The pulmonary tissue response to these metal tags was slight. A photomicrograph of a fixed air dried lung from a dog 2 weeks after tag insertion is shown in Figure 3. The metal tag was removed prior to microtome sections, and the remaining capsule is composed of compressed alveoli with slight

---

* Presentation at fall meeting of American Physiological Society, University of Kansas Medical School, Lawrence, Kansas, August 17, 1971.

inflammation and fibrous tissue; and is approximately 2 to 3 alveoli thick. To date, in autopsies of 11 dogs with parenchymal tag insertion, no pulmonary pathology, other than that seen in this figure, or pleural adhesions have been noted.

The dogs were studied 2 weeks after tag insertion in a molded 1/2 body supine cast mounted in a metal cage shown in Figure 4. This facilitated changing the dog's position from prone to head up/or head down, with minimal movement of the limbs, and neck or chest displacement. All pleural, esophageal and vascular pressures and the parenchymal tag positions were referenced to the spinous process of the 6th thoracic vertebra, which is approximately at the longitudinal and right to left midpoint of the lung. Simultaneous pressure records and Biplane orthogonal roentgenograms were obtained from each dog in the prone, head up and head down position at functional residual capacity and at the end of a spontaneous inspiration, and during brief sustained inflations by 10 and 20 cm H_2O airway pressure.

Figure 5 shows the biplane orthogonal x-ray system with the cube representing the dog's chest within the transradiated space. The exact dimensions of the orthogonal x-ray system (s,q,t,p) and the x'y' and z' co-ordinates of each tag from the central axes of the two systems must be known in order to correct for the magnification inherent in a divergent x-ray system.

This magnification correction was facilitated by transferring the x',y',z' coordinates of each tag from paired orthogonal x-rays into a CDC 3500 digital computer via an electronic plotting table and an analog to digital converter. The accuracy of the x-ray, plotting table, computer computational and display systems was assessed by the double blind determination of distances between beads placed obliquely, known distances a part, in the space transradiated by the biplane orthogonal x-ray system. These results are shown on the next Figure 6.

Using this system, the shift in pulmonary parenchymal tags following changes in body position can be examined, as shown in Figure 7. This is the computer generated plot of lung bead motion during a shift from the prone to the head up body position with the measurements made at functional residual capacity. The pulmonary parenchymal tag positions at end inspiration in three dogs in the head up and head down positions are shown on the next Figure 8. It is apparent that the weight of the abdominal contents and their influence

on diaphragm position greatly influences the spatial distribution of the pulmonary parenchyma. In all dogs in both head up and head down position, the parenchymal tags moved downward relative to T_6 spinous process. The functional residual capacity determined by the helium dilution method increased in all dogs upon movement from the prone to head up position and decreased upon moving from the prone to head down position. Note that the parenchymal tag motion closely parallels diaphragm motion and that the position of the chest wall is relatively unchanged. Note also that there is an increased gradient movement from the apex to the diaphragm.

We next examined the effect of a spontaneous inspiration upon the spatial distribution in the head up, prone and head down position. The typical changes in position of the parenchymal tags in one dog in the head up and head down positions following inspiration are shown in Figure 9.

In general the dogs' respiratory tidal volume was decreased in the head down position but the percent volume change from functional residual capacity was approximately the same in the two positions. There was less caudal displacement of the tags in the head down than the head up positions. This is compensated to some extent by a more lateral displacement of the parenchymal tags during inspiration in the head down position. Movement of the parenchymal tags following inspiration in the prone dogs was intermediate between these two patterns.

Finally we examined the pattern of parenchymal tag movement following both spontaneous inspiration and positive pressure inflation. In all body positions the direction of tag movement following position pressure inflation of the lungs or spontaneous inspiration were similar (Figure 10).

This figure shows parenchymal tag movement in a prone dog during a spontaneous and a 20 cm H_2O positive pressure inflation of the lungs. Only the magnitude of the bead movement differs and this is proportional to the difference in tidal volume under the two conditions.

Summary

A method for determining regional pulmonary parenchymal movements in the intact animal is described. Preliminary descriptive evidence indicates that the weight of the abdominal viscera significantly influences regional pulmonary displacement, and should be considered in any estimation of the spatial distribution of the pulmonary parenchyma. This method also allows

calculations of changes in regional lung volumes which together with regional pleural pressure determinations may provide information regarding regional lung compliance in the intact animal. Use of this lung parenchymal tagging procedure for quantitative analysis of changes in regional pulmonary volumes during changes in body position and changes in the magnitude of the gravitational inertial force environment procedure on a human centrifuge has been carried out by Greenleaf and co-workers (Physiologist. 14:155 (August) 1971.)

ASSEMBLY FOR PERCUTANEOUS INSERTION OF METAL TAGS FOR STUDY OF REGIONAL MOVEMENTS OF LUNG PARENCHYMA IN INTACT DOGS

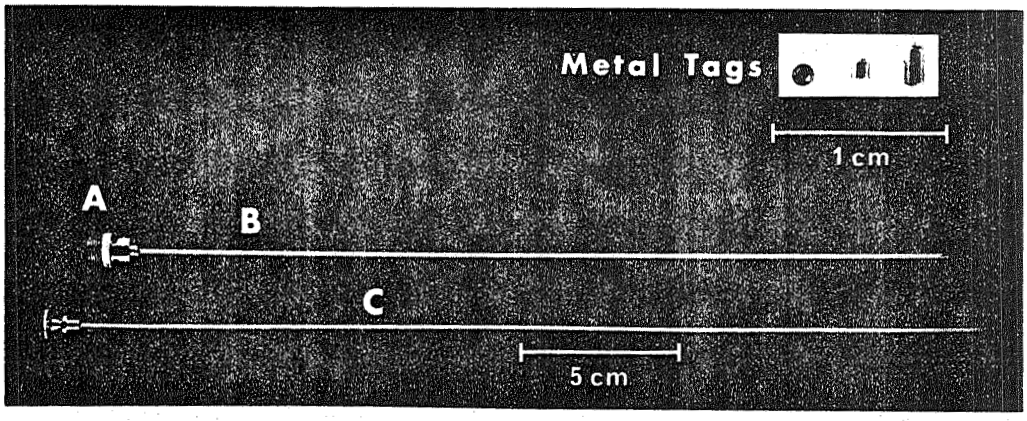

Figure 1

ORTHOGONAL ROENTGENOGRAMS OF DOG IN PRONE POSITION SHOWING LOCATION OF PARENCHYMAL TAGS AT END-INSPIRATION

(Dog 21.5 kg, Morphine-Pentobarbital Anesthesia)

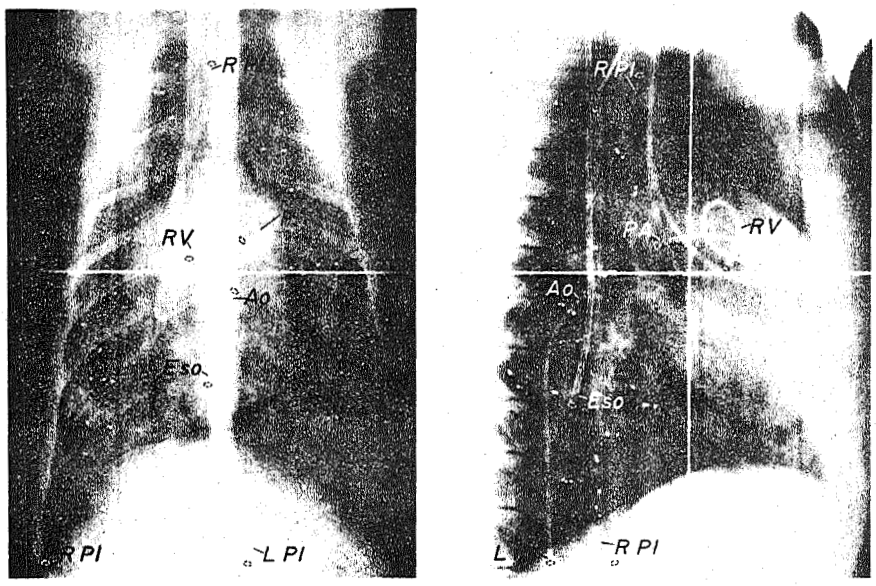

Figure 2

SECTION OF INFLATED AIR-DRIED LUNG

(Capsule Surrounding Metal Tag, 2 Weeks After Insertion)

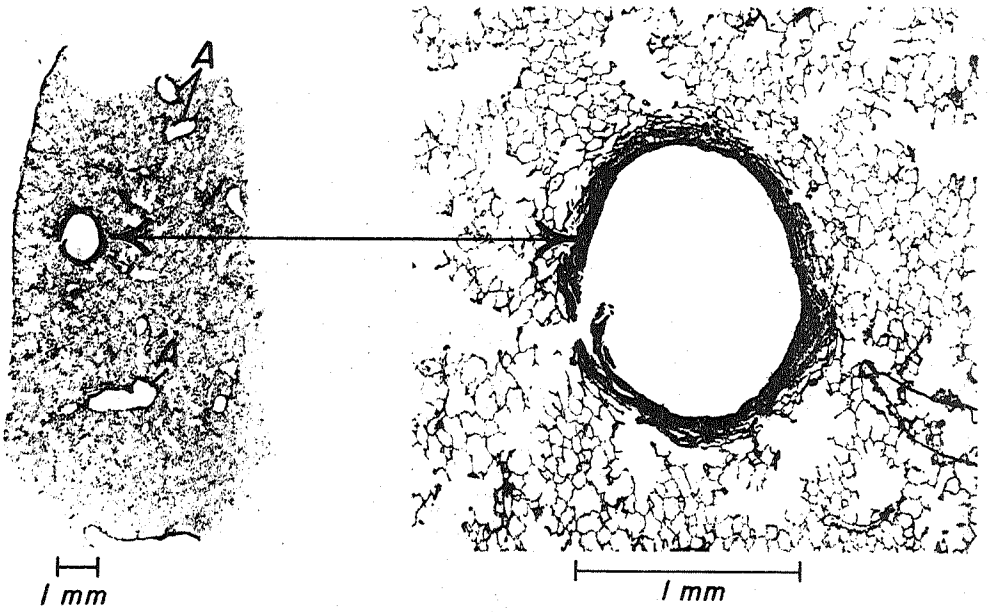

Figure 3

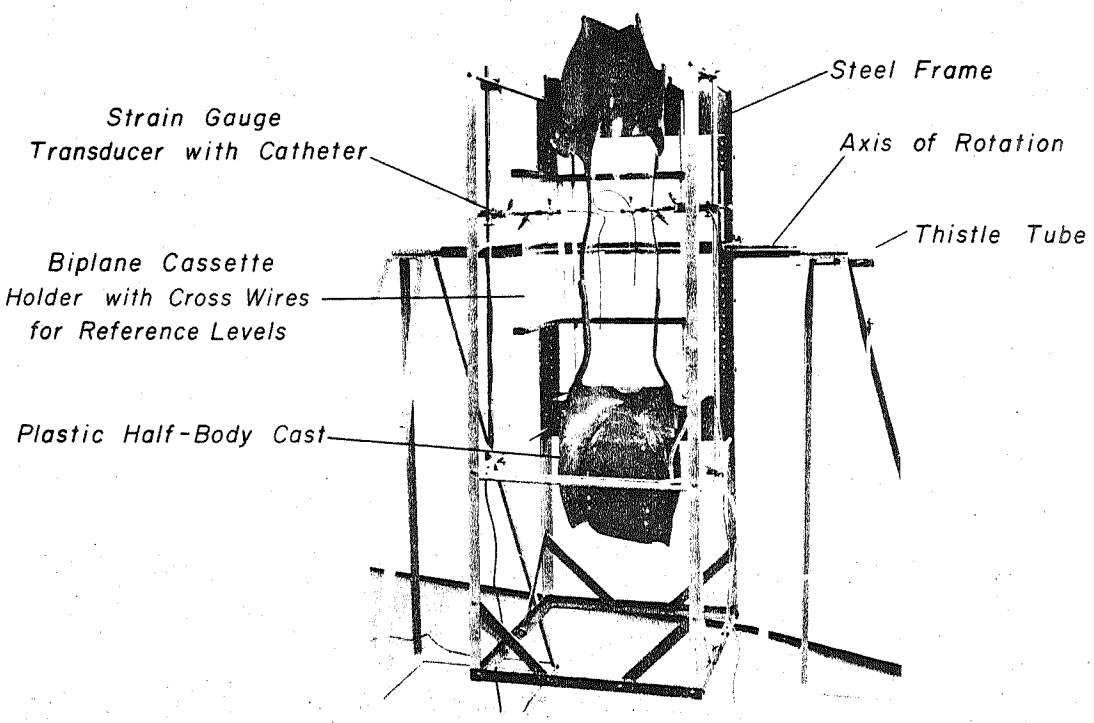

Figure 4

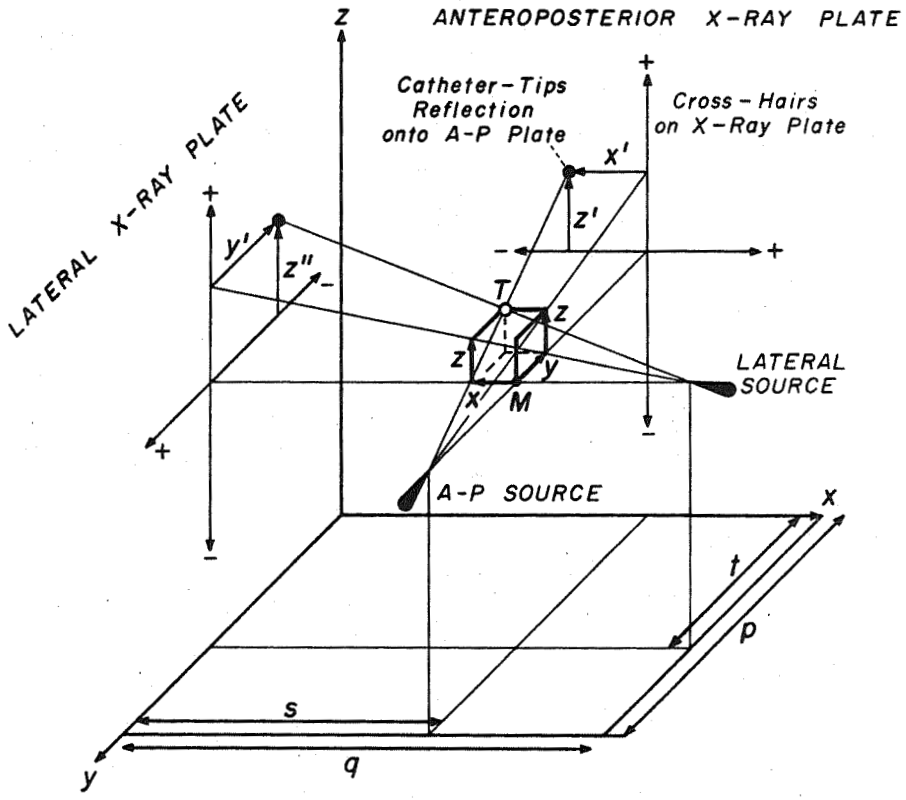

Figure 5

COMPARISON OF ACTUAL vs ROENTGENOGRAPHIC MEASURED DISTANCE BETWEEN RADIOPAQUE BEADS DISTRIBUTED IN SPACE TRANSRADIATED BY ORTHOGONAL BIPLANE X-RAY SYSTEMS

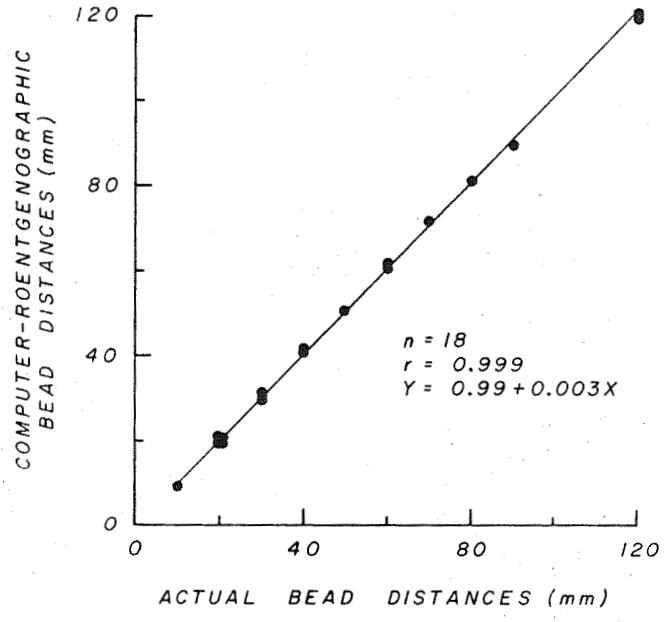

Figure 6

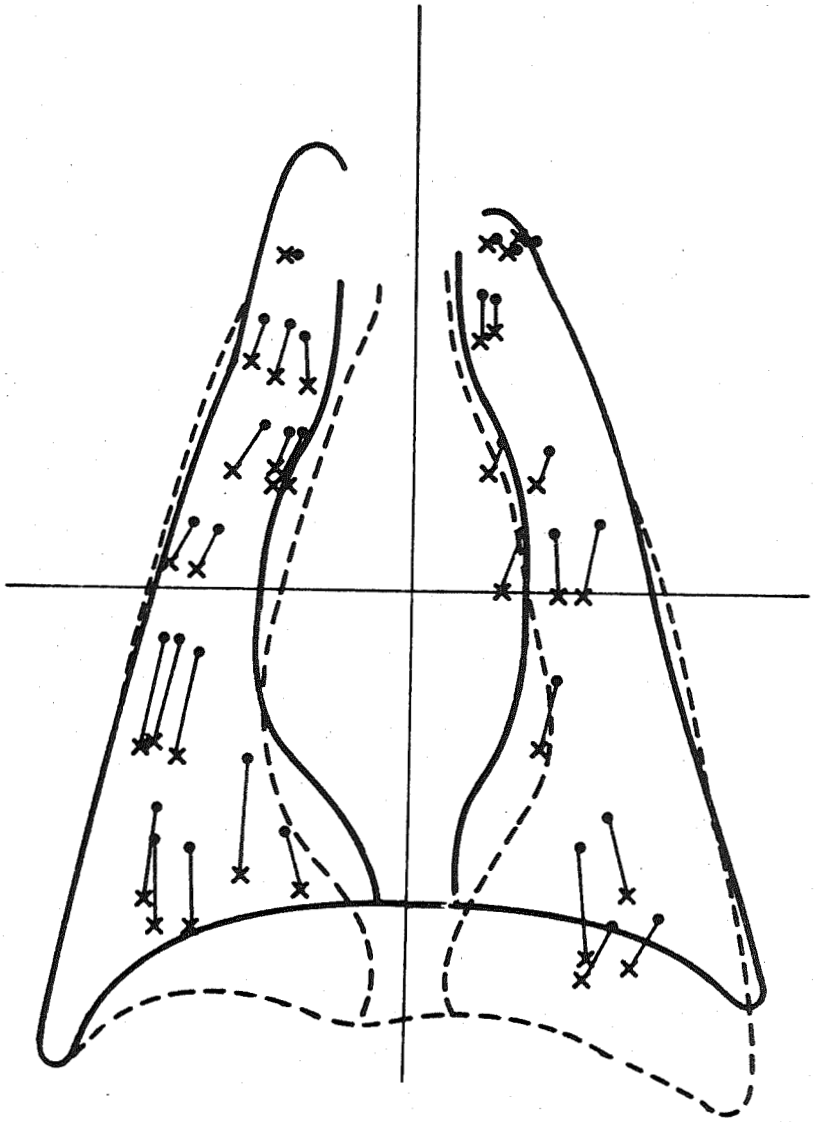

Figure 7

REGIONAL DISPLACEMENT OF LUNG PARENCHYMAL TAGS AT FRC DURING CHANGE IN BODY POSITION FROM PRONE TO HEAD-UP AND HEAD-DOWN POSITIONS

(3 Dogs, Morphine-Pentobarbital Anesthesia, 37-40 Tags/Dog)

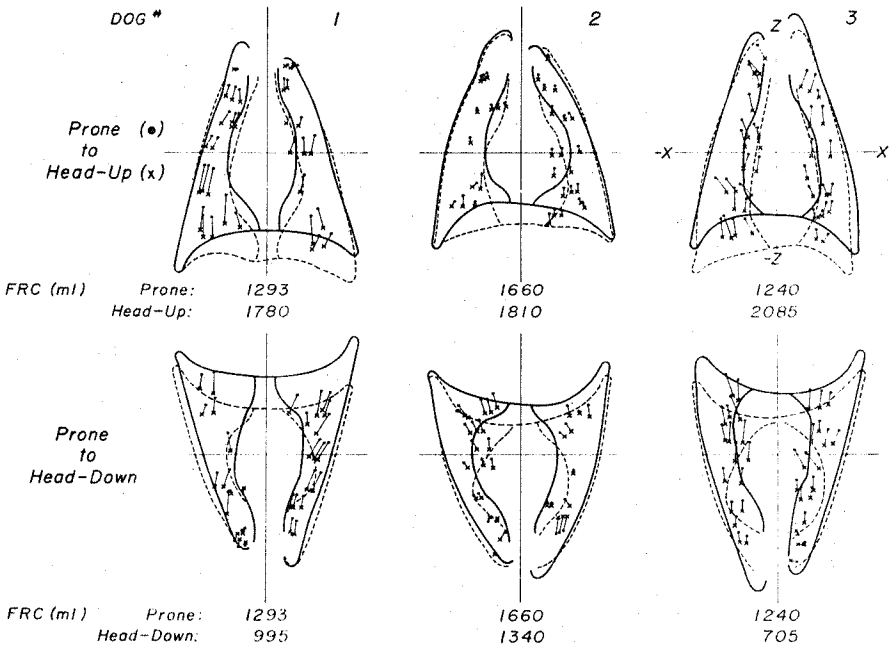

Figure 8

COMPARISON OF REGIONAL DISPLACEMENT
OF LUNG PARENCHYMAL TAGS DURING SPONTANEOUS
INSPIRATION IN THE HEAD-UP AND HEAD-DOWN POSITIONS

(Dog-21.5 kg, Morphine-Pentobarbital Anesthesia)

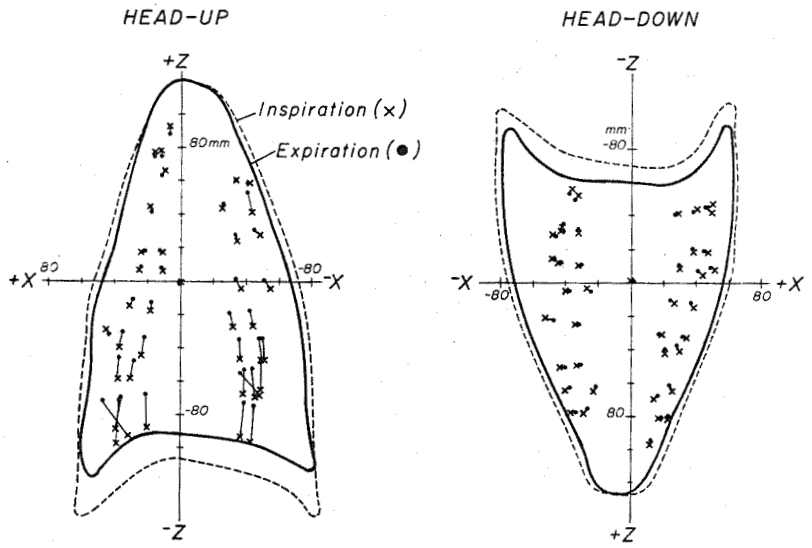

Figure 9

COMPARISON OF DISPLACEMENT OF LUNG
PARENCHYMAL TAGS FROM FRC DURING SPONTANEOUS
INSPIRATION AND POSITIVE PRESSURE INFLATION

(Dog-21.5 kg, Morphine—Pentobarbital Anesthesia, Prone Position)

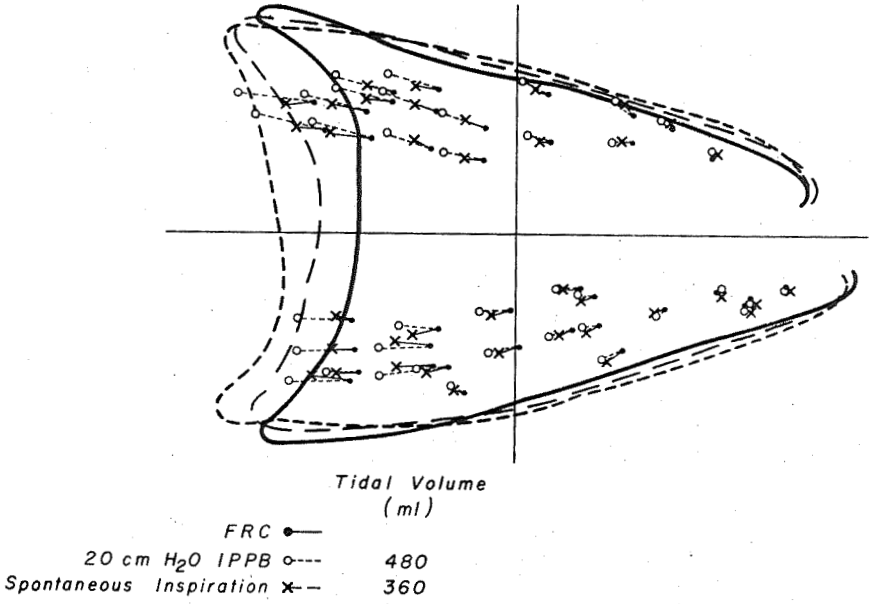

Figure 10

Section VII

Effect of Changes in the Magnitude and Direction of the Force Environment on Regional Distortion of Lung Parenchyma in Dogs*

J. F. Greenleaf, H. C. Smith, A. A. Bove, D. J. Sass, and E. H. Wood

It has been known for some time that posture affects the geometry of the lung due to changes in the gravitational force vector.

Figure 1 indicates a model of a mechanism by which the inertial force environment may effect the lung parenchyma.

The circles are the air containing tissue while the surrounding regions are the blood containing vessels and lung parenchyma. In the presence of gravity hydrostatic pressure gradients in the vessels and the weight of parenchymal tissue and mediastinal structures cause vertical gradients in volume of the air containing parts of the lung. An increased gravitational inertial force environment exaggerates the differences in weight of the air containing alveoli and the surrounding blood and tissue and hence causes higher gradients in volume down the lung.

Study of the effects of the normal gravitational inertial force environment on the lung can be facilitated by magnifying such effects with the use of a centrifuge.

During an increased force environment such as induced by centripedal acceleration in a centrifuge shifts in the heavier than lung chest walls and abdominal contents which cause diaphragmatic distortions can be minimized if the body is supported by immersion in a liquid (water) with specific gravity similar to that of blood and tissue. In addition to better body support, enclosure of the animal in a water immersion respirator provides the capability of accurate control of the respiratory rate plus tidal and residual volumes.

Figure 2 is a schematic diagram of the water immersion respirator. The animal is enclosed in a rectangular lucite chamber filled with isotonic saline. His airway is open to the outside and air is pushed in and out of the lungs by the variation in pressure over the entire surface of the body produced by sinusoidal additions and withdrawal of water from the chamber by the respiration pump. Thus, the effect of gravitational and inertial forces on the animal's body are minimized since the entire animal is supported in water.

We have used the method described by Smith and coworkers for measuring the position, by orthogonal x-rays, of percutaneously implanted metallic tags

---

*Presentation at fall meeting of American Physiological Society, University of Kansas Medical School, Lawrence, Kansas, Aug. 17, 1971.

to determine regional changes in position and volume of lung parenchyma of three anesthetized dogs while at 1G and during exposures to 7 times the normal inertial force environment while in a water respirator.

All dogs were in the left lateral decubitus position and were ventilated with air at about 8 breaths/min and a tidal volume of 480 ml. The positions of the metallic markers were measured from orthogonal thoracic roentgenograms with corrections for geometric distortions due to the divergent character of the x-ray beams.

Each dog had 30-40 markers distributed in a roughly grid-like pattern throughout the lungs. Movements of the resulting 90-120 markers from the three animals were averaged-depending on their position within the lung - in a manner whose description can be facilitated by reference to Figure 3.

The zero reference point for the three-dimensional coordinate system used for all of the dogs was set at the mid-point of the body of the sixth thoracic vertebra. This point is approximately at the caudad to cephalad and left to right mid-points of the normal lungs.

The position of each parenchymal tag, and the outlines of the lung borders in relation to this reference point were fed into a 3500 CDC computer by means of an electronic cursor device. The computer was programmed to divide lungs mathematically into 25 parallelapiped corridors arranged in a 5x5 array. The positions of the tags in these corridors which are 3cm x 4 cm on a side and extend from the ventral to the dorsal surface of the lungs were projected onto the coronal plane of the thorax. The position of the tags in similar corridors 3 cm x 3 cm on a side and extending from the caudad to cephalad surfaces of the lung were projected on the cross sectional plane of the thorax, since both of these anatomically designated planes are parallel to the resultant vector of the inertial force environment when the dog is in the left decubitus position, these projections portray the distribution and movement of the lung parenchymal tags in the vertical direction in relation to the vertical height in the thorax.

The average shifts in positions of all of the beads falling within each corridor are represented by the arrows whose tails (representing position at functional residual capacity in this case) are centered within their respective corridor as it is projected onto the plane of interest.

The standard error of the mean changes in position in the cephalo-caudad and right to left directions are indicated by the respective lengths of the

bars of the crosses at the ends of each line. No cross indicates there was only 1 sample.

Note the effect of the downward displacement of the diaphragm during inspiration in shifting the lung parenchyma. The tags moved caudal-wards in all regions and lateral-ward in the lateral regions of the lung during inspiration in the normal 1 g environment. The cross sectional projection indicates that the lung parenchyma shifted in the ventral direction during the inspiratory movement from their position at functional residual capacity.

This figure portrays only the changes in position of parenchymal tags located in different regions of the lung. However, the changes in regional volumes of the lung calculated from the differences in the changes in position of adjacent tags which occur during a breath (i.e., regional ventilation) or under conditions of increased inertial force environment are also of interest. Regional volumes were calculated by taking pairs of markers falling within each corridor to represent diametrically opposite points on a sphere of parenchyma. The percent change in volume of this sphere between two states of interest was then taken to represent the regional change in volume. Volumes were calculated for all combinations of two markers falling within each corridor for each dog and the average % volume change with its standard error were calculated for each corridor.

The regional changes in volume calculated from the changes in position, shown in Figure 3, from functional residual capacity to end inspiration (i.e., regional ventilation) are shown in Figure 4. The circles with a continuous outline all have the same diameter, representing the control state (in this case end expiration, i.e., FRC), and are centered in their respective corridor. The circles with dashed outline and varying diameters represent the volume at the second state (end inspiration) and are centered on the position to which the control element moved. The numbers represent the percent change in volume $\pm$ one standard error. The absence of a standard error value indicates that only one pair of markers was found in that corridor.

Note the distribution of % change in volume is relatively uniform in the dorsal-ventral projection with no discernible regional pattern. The cross sectional projection indicates a like result.

In order to discuss the respiratory cyclic changes during exposure to an inertial force environment 7 times normal, we will first indicate the effect of increased inertial forces on the lung parenchyma when the animal

is at functional residual capacity under these two conditions.

Figure 5 illustrates the average regional change in position and volume of lung parenchyma at end expiration during a 1 minute exposure to a force environment of 7 G_y.

The solid circles and dots represent the 1G control state and the dashed circles and standard errors the 7G state.

Note the loss of volume in the dependent portion of the lung and the gain of volume in the superior portions and the general shift of the parenchyma in the cephalad direction in the dependent-lung and concomitant caudad shift superiorly caused by this increased inertial force environment.

The cross sectional projection indicates an almost vertically downward displacement of the parenchyma again with a loss of volume in the dependent region and an increase in the superior region.

Figure 6 shows the regional change in parenchymal position and volume with inspiration during an inertial force environment 7 times normal. Note the larger change in volume in a region slightly above mid-lung and the relatively small or no change in volume in most of the dependent regions.

Note as well that the parenchyma tends to shift both caudally and in the dependent direction during inspiration rather than evenly toward the diaphragm and bilaterally as in the 1G case.

To facilitate study of changes in regional volume in relation to vertical height in the thorax, we divided the lung into 10 sagittal sections each 1.5 cm thick and projected the average change in volume in each sagittal section onto the coronal plane in order to obtain a plot of change in regional volume versus vertical height in the thorax. The regional changes in volume with inspiration in the normal 1G gravitational force environment is shown in Figure 7.

Note that the inspiratory changes in regional volumes (regional ventilation) of the dependent left lung and superior right lung were not significantly different.

The regional changes at end expiration caused by an exposure to 7 times the normal gravitational inertial force environment are shown in Figure 8.

As would be expected on the basis of the great differences in specific gravity of the air containing alveoli and the surrounding elastic parenchyma and mobile blood, there is a striking increase in regional volumes in the superior

region and decrease in the dependent region of the lung. The isovolume region appears to be near mid-lung or slightly above.

Figure 9 indicates that at 7 times the normal gravitational force environment the change in regional volume during inspiration is greatest at the mid-region of the lung.

It is particularly noteworthy that this region is at approximately the same vertical height in the thorax where the regional changes in volume at end expiration with changes in the force environment are minimal (Figure 6) and at which prior studies have demonstrated the level of pleural and circulatory pressures are relatively independent of the force environment and where regional blood flow is maximal during exposures to higher force environments.

These data indicate that under conditions of increased acceleration the lung parenchyma tends to shift as though it consisted of bubble like bouyant chambers somewhat free to float upward. Calculated changes in regional volume based on differences in displacement of adjacent lung parenchymal tags indicated that large increases in regional volume in superior regions of the lung occur during exposures to an increased force environment, concomitantly, with striking decreases in regional volumes in dependent regions.

The calculated changes in regional volume during inspiration indicate that ventilation is shifted into the mid-region of the lung during exposure to high force environments.

DIAGRAM OF THE EFFECTS OF FORWARD ($+G_x$) ACCELERATION ON INTRATHORACIC PRESSURES

(Dorso–Ventral Dimension of Lung: 20 cm.)

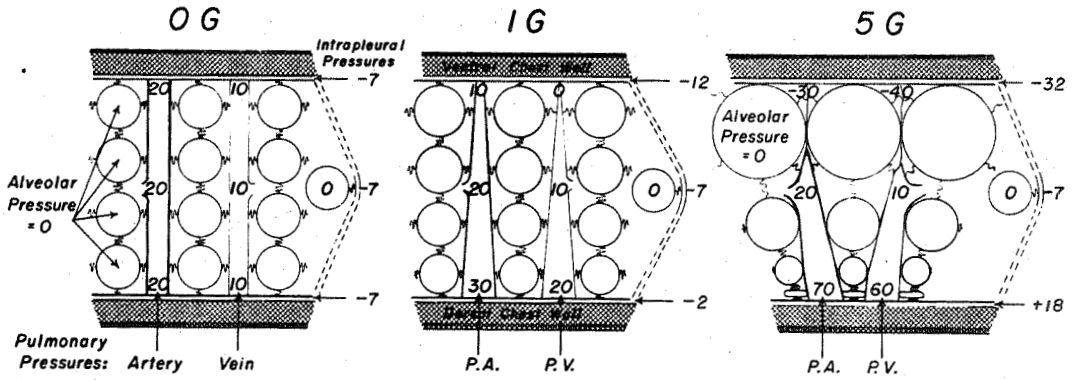

Numerals = Pressures in cm. H_2O

O Reference Level = Atmospheric Pressure at Mid Dorso–Ventral Chest Level

Figure 1

ASSEMBLY FOR STUDY OF EFFECTS OF WATER IMMERSION ON INTRATHORACIC PRESSURE RELATIONSHIPS

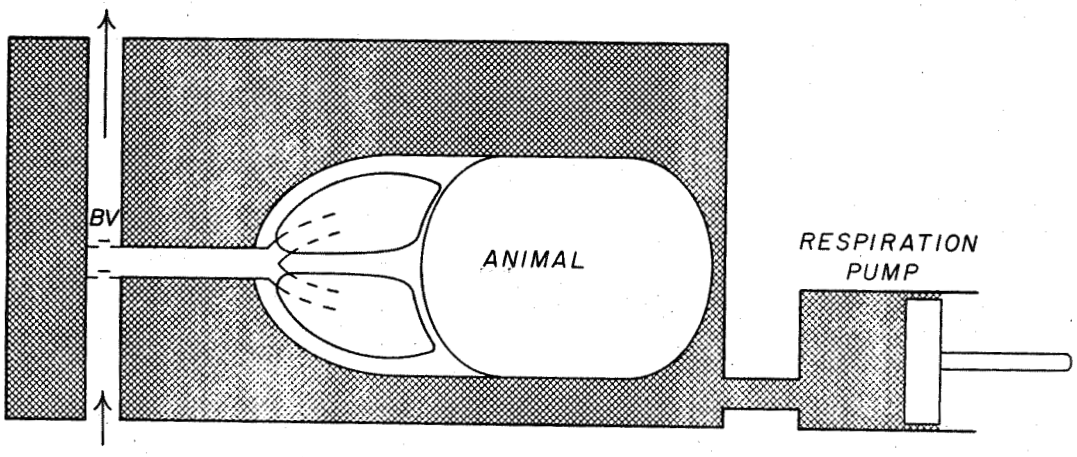

BV = Breathing Valve

Saline

Figure 2

CHANGES IN POSITION OF LUNG PARENCHYMAL TAGS DURING RESPIRATORY CYCLE IN WATER-IMMERSION RESPIRATOR

3 Dogs, Morphine-Pentobarbital Anesthesia, Left Decubitus Position
(+) SE of Inspiratory Change In Y and Z Coordinates

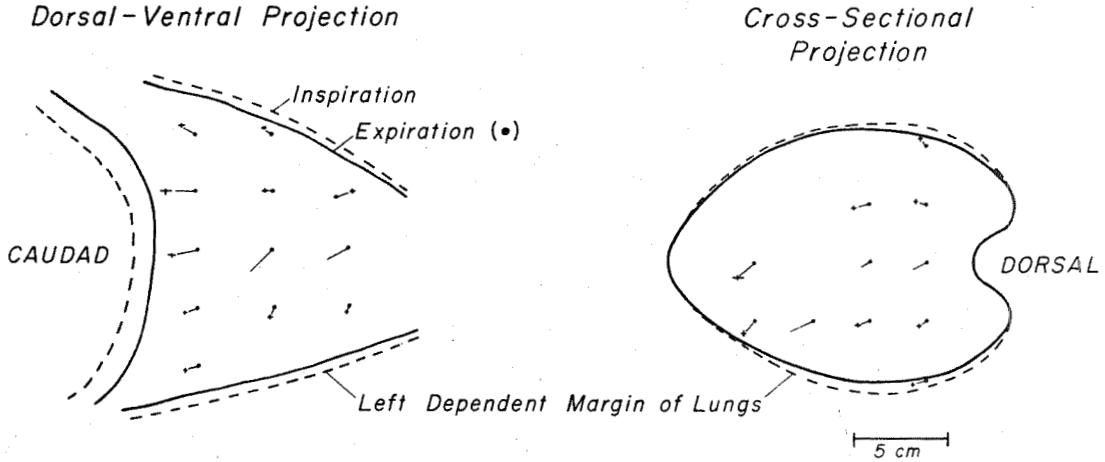

Figure 3

CHANGES IN POSITION OF LUNG PARENCHYMAL TAGS DURING RESPIRATORY CYCLE IN WATER-IMMERSION RESPIRATOR

3 Dogs, Morphine-Pentobarbital Anesthesia, Left Decubitus Position
(+) SE of Inspiratory Change In Y and Z Coordinates

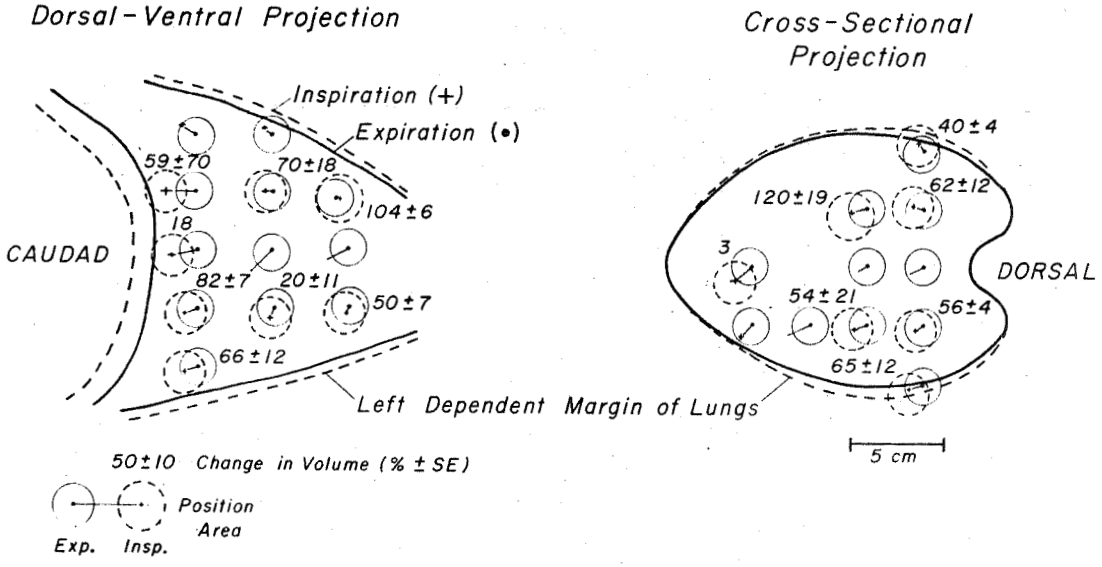

Figure 4

EFFECT OF INCREASED FORCE ENVIRONMENT ON REGIONAL POSITION OF LUNG PARENCHYMAL TAGS AND CALCULATED REGIONAL VOLUMES AT END-EXPIRATION IN WATER-IMMERSION RESPIRATOR

3 Dogs, Morphine-Pentobarbital Anesthesia, Left Decubitus Position
(+) SE of 1 G_y to 7 G_y Change in Y and Z Coordinates

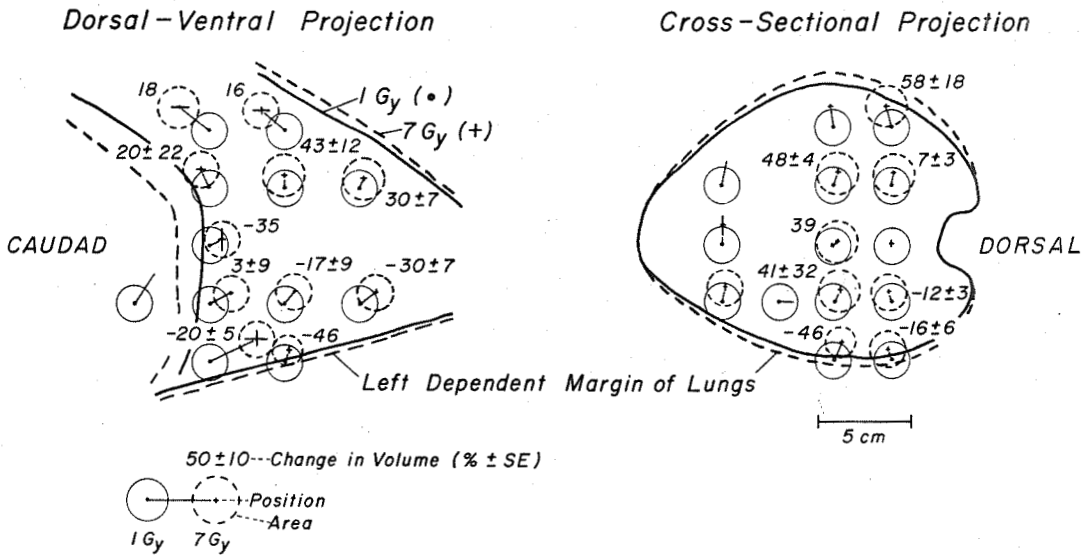

Figure 5

CHANGES IN POSITION OF LUNG PARENCHYMAL TAGS AND CALCULATED REGIONAL VOLUMES IN RESPIRATORY CYCLE DURING EXPOSURE TO FORCE ENVIRONMENT OF 7 G_y IN WATER-IMMERSION RESPIRATOR

3 Dogs, Morphine-Pentobarbital Anesthesia, Left Decubitus Position
(+) SE of Inspiratory Change in Y and Z Coordinates

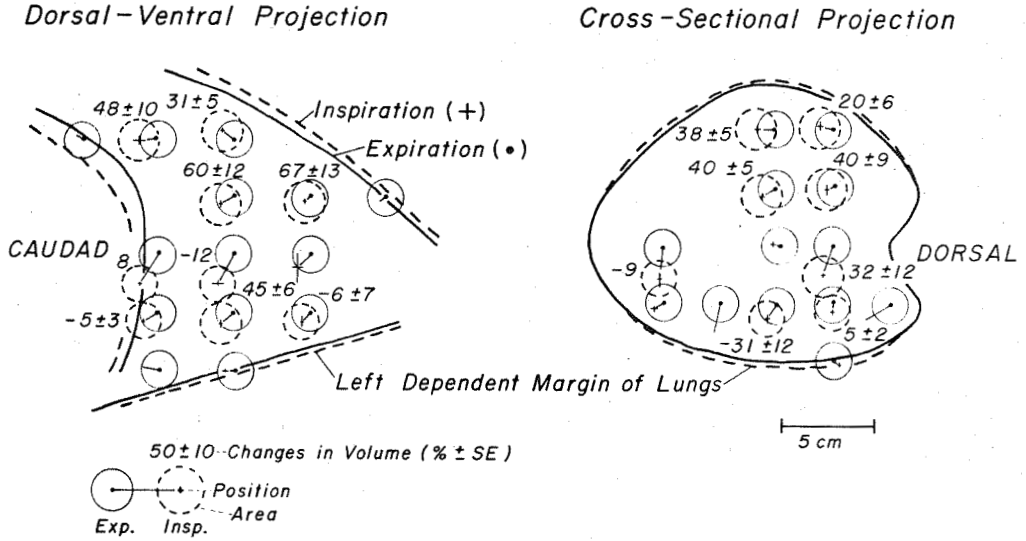

Figure 6

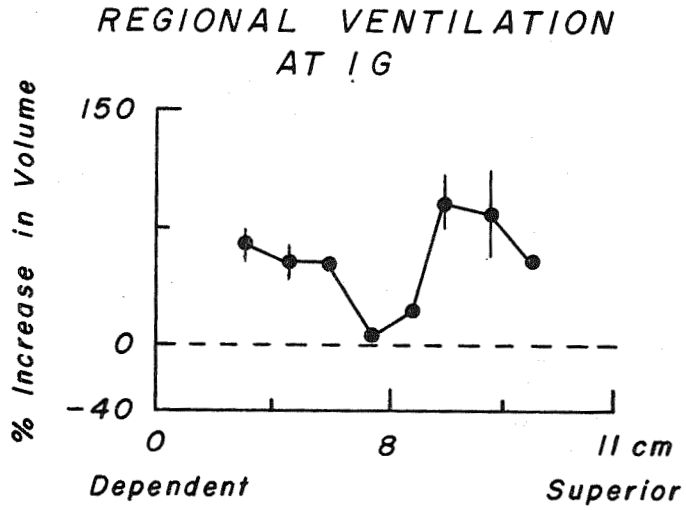

Figure 7

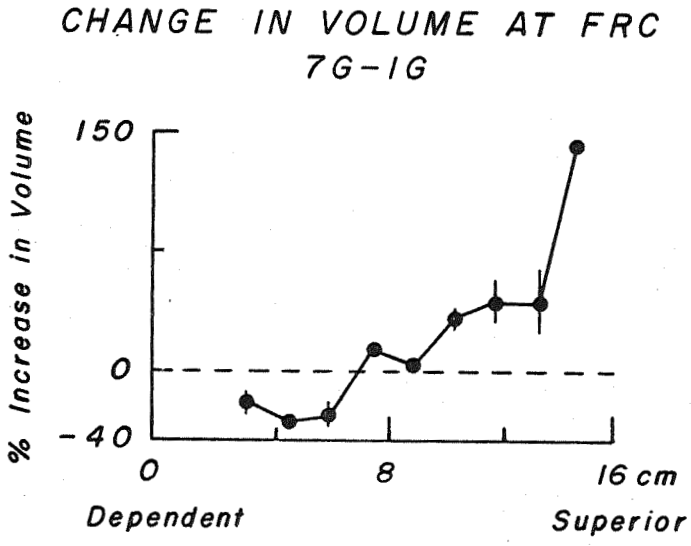

Figure 8

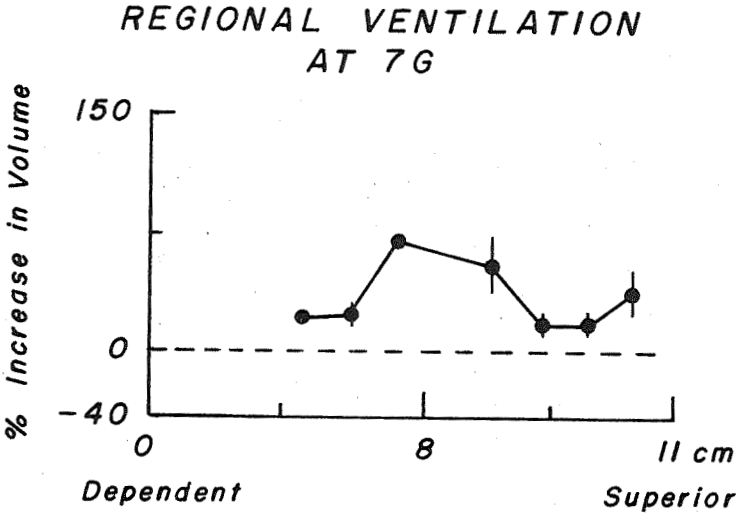

Figure 9

Section VIII

RESPIRATORY VARIATIONS IN LEFT VENTRICULAR STROKE VOLUME DURING LIQUID BREATHING *

D. J. Sass, M.D., E. L. Ritman, M.B., P. E. Caskey, B.S., W. Van Norman, B.S., and E. H. Wood, M.D. Ph.D.
Mayo Foundation, Mayo Graduate School of Medicine, Rochester, Minnesota 55901

In a previous study in dogs breathing oxygenated liquid fluorocarbon (FC 80, 3 M Company) in a water-immersion respirator, the oxygen saturation of blood continuously withdrawn from the thoracic aorta and left (dependent) pulmonary vein could be maintained at 100%; however, the oxygen saturation in mixed systemic (pulmonary artery) blood varied in an approximately sinusoidal manner with the same frequency but not in phase with respiration. These variations were thought to be caused by changes in cardiac output consequent to the sinusoidal changes in external and internal body pressures produced by the respirator (1). The purpose of the present investigation was to study the beat-to-beat changes in left ventricular stroke volume in relation to the phase of respiration in right lateral decubitus dogs breathing first air, then oxygenated liquid fluorocarbon in a water-immersion respirator providing control of respiration rate, tidal and residual lung volumes.

Methods

Slide 1 illustrates the whole-body water-immersion respirator, liquid respiration assembly. The anesthetized dog was positioned on its right side in the transparent acryclic immersion tank which was then filled with saline at 37°C. A flexible tygon endotracheal tube, introduced through a tracheotomy, was connected to an inspiratory-expiratory breathing valve near the animal's neck. Separate tygon lines connected the inspiratory and expiratory ports of the breathing valve to a pair of two-way manually operated valves mounted on the outside of the immersion tank. Thus, the animal's airway could be connected via these valves to either room air or to the breathing compartment containing oxygenated FC 80 liquid fluorocarbon. FC-80 has been used as a respirable liquid in previous animal experiments in this and other laboratories (1,2). The solubilities of oxygen and carbon dioxide in FC 80 are approximately 40 ml of oxygen and 160 ml carbon dioxide per 100 ml FC 80 at 37°C and 1 atmosphere (3,4).

During the air breathing experiments, the respiration pump ventilated the animal by pumping saline to and from the immersion tank in a nearly sinusoidal manner. Respiration rate and tidal volume were continuously variable between 0 and 20 cycles per minute, and 0 and 480 milliliters per stroke, respectively. Residual lung volume was adjusted by either adding or removing saline to or from the immersion tank. Tidal volume was measured with a spirometer, and residual lung volume by application of a Boyle's law technique.

During the liquid breathing experiments, the animal's airway was connected to the breathing compartment, an open reservoir containing approximately 4 liters of oxygenated FC 80 with the liquid level adjusted to the midchest level of the animal. Liquid fluorocarbon flowed passively between the airway and reservoir in response to the alterations in body surface pressure developed in the immersion tank by the respiration pump. Partial closure of the major airways during part of the expiratory phase of liquid respiration occurred when the liquid level in the breathing compartment was more than a few centimeters below the animal's midchest level.

Fluorocarbon was oxygenated and carbon dioxide removed by flowing the liquid over an 8-inch spinning disc (3600 rpm) to aerosolize the liquid in a 100% oxygen atmosphere maintained by a 5 liters per minute flow of oxygen through the oxygenator. The recirculation pump replenished the breathing compartment with freshly oxygenated fluorocarbon.

Nine weeks prior to this study, a dual-channel square-wave electromagnetic flowmeter (Carolina Medical Electronics model 322) was implanted around the root of the aorta of a 13.5 kg dog, and eight weeks prior to the study, complete heart block was produced in this animal by formaldehyde injection into the A-V bundle by a percutaneous technique (5). On the day of the study, catheters were introduced percutaneously into the vascular system and their tips positioned under fluoroscopic control as follows: two catheters in the main pulmonary artery (pressure recording and sampling), one each in the thoracic aorta (pressure) and abdominal aorta (sampling), right atrium, right ventricle, and one in the inferior vena cava for reinfusion of blood withdrawn through the cuvette oximeters. The right atrial and right ventricular catheters also incorporated electrodes for electrical pacing of the heart in addition to their use for pressure recording. Two catheters were introduced without thoracotomy into the left and right pleural spaces, and their tips manipulated under fluoroscopic control to the most superior and dependent margins of the lungs, respectively. An esophageal catheter was used for recording pressure and aspiration, and a gastric catheter was placed for aspiration only. Two concentric catheters recorded pressures from the endotracheal tube (outer catheter) and lower trachea (inner) for detection of partial closure of the trachea if it occurred during liquid respiration.

The positions of most of the catheters and the flowmeter probe are shown in the lateral roentgenogram obtained during the catheterization procedure (left-hand panel of Slide 2). All catheters were filled with heparinized Ringer's solution and were connected via individual ports in the side of the immersion tank to strain gauge manometers mounted outside the tank at approximately midchest level of the dog. This level, determined from P-A roentgenograms, was used as the zero-pressure reference for all manometers. The vertical distances of the pleural and esophageal catheter tips

* Presented at the Aerospace Medical Assn. meeting, Houston, Texas, April 26-29, 1971.

relative to the midlung level were measured from biplane roentgenograms, and these distances were used to correct the pleural and esophageal pressures to their respective catheter tip levels.

Oxygen saturation was measured continuously in blood sampled from the pulmonary artery and femoral artery by withdrawal through cuvette oximeters. Cardiac output was measured with the indocyanine green dye technique at different phases of respiration, and these values were used to calibrate the flowmeter when the dog breathed room air spontaneously at the start of the study. The oximeter and densitometer signals were digitized and analyzed by an on-line CDC 3300 digital computer by techniques previously described (6). The flowmeter signal, all strain gauge data, pneumotachograph signal, ECG, respiration pump displacement, cuvette and densitometer signals, and other variables were recorded in parallel on digital tape, analog tape, and two paper photokymographic recorders. Blood and liquid fluorocarbon gas tensions were measured periodically with an IL 113 blood gas analyzer. The heart was electrically paced at 140 per minute with an A-V delay of 100 milliseconds throughout the study.

Baseline recordings of oxygen saturation, blood gas tensions, cardiac output, left ventricular stroke volume (flowmeter), pressures, biplane roentgenograms, and other data were first obtained with the dog breathing air spontaneously. The immersion tank was then filled with isotonic saline at 37°C, and the volume of saline adjusted until the variations in tank pressure produced by the respiration pump were balanced around zero, measured at midchest level. All measurements were repeated with the dog immersed and mechanically ventilated with room air at approximately ten to twelve 320 ml breaths per minute. The animal was then ventilated with 100% oxygen for 10-15 minutes to remove nitrogen from the respiratory tree and body tissues before connecting the animal's airway to the breathing compartment containing oxygenated liquid fluorocarbon at 37°C. The respiration rate was then reduced to approximately three to four 480 ml breaths per minute and the liquid breathing studies performed. The water immersed dog was also subjected when breathing first air and then fluorocarbon to one-minute exposures to -4Gy and -7Gy force environments produced by the human centrifuge, but the results of these experiments will not be reported here.

Anesthesia was maintained at all times with sodium pentobarbital and morphine.

Results

Left ventricular stroke volume was calculated from the flowmeter signal by an on-line CDC 3300 digital computer and the beat-to-beat values were plotted versus time by a computer driven incremental plotter (Calcomp) along with concomitant measurements of intrathoracic pressures and other variables. The left-hand panel of Slide 3 is an example of one such computer-generated plot of stroke volume, right pleural pressure, and airway pressure obtained during an experiment in which the water-immersed dog was ventilated with room air. The right-hand panel of Slide 3 is a similar plot obtained during a liquid breathing experiment.

The plots of left ventricular stroke volume versus time were approximately sinusoidal and synchronized with respiration (9-10 per minute when breathing air and 3-4 per minute when breathing liquid fluorocarbon), as illustrated in Slide 4. Maximum stroke volume occurred soon after the start of the inspiratory phase when the dog breathed air, and just prior to full inspiration when the dog breathed fluorocarbon. The average stroke volume was approximately 1/3 greater, and the peak-to-peak changes in stroke volume were roughly twice as great, comparing plots from liquid breathing and air breathing experiments, respectively.

Slide 5 is a plot of right (dependent) and left (superior) pleural pressures, and pressures in the esophagus measured at the respective catheter tips during maximum expiration versus the vertical distance of the catheter tip from the midlung level. During both air-breathing and liquid-breathing experiments, the pressure in the superior pleural space was more negative than in the dependent space. However, when breathing air, the vertical gradient in the pleural pressures averaged 0.49 cm H_2O/cm, a value consistent with results from previous studies in air-breathing dogs and chimpanzees measured in this laboratory (6), whereas, during liquid breathing, the gradient was nearly 1.0, a value which would be predicted from hydrostatic principles if the catheter tips were positioned at different levels in a liquid-filled container.

Important to these results, is the fact that this dog developed a chronic pleural effusion shortly after implantation of the flowmeter probe and required frequent aspirations of pleural fluid both before and during the present experiments. All of the biplane roentgenograms obtained during the present study clearly demonstrate remaining fluid in both pleural spaces which could not be completely aspirated through the pleural catheters. We, therefore, conclude that the pleural pressure gradient of nearly 1.0 resulted from both catheter tips being positioned in two vertical hydraulic spaces separated only by the thin, nearly horizontal anterior and posterior mediastinal membranes.

The results of this study indicate that the phasic variations in body surface pressures and concomitant induced changes in intrathoracic, airway, and other internal body pressures required to maintain adequate respiratory gas exchange with liquid fluorocarbon produce large variations in cardiac output which are reflected by variations in the oxygen contents of mixed venous blood. These results also indicate that indicator-dilution methods cannot be used to accurately measure cardiac output during liquid ventilation.

Supported by USAF41609-C-0058, U.S. Navy, AHA CI 10.

1. Sass et al, NATO/AGARD, Garmisch, 1970, Germany.
2. Clark and Gollan, Science 152:1755, 1966.
3. 3M Company Bulletin, St. Paul, Minn. 1965.
4. Unpublished data (this laboratory) 1971.
5. Williams et al, J Appl Physiol 27:740, 1969.
6. Wood et al, SAM TR 70-6, Brooks AFB, Feb. 1970.

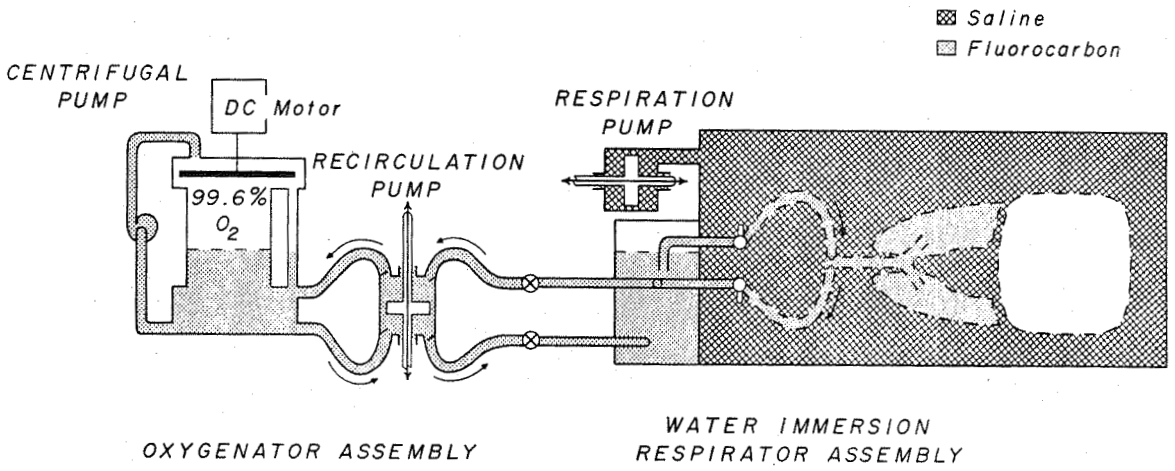

Figure 1 Diagram of water-immersion respirator and fluorocarbon oxygenator assembly used for liquid breathing experiments.

The dog, who is completely immersed in isotonic saline, is represented by a diagrammatic sketch of fluorocarbon-filled lungs and a blank space of the remainder of his body.

THORACIC ROENTGENOGRAMS SHOWING POSITION OF SENSING DEVICES FOR BREATHING LIQUID FLUOROCARBON

(13.5 kg Dog, Right Decubitus Position, Morphine - Pentobarbital Anesthesia)

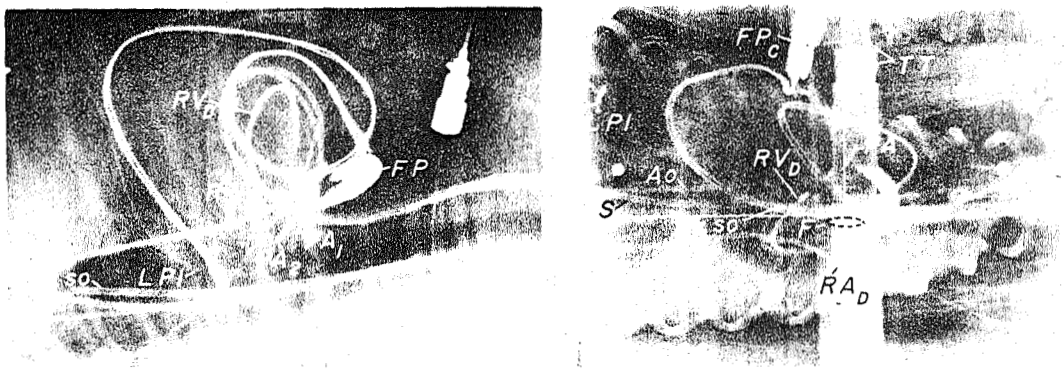

Figure 2 Lateral roentgenogram before beginning of liquid breathing (left) and dorsal-ventral roentgenogram during liquid breathing (right).

FP and FP_C; electromagnetic flow probe chronically implanted around ascending aorta, and its cutaneous connector, respectively.

RV_D and RA_D; electrode catheters with tips positioned in right ventricular outflow tract and in right atrium near the superior caval orifice, respectively, for control of heart rate and atrial-ventricular systolic interval.

LPl and RPl catheters with tips positioned in pleural space at left superior and right dependent margins of lungs, respectively.

PA_1 and PA_2 catheters with tips positioned in pulmonary artery.

Eso, Ao, and S catheters with tips positioned in esophagus, thoracic aorta, and stomach, respectively.

ECG; electrocardiographic leads.

TT; bilateral fluid-filled tubes with menisci (F) at midlung level for recording this zero reference level for each strain gauge-catheter manometer system by connecting each gauge via its respective remotely controlled three-way stopcock to this hydraulic pressure reference system.

Note in the right panel that: 1) the lung ields appear as lighter areas in relation to the darker silhouette of the heart, which is less dense than the fluorocargon filled lungs; 2) the dark margin between the superior border of the lungs and the parietal margin of the thoracic wall caused by pleural fluid displaced upward by the heavier fluorocargon-filled lungs. The sterile pleural effusion present in this dog was a non-infectious reaction to the implanted flowmeter.

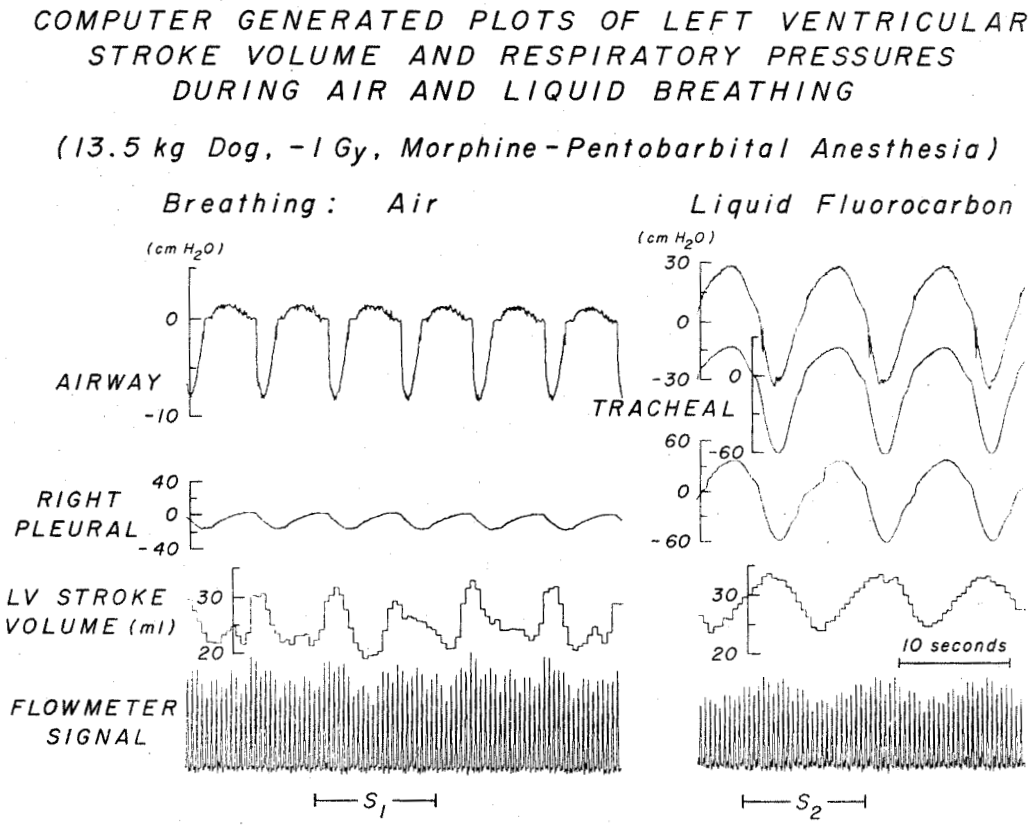

Figure 3 Computer generated plots illustrating the phasic relationships between the respiratory cyclic changes in airway and pleural pressures generated by the water immersion respirator and the associated variations in left ventricular stroke volume.

S_1 and S_2 indicate the time intervals in their recordings, tracings from which are displayed on a faster time base in Figure 4.

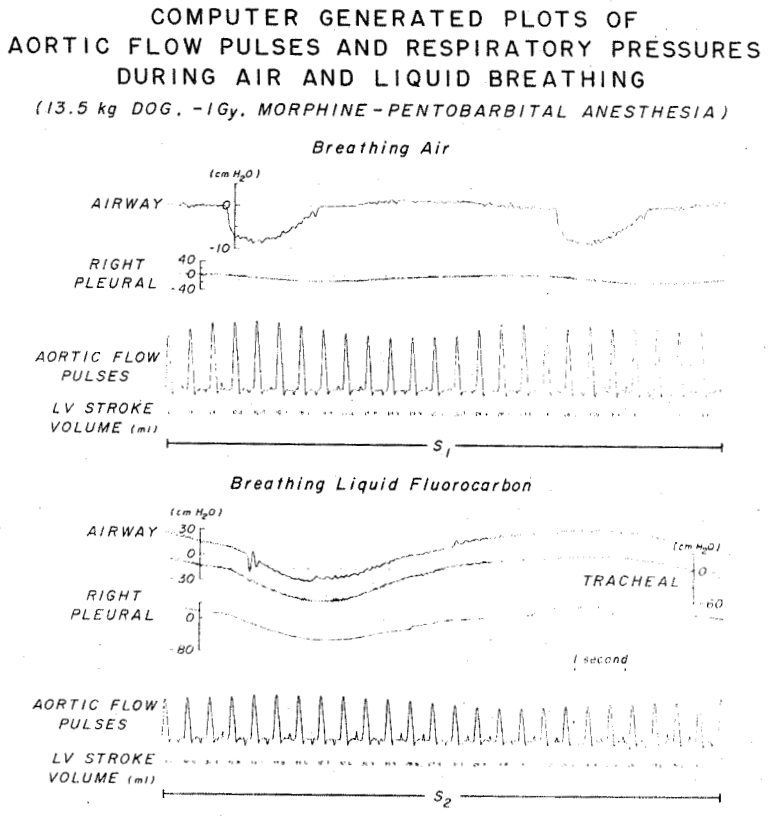

Figure 4 Computer generated plots of aortic flow pulses and respiratory pressures during air and liquid breathing.

See legend of Figure 3 for additional details.

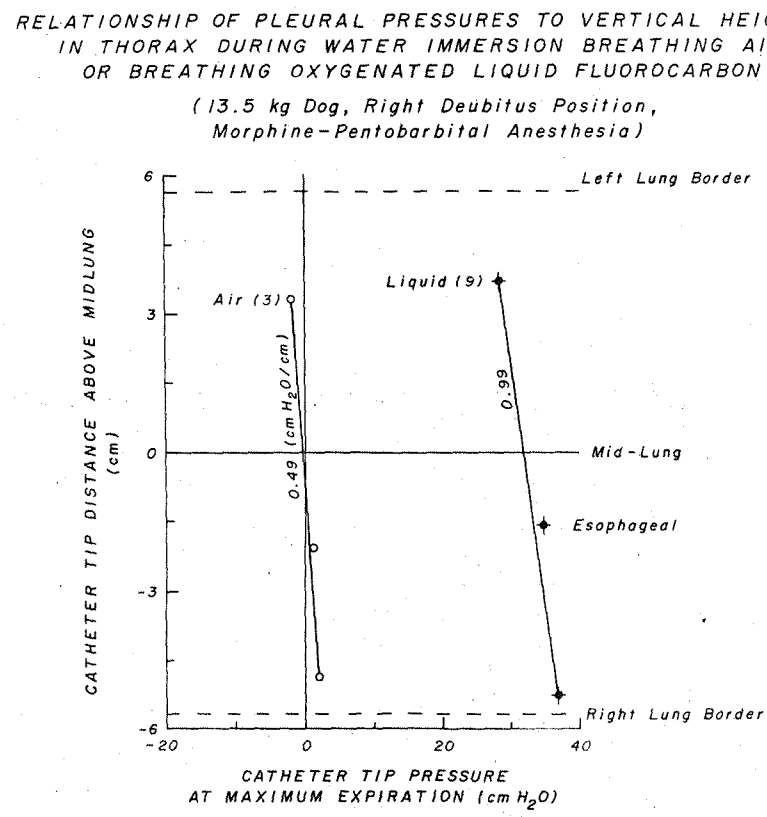

Figure 5 Relationship of pleural pressures to vertical height in thorax during water immersion breathing air or breathing oxygenated liquid fluorocarbon. Note the increased mean vertical gradient in pleural fluid pressures when breathing liquid fluorocarbon.

Section IX

EFFECTS OF ACCELERATION ON PULMONARY BLOOD FLOW IN DOGS BREATHING ORGANIC LIQUIDS*

D. J. Sass, J. F. Greenleaf, H. C. Smith, A. A. Bove, and E. H. Wood

Introduction

We measured the distribution of pulmonary blood flow in dogs breathing first air and then either the liquid fluorocarbon, FC 80, which has a specific gravity of about 1.8 (1), or silicone oil, DC 200, which has a specific of 0.8 (2). Pulmonary blood flow was measured by injecting radioactive 15 micron microspheres into the right ventricle, excising and drying the lungs which were then held inflated with air by a steady tracheal pressure of 30 cm H_2O (Figure 1). The dried lungs (left panel) were potted in a polyurethane foam block and sliced transversely on a bandsaw into 20-25 1-cm thick sections (as shown in the right panel). The complete cephalad surface of each section was scanned to determine the blood flow per cubic centimeter of inflated lung tissue, using a high resolution computer controlled scintillation scanner assembly previously developed in this laboratory (3). Up to four injections of differentially tagged microspheres could be made in each dog. The spatial distribution of blood flow was determined for each injection on the basis of the different energy spectra of the respective isotope tags. Blood flow was determined at 1 and 7G with the dog on its left side, breathing first room air and then an organic liquid.

Methods

A water immersion respirator (Figure 2) was used to control respiratory rate, tidal, and residual lung volume. The dogs were placed on their left side in the lucite immersion tank which was then completely filled with isotonic saline at 37°C. The airway was connected to either room air or to the oxygenated liquid via two external valves. The respiration pump

---

*Presentation at fall meeting of American Physiological Society, University of Kansas Medical School, Lawrence, Kansas, Aug. 17, 1971.

moved saline in and out of the tank sinusoidally, and either room air or liquid flowed passively in and out of the lungs in response to the alternating pressures applied to the entire body surface by the pump. The exhaled liquid received in the exhalation compartment was pumped upward and flowed over a rapidly spinning horizontal disc, which nebulized it into a 100% oxygen atmosphere. The level of freshly oxygenated liquid in the inhalation chamber was maintained at midchest level, and heaters regulated its temperature at 37°C. Residual lung volume was controlled by adding or removing saline from the immersion tank and was measured by reading the liquid levels in the two chambers.

Figure 3 shows thoracic roentgenograms obtained when the dog breathed room air at 1 and 6G (left panels), and in the two right panels, when the same animal breathed fluorocarbon at 1 and 6G. Catheters visible in the roentgenogram were introduced without thoracotomy and positioned in the pulmonary artery, left and right atria, aorta, left pulmonary vein, and trachea or bronchus. Two saline-filled catheters were introduced into the left and right pleural spaces, also without thoracotomy, and their tips positioned over the lateral margins of the superior right and dependent left lungs. Microspheres were injected into the right ventricle by a pneumatically driven syringe.

Figure 4 shows a photokymograph recording of the multiple physiological pressures and other variables measured in all dogs to illustrate the conditions under which the microspheres were injected; in this case during an exposure to a force environment of 7Gy when breathing air (top panel) and breathing silicone oil (lower panel). The sinusoidal variations in the pressure traces are due to the sinusoidal alterations in body surface pressure produced by the respiration pump. The pump was stopped in the inspiratory phase of the cycle, and the pressures allowed to stabilize for several seconds before the microspheres were injected. During the 7G exposures, the microspheres were injected 120 seconds after the centrifuge reached the 7G plateau.

The three-dimensional array of counts generated by scanning the entire cephalad surface of every lung section successively from the apex to the costophrenic angles can be, depending on the computer program used, displayed in any projection or section of the lung desired in correct anatomical relationship to the topography of the inflated lung.

Results

Figure 5 is a dorsal-ventral projection of the vertical distribution of pulmonary blood flow in one dog; first (in the right panel) when breathing air at 1Gy (solid line) and at 7Gy (dashed line) and then when breathing liquid fluorocarbon under the same conditions, right panel. The blood flow is expressed as the fraction of cardiac output per cubic centimeter of inflated lung tissue on the ordinate against vertical height above the mid-sagittal plane of the inflated lungs on the abscissa. The dependent left border of the lungs is plotted on the left.

During the exposure to 7Gy, when this dog was breathing air, blood flow to the most superior portions of the lungs was abolished, while concomitantly, it was relatively unchanged in the most dependent region and was increased in the midthoracic regions of the lung parenchyma.

The results with fluorocarbon breathing were similar in all five dogs. At 1G, blood flow was greater in the superior lung and increased further to the superior and decreased in the dependent lung during the exposures to 7Gy, as would be predicted since the specific gravity of blood (1.0) is less than that of fluorocarbon (1.76).

The average and variability of changes in vertical distribution of pulmonary blood flow produced by an increase in the force environment from 1 to 7Gy in all five dogs when breathing air and liquid fluorocarbon are shown as a dorsal-ventral projection in Figure 6.

In the left panel, the change in blood flow, plotted on the ordinate, is expressed as the fraction of cardiac output traversing successive 7-mm thick sagittal sections of the lungs extending from the left lateral dependent border of the lung on the left, to the right lateral superior border of the right lung, on the right . The average change in flow per cubic cm of lung tissue in each of these cross sections is shown in the right panel.

The changes produced by an increase in force environment when breathing air were similar to those reported previously in that, as would be expected from hydrostatic considerations based on the much greater specific gravity of blood than air-filled alveoli, a striking decrease in flow was observed in superior regions of the lungs. However, contrary to such considerations, no significant change was observed towards the dependent margin of the lungs in spite of the large increase in intravascular pressures present in this region, but rather the maximum increase in flow occurred in the midthoracic regions

Filling the alveoli with a liquid of greater specific gravity than blood reversed these changes. Flow increased in the superior and decreased in the dependent lung, respectively, during an increase in the force environment.

The predominant role of the specific gravity of the liquid being breathed as a determinant of the vertical distribution of pulmonary blood flow during liquid breathing can be illustrated by comparing the changes in vertical distribution of blood flow caused by an increase in force environment during breathing of a liquid with specific gravity greater than and one with less than that of blood, respectively (Figure 7). As would be predicted from hydrostatic considerations, blood flow is increased to the upper regions of the lung and decreased in dependent regions when the alveoli are filled with a liquid, FC 80, heavier than blood, and the opposite effect is seen when the alveoli are filled with a liquid less dense than blood; silicone oil.

This figure illustrates that when the alveoli were filled with a liquid with a specific gravity less than that of blood and tissue, the blood flow to the superior lung decreased during an increase in the force invironment, similar to the effects when breathing air. However, contrary to the results with air breathing, there was relatively little change in blood flow near the mid line of the lung when breathing silicone oil, and flow was increased at all levels dependent to this point.

Since silicone oil, like air, has a specific gravity less than blood, it might be expected that an increase in the force environment would have a qualitatively similar effect on the pattern of the vertical distribution of pulmonary blood flow when breathing these two substances. That this is not the case is illustrated by comparison of the changes in vertical distribution of blood flows in one dog caused by an increase in force environment from 1 to 7Gy when breathing air and silicone oil (Figure 8).

The pattern of the decrease in blood flow to the superior lung was similar in the two instances as might be expected from hydrostatic considerations. However, in the dependent lung the vertical distribution of the change in blood flow per cubic cm of lung parenchyma was strikingly different when breathing air and silicone oil. Flow was increased throughout the dependent lung when breathing silicone oil in accord with hydrostatic considerations. In contrast, during air breathing, flow/cm^3 actually decreased in the most dependent two centimeters of lung parenchyma in spite

of the fact that intravascular pressures were highest in this region and, if the alveoli and airways remained open, no concomitant increase in alveolar or airway pressure would be expected to counteract the increased intravascular pressures when breathing air.

The mechanisms which prevent an increase or cause an actual decrease in blood flow to the most dependent regions of the lung during an increase in the force environment when breathing air have not been delineated with certainty.

A one-hundred per cent arterial-venous shunt is a consistent finding in the most dependent regions of the lung during exposures to a force environment of 6 to 7G breathing air, and it has been postulated that the associated low oxygen and high carbon dioxide tensions may cause localized vasoconstriction in these regions (4-6).

Liquid breathing greatly decreased or eliminated dependent pulmonary arterial-venous shunting during exposures to high force environments and hence the possible effects of localized changes in respiratory gas tensions on vascular resistance (7). Concomitantly, the degree of inertial displacement of the heart and lung parenchyma is greatly reduced during liquid breathing (7). The qualitative differences in the pattern of vertical distribution of blood flow in the lungs between air and liquid breathing may be due in part to the differences in gas tensions in pulmonary capillary blood and tissue as well as to the purely physical factors associated with the large differences in specific gravity and compressibility between air and liquid containing alveoli and the blood perfusing these structures under the two conditions.

The pleural fluid pressures recorded at or near the superior and dependent surfaces of the lungs when breathing air and liquids of different specific gravity are shown in figure 9. The average vertical gradient obtained by dividing the difference between the pressures recorded at the superior and dependent sites in the thoracic cavity by the vertical distance separating those recording sites was slightly but significantly less than 1 when breathing air and slightly but not significantly greater than 1 when breathing liquid fluorocarbon. Since the specific gravity of the thoracic contents is certainly greater than 1 when breathing fluorocarbon (sp. Gr.: 1.76) these results indicate that the specific gravity of the thoracic contents and the magnitude and direction of the force environment

are not the sole determinants of the magnitude of the vertical gradient in pleural pressure.

The interrelationships of intra-thoracic circulatory and pleural pressures and the vertical distribution of pulmonary blood flow in relation to the zonal perfusion pressures based on the calculated differences between mean arterial, left atrial, and alveolar pressures in different regions of the lungs are shown in figure 10. These data support the findings of prior studies in this and other laboratories which indicate that the spatial distribution of pulmonary blood flow can not be fully explained on the basis of a zonal perfusion pressure model based solely on the differences between pulmonary arterial, alveolar, pulmonary venous and presumed interstitial pressures in different regions of the lung.

BIBLIOGRAPHY

1. 3M Technical Bulletin, "Fluorinent" Brank Electronic Liquids, Minnesota Mining and Manufacturing Co., St. Paul, Minn., 1965.
2. Dow Corning Company, Midland, Michigan.
3. Coulam, C. M., W. H Dunnette, and E. H. Wood: A computer-controlled scintiscanning system and associated computer graphic techniques for study of regional distribution of blood flow. Computers and Biomedical Research 3:249-273 (June) 1970.
4. Vandenberg, R. A., A. C. Nolan, J. H. Reed, Jr., and E. H. Wood: Regional pulmonary arterial-venous shunting caused by gravitational and inertial forces. Journal of Applied Physiology. 25:516-527 (November) 1968.
5. Katori, R., D. DeS Amorim, R. A. Theye, and E. H. Wood: Influence of body position on regional pulmonary arterial-venous shunts in intact dogs. Journal of Applied Physiology. 29:288-296 (September) 1970.
6. Reed, J. H., Jr., and E. H. Wood: Effect of body position on vertical distribution of pulmonary blood flow. Journal of Applied Physiology. 28:303-311 (March) 1970.
7. Sass, D. J., E. L. Ritman, P. Caskey, J. Greenleaf, N. Banchero, D. Mair, and E. H. Wood: Effects of +Gy acceleration on blood oxygen saturation and pleural pressure relationships in dogs breathing first air, then liquid fluorocarbon in a whole body water immersion respirator. Proceedings of 27th meeting Aerospace Medical Panel, AGARD-NATO, September 15-17, 1970, Garmisch-Partenkirchen, Germany pp 7-1 thru 7-13.

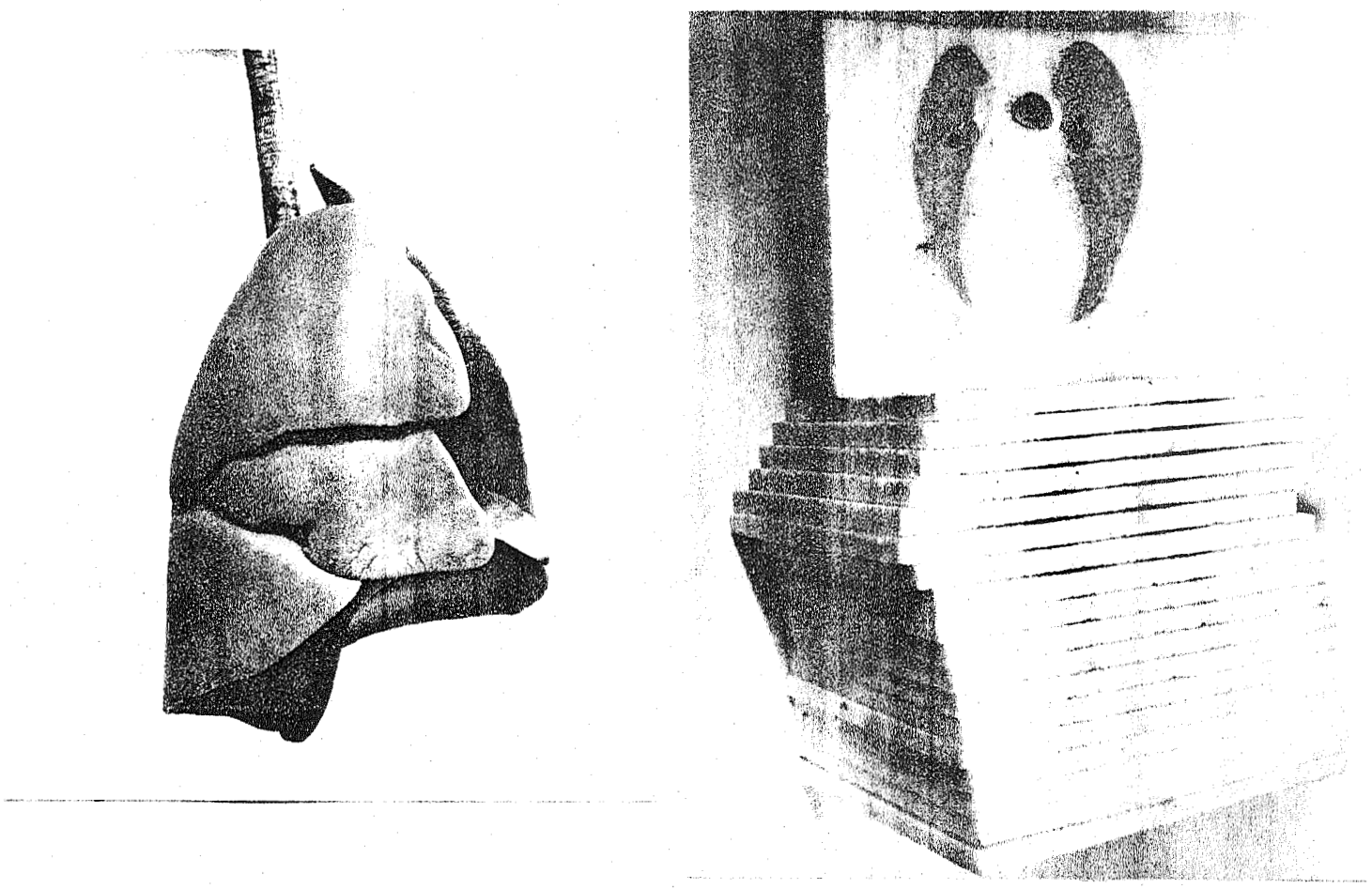

Figure 1

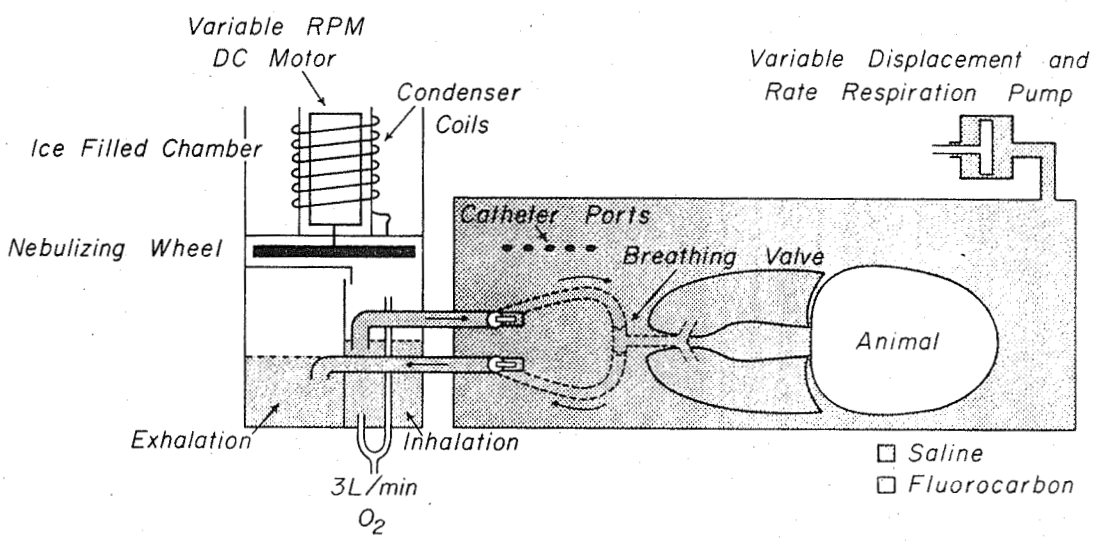

OXYGENATOR ASSEMBLY

WHOLE-BODY, WATER-IMMERSION RESPIRATOR ASSEMBLY

Figure 2

THORACIC ROENTGENOGRAMS DURING RESPIRATION WITH AIR (A,C) AND LIQUID FLUOROCARBON (B,D)
(Dog 14.5 kg, Morphine-Pentobarbital Anesthesia, Water Immersion Restraint)

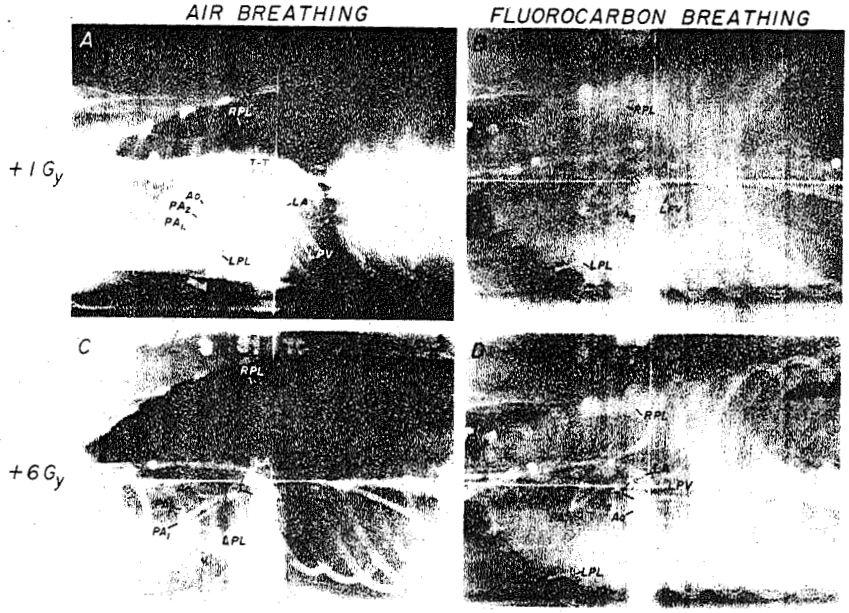

Figure 3

MULTIPLE PHYSIOLOGIC VARIABLES RECORDED DURING EXPOSURE TO 7 G_Y IN WATER-IMMERSION RESPIRATOR
(DOG 17 kg, MORPHINE-PENTOBARBITAL ANESTHESIA)

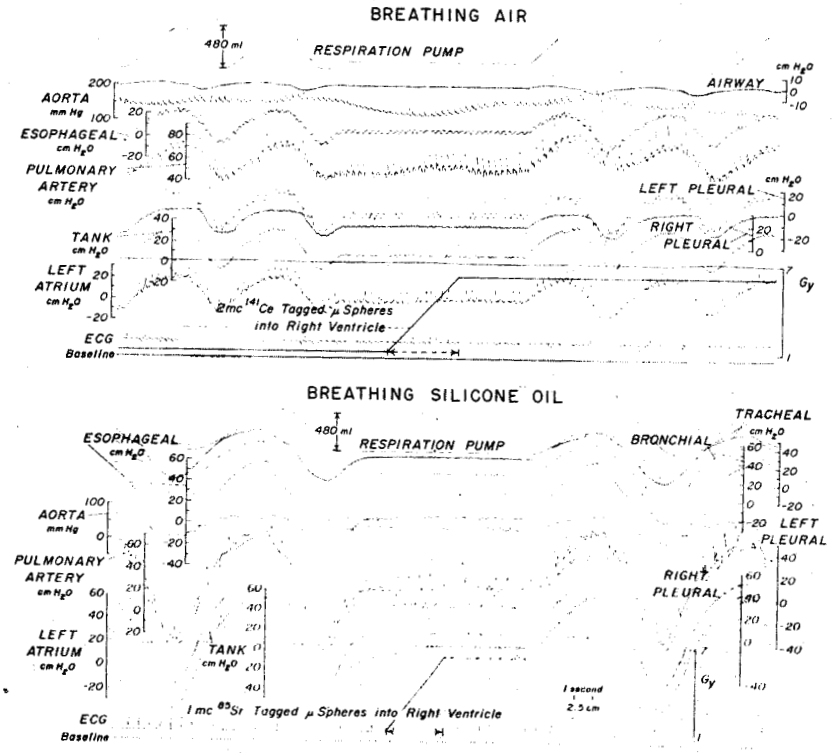

Figure 4

COMPARISON OF EFFECT OF INCREASE IN FORCE ENVIRONMENT ON VERTICAL DISTRIBUTION OF PULMONARY BLOOD FLOW WHEN BREATHING AIR OR LIQUID FLUOROCARBON (FC 80) IN WATER-IMMERSION RESPIRATOR - INSPIRATORY POSITION

(Dog 18 kg, Morphine - Pentobarbital Anesthesia, Left Decubitus Position)

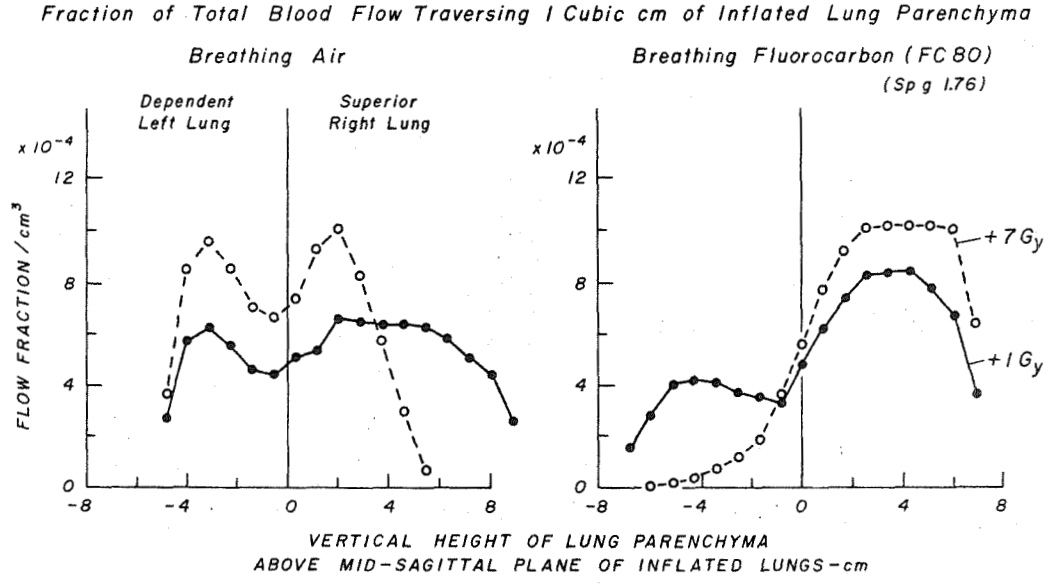

Figure 5

COMPARISON OF EFFECT OF INCREASE IN FORCE ENVIRONMENT ON VERTICAL DISTRIBUTION OF PULMONARY BLOOD FLOW WHEN BREATHING AIR OR LIQUID FLUOROCARBON IN WATER IMMERSION RESPIRATOR-INSPIRATORY POSITION

(5 Dogs, Morphine Pentobarbital Anesthesia, Left Decubitus Position)

Change In Fraction of Total Blood Flow Traversing:

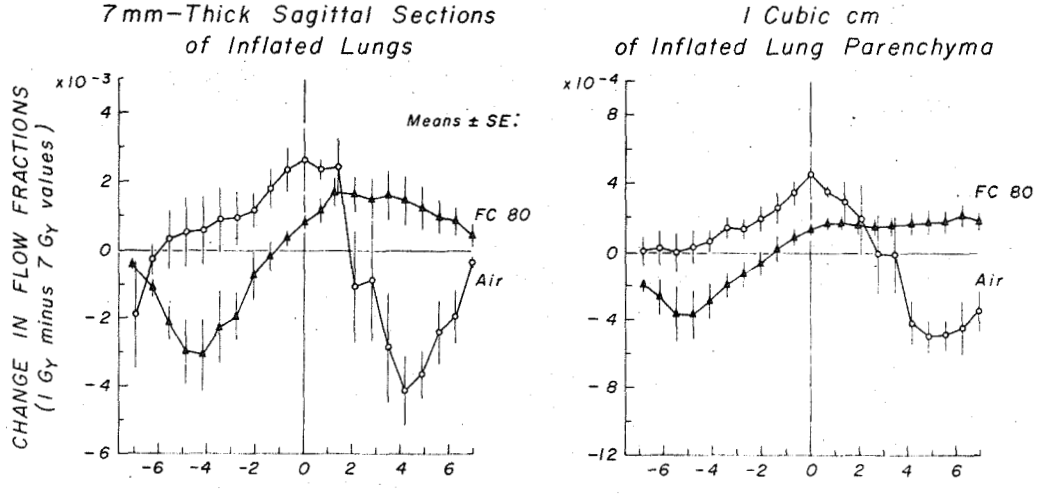

Figure 6

COMPARISON OF EFFECT OF INCREASE IN FORCE ENVIRONMENT ON VERTICAL DISTRIBUTION OF PULMONARY BLOOD FLOW WHEN BREATHING LIQUIDS OF DIFFERENT SPECIFIC GRAVITY IN WATER-IMMERSION RESPIRATOR-INSPIRATORY POSITION

(5 Dogs, Morphine Pentobarbital Anesthesia, Left Decubitus Position)

Change In Fraction of Total Blood Flow Traversing:

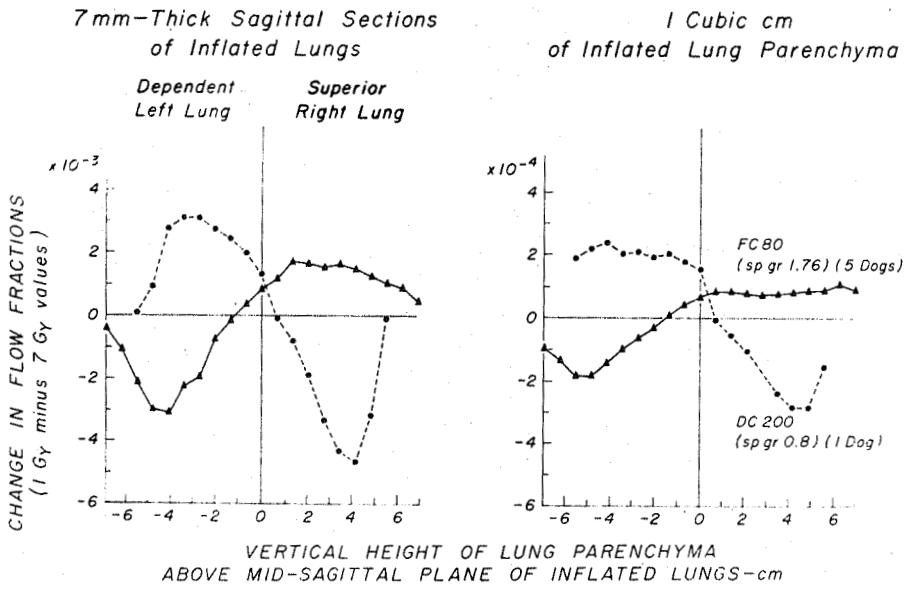

Figure 7

COMPARISON OF EFFECT OF INCREASE IN FORCE ENVIRONMENT ON VERTICAL DISTRIBUTION OF PULMONARY BLOOD FLOW WHEN BREATHING AIR OR LIQUID SILICONE OIL IN WATER-IMMERSION RESPIRATOR-INSPIRATORY POSITION

(5 Dogs, Morphine Pentobarbital Anesthesia, Left Decubitus Position)

Change In Fraction of Total Blood Flow Traversing:

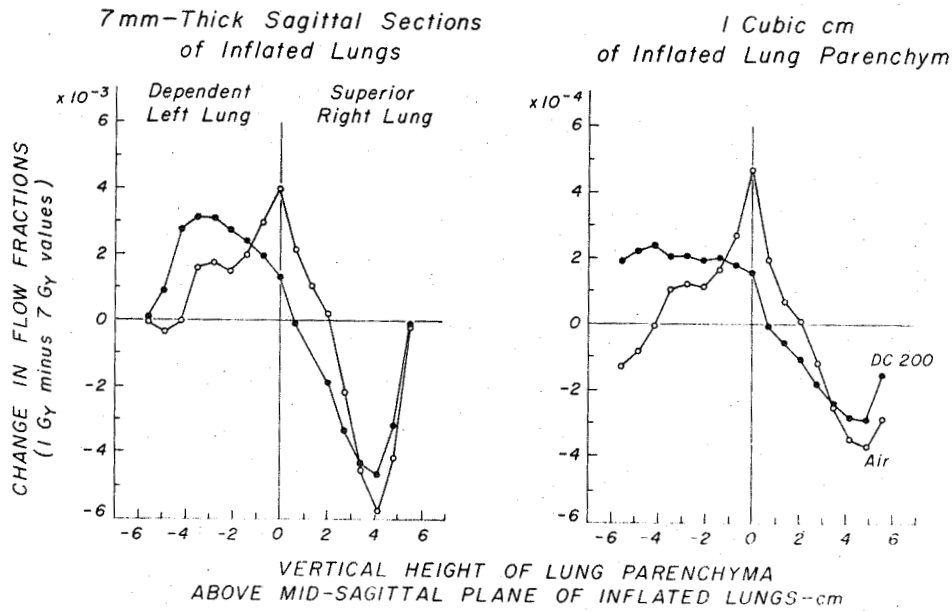

Figure 8

RELATIONSHIP OF PLEURAL FLUID PRESSURE TO VERTICAL HEIGHT IN THORAX OF DOGS BREATHING AIR, LIQUID FLUOROCARBON OR SILICONE OIL IN WATER IMMERSION RESPIRATOR IN LEFT DECUBITUS POSITION

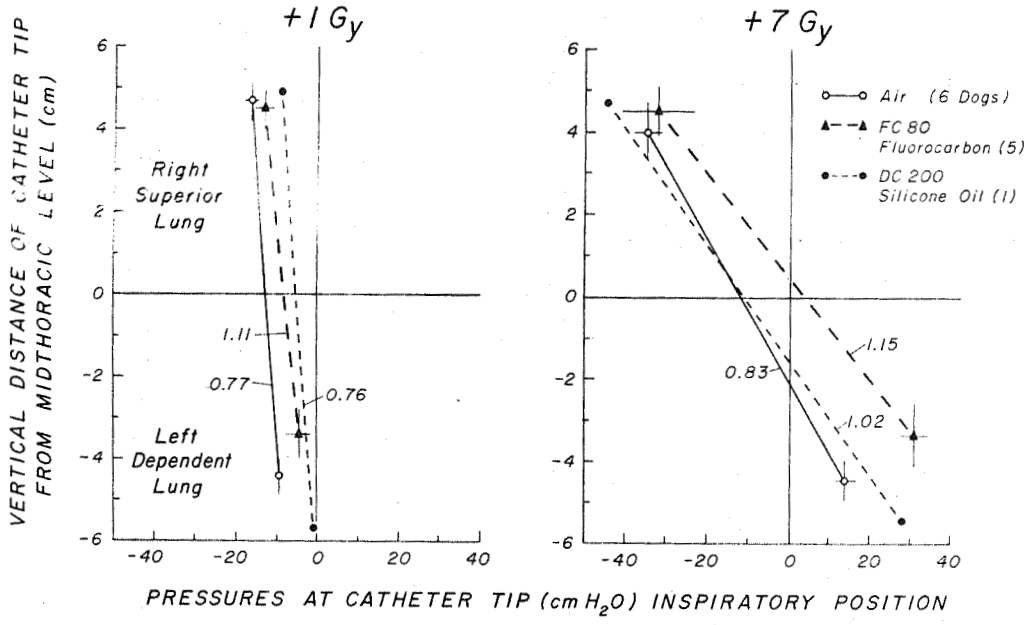

Figure 9

COMPARISON EFFECTS OF FORCE ENVIRONMENT ON VERTICAL DISTRIBUTION OF BLOOD FLOW AND INTRATHORACIC PRESSURES WHEN BREATHING AIR OR LIQUIDS OF DIFFERENT SPECIFIC GRAVITY IN WATER IMMERSION RESPIRATOR – INSPIRATORY POSITION

(MORPHINE – PENTOBARBITAL ANESTHESIA, LEFT DECUBITUS POSITION)

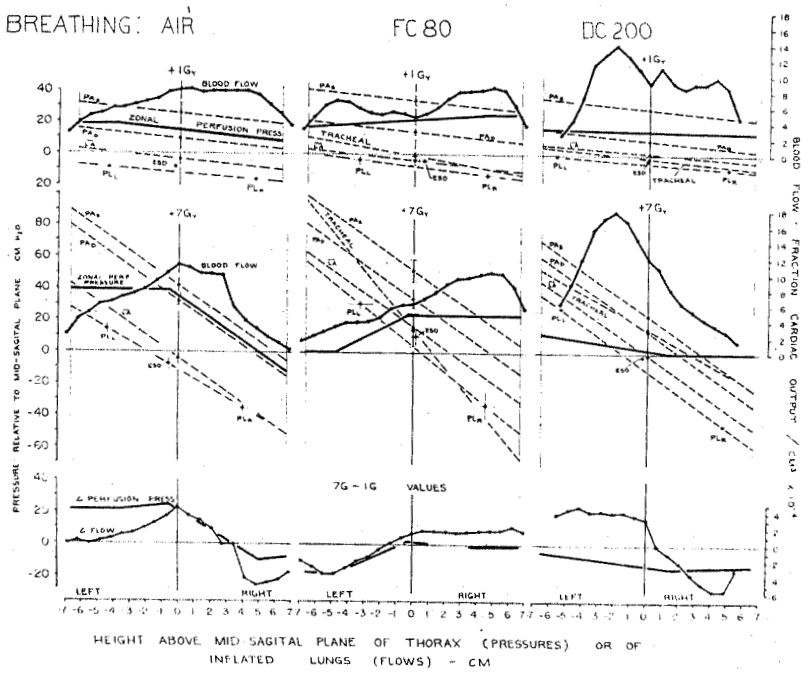

Figure 10

Section X

CALIBRATION OF CHRONICALLY IMPLANTED TRANSDUCERS FOR CARDIORESPIRATORY STUDIES IN INTACT CHIMPANZEES

In May 1971, a series of hemodynamic-respiratory studies were carried out on three intact chimpanzees in whom multiple transducers had been implanted in their thoraces several weeks previously by Dr. Harold Sandler of NASA, Ames Research Center, and Dr. H. Lowell Stone of Brooks Air Force Base.

The objective of these studies was:

1) To calibrate the implanted transducers against conventional external transducers sensing pressures obtained simultaneously via percutaneously inserted aortic, pleural, right and left atrial, pulmonary artery, and left ventricular catheters, and,

2) To assess the feasibility of use of chronically implanted transducers for quantitative cardiorespiratory studies of intact large primates during prolonged space flights.

These technically difficult experiments were carried out successfully. The very extensive data obtained are being analyzed by Dr. Harold Sandler and colleagues at NASA, Ames Research Center, in collaboration with this laboratory.